Department of Chemical and Metallurgical Engineering

Hydrotreatment of lignocellulose-derived molecules to renewable fuels and chemicals

Eveliina Mäkelä

Aalto University

DOCTORAL DISSERTATIONS

Aalto University publication series
DOCTORAL DISSERTATIONS 111/2021

Hydrotreatment of lignocellulose-derived molecules to renewable fuels and chemicals

Eveliina Mäkelä

A doctoral dissertation completed for the degree of Doctor of Science (Technology) to be defended, with the permission of the Aalto University School of Chemical Engineering (Kemistintie 1, Espoo, Finland), at a public examination held at the Auditorium KE1 of the school on 8th of October 2021 at 12:00.

Aalto University
School of Chemical Engineering
Department of Chemical and Metallurgical Engineering
Catalysis Research Group

Supervising professor
Associate Professor Riikka L. Puurunen, Aalto University, Espoo, Finland

Thesis advisors
D.Sc. (Tech.) Reetta Karinen, Aalto University, Espoo, Finland
D.Sc. (Tech.) Marina Lindblad, Neste Corporation, Finland

Preliminary examiners
D.Sc. (Tech.) Satu Ojala, University of Oulu, Oulu, Finland
Professor Magnus Rønning, Norwegian University of Science and Technology, Trondheim, Norway

Opponent
Professor Anders Riisager, Technical University of Denmark, Lyngby, Denmark

Aalto University publication series
DOCTORAL DISSERTATIONS 111/2021

ISBN 978-952-64-0479-0 (printed)
ISBN 978-952-64-0480-6 (pdf)
ISSN 1799-4934 (printed)
ISSN 1799-4942 (pdf)
http://urn.fi/URN:ISBN:978-952-64-0480-6

Unigrafia Oy
Helsinki 2021

Finland

NORDIC SWAN ECOLABEL
Printed matter
4041-0619

Author
Eveliina Mäkelä

Name of the doctoral dissertation
Hydrotreatment of lignocellulose-derived molecules to renewable fuels and chemicals

Publisher School of Chemical Engineering

Unit Department of Chemical and Metallurgical Engineering

Series Aalto University publication series DOCTORAL DISSERTATIONS 111/2021

Field of research Chemical Engineering

Manuscript submitted 16 April 2021 **Date of the defence** 8 October 2021

Permission for public defence granted (date) 22 June 2021 **Language** English

☐ **Monograph** ☒ **Article dissertation** ☐ **Essay dissertation**

Abstract

Lignocellulose is an abundant, non-edible source of biofuels and biochemicals. It can be processed into several platform molecules, such as furfural, levulinic acid (LA), and phenols. In this thesis, the hydrotreatment of lignocellulose-derived molecules to obtain biofuels and renewable chemicals was studied using batch reactors. Instead of traditional hydrotreatment catalysts (sulfided NiMo and CoMo on γ-Al_2O_3) and toxic copper chromite (industrial furfural hydrotreatment), noble and base metal catalysts on metal oxides as well as on bio-based carbon supports were used.

Furfural hydrotreatment to 2-methylfuran (MF) was conducted using Pt, Ru, and Ni catalysts on wood-based activated carbons (ACs) from spruce and birch and with Cu/Ni catalysts on bio-based activated carbon foams (ACFs) from tannic acid and pine bark extracts and on spruce-based AC. The highest MF yields of 49%–58% were obtained with 1.5–3 wt.% Pt and Ru catalysts and with 5/5 wt.% Cu/Ni catalyst on ACs in liquid phase at 230–240 °C and 40 bar H_2 pressure. The suitability of ACFs as catalyst supports was also confirmed, and MF selectivity was increased by acid treatments. The important catalytic factors affecting the MF selectivity were metal particle size and dispersion as well as the support's porosity and surface groups.

Hydrotreatment of LA dimers was first studied with a model compound, γ-nonalactone, using 3 wt.% Pt, Pd, Ru, and Rh catalysts on ZrO_2 at 280 °C and at an average pressure of 57.5 bar H_2. The highest selectivity to hydrocarbons (nearly 24%) was obtained with the Ru catalyst. The initial conversion of the catalysts (Rh >> Ru) correlated with the amount of detected surface metal atoms. Further, the hydrotreatment of LA dimers was demonstrated with a 3.6 wt.% Ru/ZrO_2 catalyst at 250–300 °C and 47.5 bar average H_2 pressure to obtain increased carbon-chain-length (>C_6) products. Deoxygenation, the formation of volatile products, and the formation of aromatics increased at high temperature. The volatile products mainly comprised not only acids, esters, and ketones but also linear, branched, and cyclic hydrocarbons.

Hydrotreatment of 4-propylphenol to propylbenzene was studied with 3 wt.% Pt catalysts on Nb_2O_5, TiO_2, and ZrO_2 supports in liquid organic phase at 350 °C and 20 bar H_2 pressure. The highest selectivity of 77% at 98% conversion level was obtained with the Pt/Nb_2O_5 catalyst. Nb_2O_5- and TiO_2-supported catalysts had activity superior to ZrO_2-supported catalyst, which was thought to be attributable to oxophilic sites created during catalyst reduction.

In this thesis, high MF yields were obtained using catalysts on wood-based ACs. To the best of the author's knowledge, AFCs were tested as catalyst supports, for the first time. Moreover, the hydrotreatment of LA dimers with Ru catalyst was demonstrated, which offers a new route from lignocellulosic sugars to increased carbon-chain-length products. Finally, high selectivity to propylbenzene was obtained from 4-propylphenol; this is among the best results reported in the liquid-phase hydrotreatment of phenols.

Keywords catalyst, hydrotreatment, furfural, levulinic acid, 4-propylphenol, biofuel

ISBN (printed) 978-952-64-0479-0 **ISBN (pdf)** 978-952-64-0480-6

ISSN (printed) 1799-4934 **ISSN (pdf)** 1799-4942

Location of publisher Helsinki **Location of printing** Helsinki **Year** 2021

Pages 244 **urn** http://urn.fi/URN:ISBN:978-952-64-0480-6

Aalto-yliopisto

Tiivistelmä

Aalto-yliopisto, PL 11000, 00076 Aalto www.aalto.fi

Tekijä
Eveliina Mäkelä

Väitöskirjan nimi
Lignoselluloosapohjaisten molekyylien vetykäsittely uusiutuviksi polttoaineiksi ja kemikaaleiksi

Julkaisija Kemian tekniikan korkeakoulu

Yksikkö Kemian tekniikan ja metallurgian laitos

Sarja Aalto University publication series DOCTORAL DISSERTATIONS 111/2021

Tutkimusala Kemian tekniikka

Käsikirjoituksen pvm 16.04.2021 **Väitöspäivä** 08.10.2021

Väittelyluvan myöntämispäivä 22.06.2021 **Kieli** Englanti

☐ **Monografia** ☒ **Artikkeliväitöskirja** ☐ **Esseeväitöskirja**

Tiivistelmä

Lignoselluloosaa voidaan pitää potentiaalisena raaka-aineena biopolttoaineille ja -kemikaaleille. Siitä voidaan valmistaa useita erilaisia kemikaaleja, kuten furfuraalia, levuliinihappoa ja fenoleita. Tässä väitöskirjassa tutkittiin lignoselluloosasta saatavien molekyylien vetykäsittelyä panosreaktoreissa. Perinteisten hydrauskatalyyttien (rikitetyt NiMo ja CoMo γ-Al_2O_3-kantajalla) sekä myrkyllisen kuparikromiitin (teollinen furfuraalin hydraus) sijaan käytettiin jalometalleja sekä kuparia ja nikkeliä metallioksidi- ja biohiilikantajilla.

Furfuraalin hydrausta 2-metyylifuraaniksi (MF) tutkittiin käyttäen Pt-, Ru- ja Ni-katalyyttejä koivusta ja kuusesta valmistetuilla aktiivihiilikantajilla sekä käyttäen Cu/Ni-katalyyttejä biopohjaisilla tanniinihaposta ja männynkuoriuutteesta valmistetuilla aktiivihiilivaahtokantajilla ja kuusesta valmistetulla aktiivihiilikantajalla. Parhaimmat MF-saannot, 49%–58%, saavutettiin 1,5–3 m.% Pt- ja Ru- sekä 5/5 m.% Cu/Ni-katalyyteillä aktiivihiilikantajilla 230–240 °C:ssa ja 40 bar H_2-paineessa. Työssä osoitettiin aktiivihiilivaahtojen soveltuvuus katalyyttien kantajiksi. Vaahdoista valmistettujen katalyyttien selektiivisyyttä MF:ksi saatiin parannettua happokäsittelyillä. MF:n selektiivisyyteen vaikuttivat erityisesti metallikatalyytin partikkelikoko ja dispersio sekä kantajan huokoisuus ja pintaryhmät.

Levuliinihapon dimeerien hydrausta tutkittiin aluksi hyödyntäen γ-nonalaktonia malliaineena. Katalyytteinä käytettiin 3 m.% Pt-, Pd-, Ru- ja Rh-metalleja ZrO_2-kantajalla 280 °C:ssa ja 57,5 bar H_2-paineessa. Korkein selektiivisyys hiilivedyiksi (lähes 24%) saavutettiin Ru-katalyytillä. Katalyyttien alkukonversio (Rh >> Ru) korreloi aktiivisten metalliatomien määrän kanssa. Seuraavaksi levuliinihapon dimeerien hydraus suoritettiin käyttäen 3.6 m.% Ru/ZrO_2-katalyyttiä 250–300 °C:ssa ja 47,5 bar H_2-paineessa. Tarkoituksena oli tuottaa pitkän hiiliketjun (>C_6) omaavia tuotteita. Korkean reaktiolämpötilan huomattiin lisäävän hapenpoistoa sekä kevyiden tuotteiden ja aromaattien muodostumista. Kevyet tuotteet olivat pääasiassa happoja, estereitä ja ketoneita, mutta myös suoraketjuisia, haaroittuneita ja syklisiä hiilivetyjä muodostui.

4-Propyylifenolin hydrausta propyylibentseeniksi tutkittiin käyttäen 3 m.% Pt-katalyyttejä Nb_2O_5-TiO_2- ja ZrO_2-kantajilla. Reaktiot suoritettiin nestefaasissa käyttäen orgaanista liuotinta 350 °C:ssa ja 20 bar H_2-paineessa. Paras selektiivisyys propyylibentseeniksi (77%, 98%:n konversiolla) saavutettiin Pt/Nb_2O_5-katalyytillä. Nb_2O_5- ja TiO_2-kantajilla olevien katalyyttien korkean aktiivisuuden ajateltiin johtuvan katalyytin pelkistyksessä muodostuvista oksofiilisista paikoista.

Tässä väitöskirjassa saavutettiin korkeita MF-saantoja käyttäen puupohjaisia aktiivihiilikantajia sekä testattiin aktiivihiilivaahtojen soveltuvuutta katalyytin kantajiksi ensimmäistä kertaa. Työssä esitetty levuliinihapon dimeerien hydraus Ru-katalyytillä tarjoaa uuden reitin lignoselluloosan sokereista pidemmän hiiliketjun tuotteiksi. Lopuksi 4-propyylifenolin hydrauksessa saavutettiin yksi parhaista raportoiduista propyylibentseenisaannoista nestefaasi-reaktiossa.

Avainsanat katalyytti, vetykäsittely, furfuraali, levuliinihappo, 4-propyylifenoli, biopolttoaine

ISBN (painettu) 978-952-64-0479-0 **ISBN (pdf)** 978-952-64-0480-6

ISSN (painettu) 1799-4934 **ISSN (pdf)** 1799-4942

Julkaisupaikka Helsinki **Painopaikka** Helsinki **Vuosi** 2021

Sivumäärä 244 **urn** http://urn.fi/URN:ISBN:978-952-64-0480-6

Acknowledgements

The thesis work has been conducted in the research group of Catalysis at Aalto University School of Chemical Engineering from 2016 onward. I thank the Aalto University School of Chemical Engineering for funding this work. I would also like to acknowledge the HDO catalyst development project between Aalto University and Neste Corporation. Finnish Foundation for Technology Promotion, KAUTE Foundation, and Walter Ahlström Foundation are acknowledged for providing encouragement grants.

I am most grateful to my supervising Associate Professor Riikka Puurunen for guiding me through this journey. I would also like to thank Research Professor Juha Lehtonen for initially offering the possibility to pursue doctoral degree at Aalto University and my instructors D.Sc. (Tech.) Reetta Karinen and D.Sc. (Tech.) Marina Lindblad for their valuable suggestions and ideas. I am also thankful to my pre-examiners D.Sc. (Tech.) Satu Ojala and Professor Magnus Rønning for their time and interest in this topic. I would like to express special thanks to my co-author, Mr. José Luis González Escobedo, for the endless discussions, ideas, and support during the years of working together. I would also like to thank all my other co-authors, especially Professor Ulla Lassi, Ph.D. Henrik Romar, Ph.D. Tao Hu, Ph.D. Toni Varila and Mrs. Riikka Kupila from University of Oulu and D.Sc. (Tech.) Mats Käldström from Neste Corporation. I am also grateful to my fellow students as well as to Mrs. Heidi Meriö-Talvio and Mr. Pekka Koivulaakso for all the help provided.

Finally, I would like to express gratitude to my family for the encouragement and support during this period and beyond. Special thanks to Yaseen and Mikaela for bringing joy to my life. Summer, sauna and good company at Lysti deserve to be mentioned as well—my favorite combination to relax and energize.

Helsinki, 22th of August, 2021
Eveliina Mäkelä

Contents

Abbreviations and symbols

Abbreviations

amu	Atomic mass unit
a.u.	Arbitrary unit
AA	Azelaic acid
AC	Activated carbon
ACF	Activated carbon foam
ACN	Acetonitrile
AMDIS	Automated mass spectral deconvolution and identification system
ATR	Attenuated total reflection
BE	Binding energy
BET	Brunauer–Emmett–Teller
BJH	Barrett–Joyner–Halenda
CHPA	Cyclohexanepropanoic acid
CI	Chemical ionization
DDO	Direct deoxygenation
DFT	Density functional theory
EDS	Energy dispersive X-ray spectroscopy
EFTEM	Energy-filtered transmission electron microscopy
EI	Electron impact ionization
EIC	Extract ion chromatogram
ESI	Electrospray ionization
+ESI	Positive mode of electrospray ionization
-ESI	Negative mode of electrospray ionization
FA	Furfuryl alcohol
FESEM	Field-emission scanning electron microscopy

FID	Flame ionization detector
FMA	Furanmethanol acetate
GC	Gas chromatograph
GNL	γ-Nonalactone
GPC	Gel permeation chromatography
GVL	γ-Valerolactone
HAA	Hydroxyalkylation–alkylation
HMF	5-Hydroxymethylfurfural
HPLC	High-performance liquid chromatography
HYD	Hydrogenation–dehydration
ICP–OES	Inductively coupled optical emission spectrometry
IR	Infrared
IWI	Incipient wetness impregnation
LA	Levulinic acid
LC	Liquid chromatography
m/z	Mass to charge ratio
MB	Methylene blue
MF	2-Methylfuran
MOA	4-Methyloctanoic acid
MS	Mass spectrometer
MSTFA	*n*-Methyl-*n*-trimethylsilylfluoroacetamide
MTHF	2-Methyltatrahydrofuran
n.a.	Not applicable
n.d.	Not determined
NIST	National Institute of Standards and Technology
NMR	Nuclear magnetic resonance
OR	Orange II
PA	Pentanoic acid
PN	2-Pentanone
POL	2-Pentanol
PTHF	2-Pentyl tetrahydrofuran
PTMEG	Polytetramethylene ether glycol

PZC	Point of zero charge
RI	Refractive index
SA	Stearic acid (standard in GPC analysis)
SA	Surface area (catalyst characterization)
SIM	Selected ion monitoring
SMSI	Strong metal–support interaction
STEM	Scanning transmission electron microscopy
TAU	Tautomerization
TC	Total carbon analysis
TCD	Thermal conductivity detector
TGA	Thermogravimetric analysis
THF	Tetrahydrofuran
THFA	Tetrahydrofurfuryl alcohol
TMCP	1,2,3-Trimethylcyclopentene
TOF	Turnover frequency
TPD	Temperature programmed desorption
TPR	Temperature programmed reduction
OSD	1-Oxaspiro(4,5)decan-2-one
UV	Ultraviolet
WHSV	Weight hourly space velocity
XPS	X-ray photoelectron spectroscopy
XRD	X-ray diffraction
XRF	X-ray fluorescence

Symbols

a_m	Surface area of a metal atom (m^2 or $Å^2$)
A	Surface area ($m^2\,g^{-1}$)
A_i	Peak area of component i
A_m	Surface area of active metal ($m^2\,g_m^{-1}$)
A_s	Peak area of standard

$C_{F,0}$	Furfural concentration in the feed (mmol g^{-1})
$C_{i,t}$	Concentration of component *i* at specified reaction time (mmol g^{-1})
$C_{F,t}$	Furfural concentration at reaction time *t* (mmol g^{-1})
C_{met}	Fraction of metal in catalyst (%)
d_{met}	Metal particle size (nm)
D	Metal dispersion (%)
i	Any product component
$f_{v,DIM}$	Fraction of evaporated liquid dimer product (%)
F_i	Response factor for component *i*
n	Stoichiometry of adsorption
$n_{A,0}$	Molar amount of 4-propylphenol in the feed (mol)
$n_{A,f}$	Molar amount of 4-propylphenol at reaction time *t* (mol)
$n_{GNL,0}$	Molar amount of GNL in the feed (mol)
$n_{GNL,t}$	Molar amount of GNL at reaction time *t* (mol)
n_i	Molar amount of component *i* (mol)
N_A	Avogadro's number (mol^{-1})
m or m_i	Mass of component *i* (mg)
$m_{DIM/C}$	Mass of the liquid product in the spent catalyst (mg)
$m_{DIM,0}$	Mass of the liquid dimer product at the beginning of the evaporation step (mg)
$m_{DIM,1}$	Mass of the liquid dimer product after the evaporation step (mg)
m_{cat}	Mass of catalyst loaded to the reactor (g)
$m_{cat,f}$	Mass of the spent catalyst after combustion (mg)
$m_{cat,0}$	Mass of the soaked, spent catalyst sample (mg)
$m_{cat,1}$	Mass of the spent catalyst after the drying step (mg)
m_f	Mass of feed (g)
m_s	Mass of solid deposits in the spent catalyst (mg)
M	Molecular weight of metal (g mol^{-1})
P_i	Mass fraction of component *i* in sample
P_s	Mass fraction of standard in sample
P_{i0}	Mass fraction of component *i* in the feed
r_{GNL}	Initial reaction rate of GNL (mol g_{cat}^{-1} s^{-1})

S_{BET}	BET surface area ($m^2\ g^{-1}$)
S_i	Selectivity of component *i* (%)
t	Reaction time (min)
t_c	Contact time (min wt.%)
T_0	GC heating program starting temperature (°C)
T_{Inlet}	GC's inlet temperature (°C)
TOF	Turn over frequency (s^{-1})
V_{ads}	Volume of irreversibly adsorbed gas ($cm^3\ g^{-1}$)
$V_{Injection}$	Injection volume in GC (µl)
V_{mol}	Molar volume ($cm^3\ mol^{-1}$)
x_{GNL}	Number of carbon atoms in GNL
x_i	Number of carbon atoms in product *i*
X	Conversion or relative change (%)
Y or Y_i	Yield of component *i* (%)
τ, τ_b or τ_B	Batch residence time ($g_{cat}\ min\ g_{feed}^{-1}$)
ν	Wavelength (cm^{-1})
ν_A	Stoichiometric factor of 4-propylphenol
ν_{GNL}	Stoichiometric factor of GNL
ν_i	Stoichiometric factor of component *i*
ρ	Density of metal ($g\ cm^{-3}$)
σ	Compressive strength (MPa)
Γ	Molar amount of surface metal sites per gram of catalyst ($mol\ g_{cat}^{-1}$)
η^1 and η^2	Furfural adsorption modes
$\sum_n m_i$	Total amount of all products (mg)

List of publications

This doctoral dissertation comprises a summary and the following publications, which are referred to in the text by their Roman numerals.

I Mäkelä, Eveliina; Lahti, Riikka; Jaatinen, Salla; Romar, Henrik; Hu, Tao; Puurunen, Riikka L.; Lassi, Ulla; Karinen, Reetta. 2018. Study of Ni, Pt, and Ru catalysts on wood-based activated carbon supports and their activity in furfural conversion to 2-methylfuran. ChemCatChem, 10, 15, 3269-3283. https://doi.org/10.1002/cctc.201800263

II Varila, Toni; Mäkelä, Eveliina; Kupila, Riikka; Romar, Henrik; Hu, Tao; Karinen, Reetta; Puurunen, Riikka L.; Lassi, Ulla. 2020. Conversion of furfural to 2-methylfuran with CuNi catalysts supported on bio-based carbon foams. Catalysis Today, 367, 16-27.
https://doi.org/10.1016/j.cattod.2020.10.027

III González Escobedo, José Luis*; Mäkelä, Eveliina*; Braunschweiler, Aki; Lehtonen, Juha; Lindblad, Marina; Puurunen, Riikka L.; Karinen, Reetta. 2019. Solvent-free hydrodeoxygenation of γ-nonalactone on noble metal catalysts supported on zirconia. Topics in Catalysis, 62, 724-737. https://doi.org/10.1007/s11244-019-01161-6

IV Mäkelä, Eveliina; González Escobedo, José Luis; Lindblad, Marina; Käldström, Mats; Meriö-Talvio, Heidi; Jiang, Hua; Puurunen, Riikka L.; Karinen, Reetta. 2020. Hydrodeoxygenation of levulinic acid dimers on a zirconia-supported ruthenium catalyst. Catalysts, 10, 2, 200.
https://doi.org/10.3390/catal10020200

V Mäkelä, Eveliina*; González Escobedo, José Luis*; Neuvonen, Jouni; Lindblad, Marina; Lahtinen, Jouko; Lassi, Ulla; Karinen, Reetta; Puurunen, Riikka L. 2020. Liquid-phase hydrodeoxygenation of 4-propylphenol to propylbenzene: reducible supports for Pt catalysts. ChemCatChem, 12, 16, 4090-4104. https://doi.org/10.1002/cctc.202000429

* These authors contributed equally.

Authors' contribution

Publication I: Study of Ni, Pt, and Ru catalysts on wood-based activated carbon supports and their activity in furfural conversion to 2-methylfuran

All authors planned the experiments and catalyst characterization. E.M. designed and performed catalytic reactor experiments and processed the obtained data. S.J. developed product analytics and E.M. analyzed the obtained products. R.L. prepared the tested catalysts and was responsible for catalyst characterization: dye molecules adsorption, physisorption, chemisorption, and carbon and ash analyses. E.M. partly conducted chemisorption measurements. T.H. performed microscopic analysis and X-ray measurements. E.M. and R.L. jointly wrote the first version of the manuscript with the help of other authors. The final version was written with contributions from all the authors.

Publication II: Conversion of furfural to 2-methylfuran over CuNi catalysts supported on bio-based carbon foams

All authors planned the experiments and catalyst characterization. E.M. designed and performed catalytic reactor experiments, analyzed the products and processed the obtained data. T.V. synthesized the activated carbon foam supports, performed all the steps required to obtain the final catalysts and did some of the characterization and analysis of the data. R.K. participated in the characterization and analysis of the data. T.H. performed the XRD, XPS, and microscopic characterizations. E.M., T.V., and R.K. jointly wrote the first version of the manuscript with the help of other authors. The final version was written with contributions from all the authors.

Publication III: Solvent-free hydrodeoxygenation of γ-nonalactone on noble metal catalysts supported on zirconia.

The first authorship is shared between E.M. and J.L.G.E., both of whom planned the research. E.M. prepared the catalysts and participated in developing the batch reactor experimental procedure. J.L.G.E. and A.B. performed most of the batch reactor experiments with the help of E.M. E.M. developed and conducted GC analyses with the help of J.L.G.E. The GC response factors of the products that lacked commercial standards were calculated by J.L.G.E, and he was also responsible for GC–MS analysis and for developing the single ion monitoring (SIM) method. E.M. participated in developing and conducting HPLC analysis and interpreting its results together with an analytical expert. Silylation method was developed by both E.M. and J.L.G.E. Karl Fisher titrations for the organic phases were conducted by E.M. and A.B., and J.L.G.E. was responsible for the elemental analysis. J.L.G.E. and A.B. interpreted the STEM images. E.M. was responsible for physisorption and chemisorption measurements, and J.L.G.E. performed the TGA and XRD measurements. The mass transfer limitations were assessed by J.L.G.E. The first version of the manuscript was written by E.M. and J.L.G.E. The final version was written with contributions from all the authors.

Publication IV: Hydrodeoxygenation of levulinic acid dimers on a zirconia-supported ruthenium catalyst

E.M. prepared the catalyst and performed all the batch reactor experiments. The experimental procedure for the batch reactor was jointly developed by E.M. and J.L.G.E. The GC–MS analysis was developed and performed by E.M., and the data were interpreted by J.L.G.E., who also proposed the for-

mation reactions of some volatile products. The Karl Fisher titrations for the organic phases were conducted by E.M. H.M.-T. and E.M. developed and performed the GPC and HPLC analyses and interpreted the results. J.L.G.E. was responsible for the elemental analysis of the organic products. E.M. and J.L.G.E. performed ATR-IR measurements, and E.M. interpreted the results, and E.M. also interpreted NMR results. For the catalysts, physisorption and chemisorption analyses were conducted by E.M., whereas J.L.G.E. performed TPR and TGA measurements. J.L.G.E. also assessed the mass transfer limitations. H.J. acquired the STEM images and EDS maps of the catalyst and interpreted the results along with J.L.G.E. The first version of the manuscript was written by E.M. and J.L.G.E. The final version was written with contributions from all the authors.

Publication V: Liquid-phase hydrodeoxygenation of 4-propylphenol to propylbenzene: reducible supports for Pt catalysts

The first authorship is shared between E.M. and J.L.G.E. Both authors equally participated in designing the content of the article. The work was initially based on J.L.G.E.'s earlier thermodynamic calculations and experimental work. The experiments were conducted by J.L.G.E and J.N. E.M. was responsible for preparing the catalysts and characterizing the fresh and spent catalysts (physisorption and chemisorption, TPR, XRF, XRD, TGA, and STEM interpretation). U.L. was responsible for TPD analysis and J.L. for XPS analysis. The Karl Fisher titrations for selected products were conducted by E.M. and J.N. The GC analysis was developed and conducted by E.M. with the help of J.N. The GC response factors of the minor liquid by-products were estimated by J.L.G.E. The analysis of liquid products with GC–MS was conducted by J.L.G.E and J.N. The study of the mass transfer limitations was performed by J.L.G.E. The first version of the manuscript was written by E.M. and J.L.G.E. The final version was written with contributions from all the authors.

1. Introduction

Owing to climate change and the increasing global energy demand, renewable fuels and chemicals have recently received research attention [1]. U.S. Energy Information Administration has projected a nearly 50% increase in global energy consumption between 2018 and 2050, and renewables are predicted to be the fastest growing sector with respect to energy consumption (3.1% annually, Figure 1) [2]. Several sources for green energy production are available, but biomass is among the raw materials with most potential for the production of liquid fuels and chemicals [3]. Biofuels can be classified into 1st and 2nd generation biofuels based on their source of origin [3]. The 1st generation biofuels (e.g., biodiesel and ethanol) are mainly produced from edible crops, which has led to increased food prices globally [4]. Lignocellulosic feedstock offers a cheap, non-edible source of plant biomass that can be used for the production of 2nd generation biofuels and renewable chemicals [4].

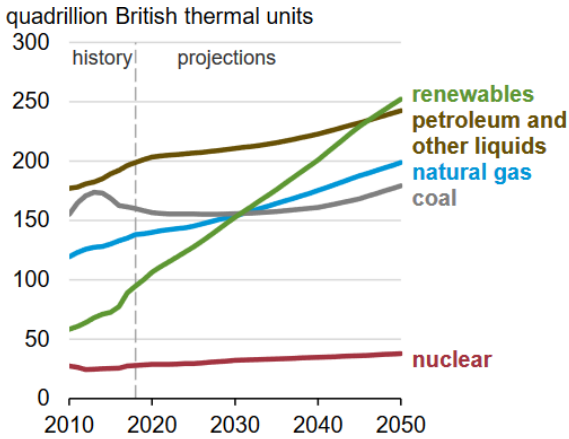

Figure 1. Global energy consumption outlook and projections for 2050 [2].

1.1 Lignocellulose as a source of fuels and chemicals

Lignocellulose comprises 40%–50% cellulose, 25%–30% hemicellulose, 15%–20% lignin, and traces of other components [5]. The structures of cellulose (a linear polymer of glucose linked together), hemicellulose (a mixture of polysaccharides with low degree of polymerization), and lignin (a complex cross-linked aromatic polymer) are presented in Figure 2 [5]. Compared with the structure of triglycerides, a traditional biodiesel raw material, lignocellulose contains more heteroatoms, especially oxygen [6]. The high oxygen content affects the processing of lignocellulosic material, which is more demanding than the quite straightforward processing of oils and fats [7]. Nevertheless, hundreds of bio-based chemicals can be obtained from lignocellulose [8].

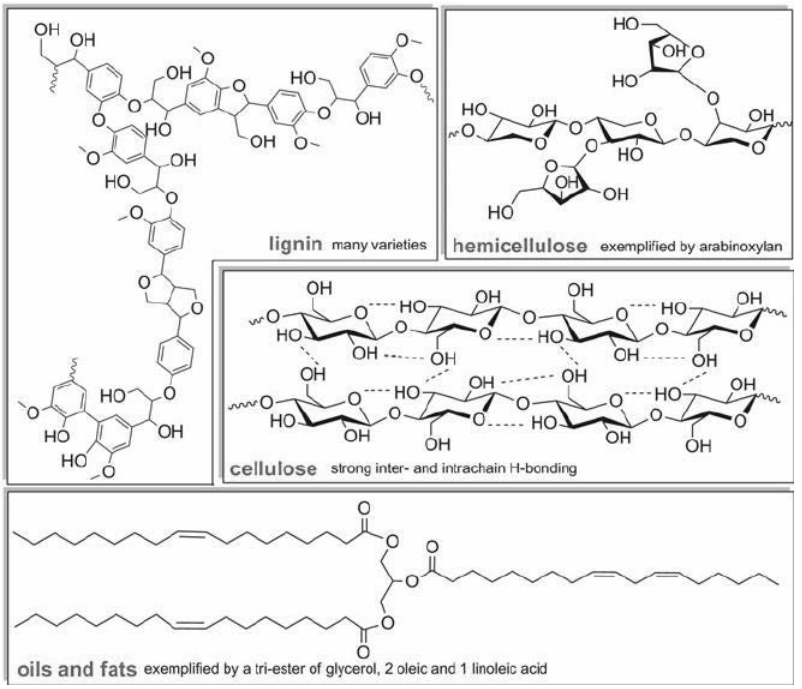

Figure 2. The structures of lignin, cellulose, and hemicellulose compared with those of fats and oils [9]. Reprinted with permission from Springer Nature, copyright (2014).

The easiest way to use lignocellulose is via combustion, which produces heat and energy. To produce liquid transportation fuels and chemicals, three processing routes have been identified to have the most potential [7,10]: gasification followed by Fischer–Tropsch synthesis [11,12], pretreatment–hydrolysis followed by fermentation [13] or catalytic hydrotreatment [14], and pyrolysis or liquefaction followed by catalytic hydrotreatment [15,16]. Here, gasification and pyrolysis involve the use of the whole lignocellulosic material, whereas hydrolysis and fermentation only use lignocellulosic sugars [10]. This thesis investigates the upgrading of molecules obtained from lignocellulosic sugars into fuel components and chemicals as well as the upgrading of phenols obtained from pyrolysis or liquefaction biocrudes into aromatic components.

Ethanol produced from starch-containing raw materials, such as corn or sugarcane, has accounted for the major share of biofuels produced globally [17]. Ethanol can be blended with fossil gasoline for use in conventional combustion engines; however, only 5% or 10% EtOH blends (E5 and E10) are approved [17,18]. Higher blending ratios also exist (E85), but they can only be used in special engines. Another drawback related to ethanol is its lower energy density compared with conventional gasoline [17,18]. Besides starch, ethanol can be obtained from lignocellulosic sugars (e.g., St1's Cellunolix® technology), although the hydrolysis of cellulose has proven to be rather difficult [7]. In addition to ethanol, the production of conventional fuel components, such as branched or linear hydrocarbons that are chemically equivalent to the fossil-based fuels, is attractive because these fuels are fully adaptable to the conventional transportation sector [17]. Nevertheless, conventional fuels need additional components to improve their properties, such as oxygenates in gasoline to enhance fuel combustion [19].

1.2 Upgrading via hydrotreatment

Hydrotreatment is a process that utilizes catalysts and hydrogen to saturate bonds as well as to completely or partially remove heteroatoms, such as oxygen, nitrogen, and sulfur [20]. Oxygen removal is often referred to as hydrodeoxygenation (HDO), which is applied in this thesis. Oxygen removal preferably occurs via the removal of water; however, carbon dioxide and carbon monoxide can also be formed through decarboxylation and decarbonylation, respectively [20]. These reactions are often considered as unwanted side reactions and they do not directly consume hydrogen. Light hydrocarbons are typically obtained through catalytic cracking or via further methanation of carbon monoxide and carbon dioxide in the presence of hydrogen [21,22]. The general reaction for the HDO of an alcohol is depicted in Reaction A.

$$R\text{–}OH + H_2 \rightarrow H_2O + R\text{–}H \quad \text{(A)}$$

Hydrotreatment can be used instead of transesterification to upgrade vegetable oils and animal fats, leading to the production of paraffinic renewable diesel [9]. In theory, hydrotreatment can be used to obtain hydrocarbons from cellulose- and hemicellulose-derived oxygenates. However, only hydrocarbons with a maximum chain length of C_6 can be obtained from lignocellulosic sugars. Thus, either a carbon chain increase reaction is needed prior to hydrocarbon production to obtain heavier compounds suitable for diesel (C_{16}–C_{20}) and jet (C_9–C_{15}) fuels [23] or the production of specialty chemicals or additional fuel components (e.g., bio-based oxygenates to gasoline [17] or bio-based aromatics to jet fuel [24]) should be targeted. Another interesting route is the hydrotreatment of pyrolysis or liquefaction biocrudes to obtain liquid hydrocarbons for use in the transportation sector [10].

1.3 Hydrotreatment catalysts

Conventional hydrotreatment catalysts include a molybdenum sulfide phase that is promoted by Ni or Co (NiMo and CoMo) and supported on γ-Al_2O_3 [25]. The sulfided catalysts deactivate by releasing sulfur in the absence of replenishment [26]. Because biomass and bio-oils typically contain only little sulfur, a sulfiding agent is often added to improve catalyst stability and to maintain its activity [27]. For the final products (e.g., fuels), sulfur specifications are low and therefore sulfur removal is needed [26]. In a particular reaction, furfural hydrotreatment, toxic copper chromite has been industrially used, but owing to environmental regulations, research has recently focused on less harmful catalysts [28,29].

Supported noble metal catalysts can be considered as alternatives for the traditional hydrotreatment catalysts, as they do not require sulfur in the system to remain active. Supported noble metal catalysts have also been found to be active in eliminating carbonyl groups from fatty acids and esters as well as oxygen from phenols [30,31]. Typical noble metals in hydrotreatment are platinum group metals, such as Pt, Pd, Rh, Ru, and Ir, which provide high activity in the hydrogenation of most functional groups under mild conditions [32]. Non-noble metals, such as Ni, Cu, and Co, are also widely used for hydrogenation [33]. Their advantage over noble metals is their significantly lower cost [33]. In addition, Ni and Cu are not included in the list of critical raw materials by the European Union [34]. The selection of the metal catalyst for a particular reaction can also have a significant effect on selectivity and impurity tolerance [35].

Hydrogenating metals can also be supported on metal oxides other than the conventional γ-Al_2O_3. In general, a metal oxide surface terminates to O^{2-} anions, which are larger in size than the metal cations [36]. The surface can also contain various defects, and the unsaturation is typically compensated by a reaction with water, leading to the formation of hydroxyls on the surface [36]. In the hydrotreatment

process, water is formed as a consequence of oxygen removal. Water can cause a partial phase transition of γ-Al_2O_3 to boehmite causing loss in catalytic activity [37], whereas other oxides, such as TiO_2, ZrO_2, and Nb_2O_5, provide higher water tolerance [38]. Moreover, the deactivation of γ-Al_2O_3 through excess coke formation could be avoided using a support with lower concentration of acid sites, such as ZrO_2 [31]. In addition, TiO_2 and Nb_2O_5 are recognized as reducible supports, which can significantly affect catalyst activity [39]. Another important factor associated with reducible metal-oxide–supported noble metal catalysts, is the so-called strong metal–support interaction (SMSI), which can increase or decrease catalyst activity [40]. Typically, it involves the metal being covered by partially reduced support species [40].

Other interesting options for catalyst support are various carbon materials, which are typically used in wastewater treatment, gas cleaning processes, and metal removal from waste streams [41,42]. Carbon-based supports are also interesting options for hydrotreatment catalysts. Because these supports are less acidic than γ-Al_2O_3, they can prevent excess coke formation [43]. Moreover, carbon supports could offer higher stability in water-containing systems (e.g., HDO) than γ-Al_2O_3 [43,44]. Carbon-based materials also possess many other advantageous features suitable for catalyst support, such as high surface area (SA), easily tailorable structure, high porosity, and relative chemical inertness [45]. The weak interaction associated with carbon-based supports is sometimes advantageous, as it can ease the reduction of the metal [46,47]. Moreover, the precious metals can be recovered from the spent catalysts by burning the carbon [45]. Several different carbon materials can be used as catalyst supports, such as activated carbon (AC), carbon black, carbon nanotubes, carbon nanofibers and graphenes. Carbon surface groups can be tailored to change catalyst acidity and hydrophobicity [45]. The surface groups containing heteroatoms (e.g., O, S, N, and H) can be divided into acidic, basic, and neutral groups, and they can act as anchoring sites for metal particles, thus facilitating high dispersion [46]. Oxygen-containing surface groups have been mostly studied and are typically produced by simply exposing the carbon material to the atmosphere or by oxidation treatments [48]. Oxygen-containing groups include carboxylic acids, lactones, phenols, carbonyl, ether, and quinone [48].

ACs are typically produced from fossil-based sources, such as bituminous coal or lignite; however, the production of alternative bio-based carbon materials from residual wood and coconut shells has been reported [49]. The residual and waste biomass-based materials are considered as low-cost alternatives [45,50,51]. However, AC materials typically have limited mechanical stability, especially abrasion resistance [52]. To enhance the mechanical stability of the AC support for high flow rate processes, briquetting [53] or foaming [54] can be applied. Moreover, the porosity of carbon-based materials can be tailored by choosing the activation method [42]. Thus, in this thesis, tannic-acid–based and pine-bark-extracts–based carbon foams were tested as catalyst supports.

1.4 Scope of the research

The aim of this work was to investigate the production of valuable bio-based fuel components and chemicals from lignocellulose-derived raw materials through catalytic hydrotreatment. Both model compounds and an industrially produced feed were used. Raw materials from lignocellulosic sugars, namely levulinic acid (LA) dimers and furfural, were studied to produce renewable chemicals and 2-methylfuran (MF), respectively. The production of alkylbenzenes from pyrolysis and liquefaction biocrudes was investigated using 4-propylphenol as a model compound. Catalysts were developed to study the previously mentioned reactions to achieve the desired product selectivities. The main targets can be summarized as follows:

1. Chemicals from lignocellulosic sugars

- Investigate the use of biomass-based activated carbons and carbon foams as catalyst supports in furfural hydrotreatment, and understand the effect of their structural characteristics on MF production [I,II].
- Study the hydrodeoxygenation of LA dimers with a model compound, γ-nonalactone (GNL), and with an industrially produced dimer feed using noble metal catalysts to obtain chemicals and fuel components [III,IV].

2. Alkylbenzenes from pyrolysis and liquefaction biocrudes
   - Compare reducible and irreducible metal oxide supports for Pt catalysts for the hydrodeoxygenation of 4-propylphenol to obtain new insights into the reaction system and maximize catalyst activity toward propylbenzene production [V].

2. Background literature

This chapter provides background information regarding the research topics discussed in this thesis. The overall process from lignocellulose to sugar-based platform molecules is briefly described, followed by further discussion on the production of furfural and LA. The routes from lignocellulose to lignin-based chemicals are also discussed, especially the thermal conversion processes. In addition, the potential of biocrudes as a source of phenols is assessed. Finally, the hydrotreatment of furfural, LA dimers, and 4-propylphenol is discussed in more detail.

2.1 From lignocellulose to sugar-based platform molecules

To separate or dissolve the different components present in lignocellulose (cellulose, hemicellulose, and lignin), pretreatment methods are applied and are an important step toward obtaining platform molecules [8]. The different pretreatment methods can be categorized as physical (e.g., mechanical milling and ultrasound), chemical (e.g., acid or alkali treatment), physico-chemical (e.g., steam explosion), and biological methods [55]. The entire separation process typically includes several methods—for example, mechanical milling is often applied prior to other methods [5,56].

After the separation of lignocellulosic polysaccharides, hydrolysis is performed, where the polysaccharides are converted into simple sugars, such as glucose (C_6 sugar) and xylose (C_5 sugar), through the cleavage of glycosidic bonds between the sugar units [57]. Typically, hydrolysis is conducted at 100–300 °C with acid or base catalysts [57] or at 45–50 °C with cellulase enzymes [56]. Furfural is formed on further dehydration of C_5 sugars, whereas the same process from C_6 sugars leads to the formation of 5-hydroxymethylfurfural (HMF) [57,58]. LA is produced by the subsequent hydration of HMF along with the formation of equivalent amounts of formic acid in acidic conditions and elevated temperatures [58]. The production of furfural and LA from lignocellulose is summarized in Scheme 1. Another important platform molecule obtained from lignocellulosic sugars is γ-valerolactone (GVL) [8], which can be produced from LA via the 4-hydroxypentanoic acid (HPA) intermediate and further cyclization using various homogeneous and heterogeneous catalysts in the liquid-phase reaction [59]. In contrast, the vapor-phase reaction proceeds via enolization to the α-angelica lactone intermediate, which is further hydrogenated to GVL [59].

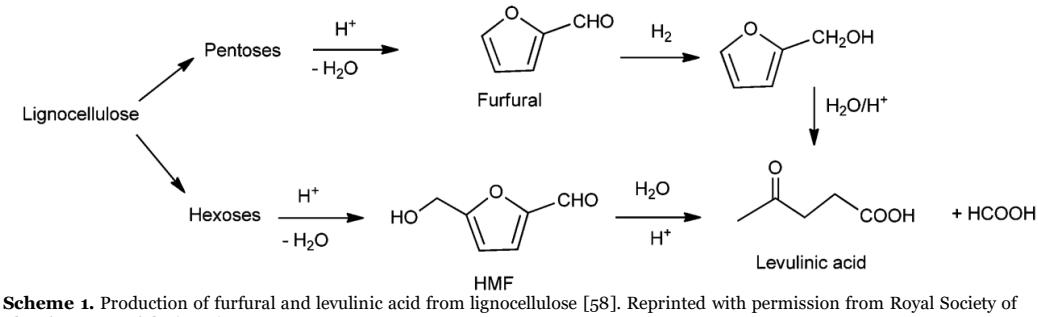

Scheme 1. Production of furfural and levulinic acid from lignocellulose [58]. Reprinted with permission from Royal Society of Chemistry, copyright (2014).

Furfural was first produced on a large scale in the 1920s by Quaker Oats Company using agricultural by-products as a feed with sulfuric or phosphoric acid catalysts at 153 °C (hydrolysis) to obtain pentoses that were further converted to furfural in a two-step process [60]. The first industrial process provided low furfural yields (<50% of sugar monomers); therefore, it was modified by Westpro and Supra Yield into continuous processes with 50%–70% (240 °C) production yields [60,61]. Another process that uses two-stage dilute acid hydrolysis (195–230 °C) is the Biofine process (by BioMetics, Inc.), which can result in up to 70% of the maximum theoretical yield of furfural from hemicellulose and 70%–80% of the maximum theoretical yield of LA from cellulose [62].

The annual production volume of furfural is around 300 ktons, of which around 70% is produced in China [63]. The price of furfural fluctuates with demand but is around $1500 per ton [64]. Furfural production from fossil-based raw materials has not been economically competitive [63]. In comparison to furfural, LA has a higher price (around $5000–8000 per ton) and smaller market size (around 3800 tons) and has been mostly produced from petrochemicals [65]. However, the development of the Biofine process has lowered the costs of producing LA from renewable sources, which should make the bio-based LA-derived chemicals economically more attractive [65].

2.2 Phenols from pyrolysis and liquefaction biocrudes

Approximately 100 million tons of lignin was produced in 2015, and an annual growth rate of 2.2% in the production was estimated [66]. Lignin has three different categories: ligno-sulphonate (88%), kraft lignin (9%), and organosolv lignin (2%) [66]. To obtain value-added products from lignin, degradation via thermal, chemical, or enzymatic pathways is necessary [66]. Pyrolysis and liquefaction are promising thermal conversion processes not only for lignin but also lignocellulose. In a pyrolysis process, the raw material is thermally decomposed in the absence of oxygen at temperatures of 375–530 °C [10]. Owing to the depolymerization and fragmentation of cellulose, hemicellulose, and lignin, biocrude containing up to 300 compounds is produced [67]. Up to 80 wt.% of the dry feed can be transformed into biocrude [10], which is typically composed of up to 30% of water and has major product groups of acids, alcohols, ketones, ethers, esters, aldehydes, furans, sugars, hydrocarbons, and phenols [67,68].

Liquefaction is a process where lignocellulose is depolymerized and partially deoxygenated to biocrude. The process includes both pyrolysis and hydrolysis, as the thermal degradation is similar to pyrolysis chemistry but proceeds in a liquid solvent at moderate temperatures (200–400 °C), which is similar to hydrolysis [69]. In addition to thermal liquefaction, hydroliquefaction can be used, which leads to more saturated and lighter biocrude [69]. The fractions of water, organics, and solids significantly depend on the selected process conditions and the biomass type; however, in general, 15%–95%

yields of the organic fractions of biocrude have been reported with major compositions of sugar derivatives and phenolic compounds [70]. The typical hydrothermal liquefaction biocrude can contain up to 65% of phenols (based on gas chromatography-mass spectrometry area-%) [71].

Pyrolysis and liquefaction biocrudes are corrosive and chemically unstable and thus inadequate to be used as fuels [68,69]. Hydrotreatment, where oxygen is removed as water, and zeolite upgrading, where oxygen is removed as CO_2, are the most typical upgrading processes in the literature when transportation fuels are considered as target products [72]. Phenolic compounds are particularly challenging to upgrade because the hydroxyl–aryl bond is strong [10]. However, they can serve as a source for obtaining aromatic compounds.

2.3 Hydrotreatment of furfural

In the past, furfural was mainly used for resin production (in foundry technologies) or as a solvent [60]. Being a versatile platform molecule with aldehyde and furan ring functional groups, furfural (furan-2-carbaldehyde) can be directly or indirectly converted into over 80 products [63]. Although various ways to modify furfural exist (e.g., oxidation, hydrogenation, amination, acetalization, and condensation) [63], the present work focuses on the hydrotreatment of furfural to obtain valuable products, such as MF.

A simplified furfural hydrotreatment reaction network is presented in Scheme 2. The most common product that can be obtained from furfural via hydrogenation is furfuryl alcohol (FA), as around 65% of furfural is used to produce this chemical [63]. FA can be used as a solvent or in different industrial processes (e.g., resin production) and can serve as a building block for other chemicals [73]. Another major product from furfural is furan, which is formed via decarbonylation. Furan is mostly hydrogenated to tetrahydrofuran (THF), which is used as a solvent and in the production of polytetramethylene ether glycol (PTMEG) [73]. Furfural can also react to afford α,ω-diols—for example 1,2-, 1,4- or 1,5-pentanediols (PDOL)—which can be used as disinfectants, in cosmetics, and in polyester and polyurethane production [74].

Tetrahydrofurfuryl alcohol (THFA) is a green solvent applied in the agricultural sector, for printing inks, and in industrial and electronics cleaners and is obtained via the hydrogenation of FA [28]. The hydrogenation of FA can also lead to furan ring rearrangement, yielding cyclopentanone and cyclopentanol, especially with water solvent; alcohol solvents favor hydrogenation and decarbonylation [75–77]. Another important product from FA is MF, which is produced via hydrogenolysis. The production of MF with high yields is challenging, as it can further react via hydrogenation to form 2-methyltetrahydrofuran (MTHF) and via ring opening to form 2-pentanone (PN) and 2-pentanol (POL). Moreover, MF can be consumed in condensation reactions, leading to, for example, 2-(2-furanylmethyl)-5-methylfuran (FMMF) (Scheme 2b).

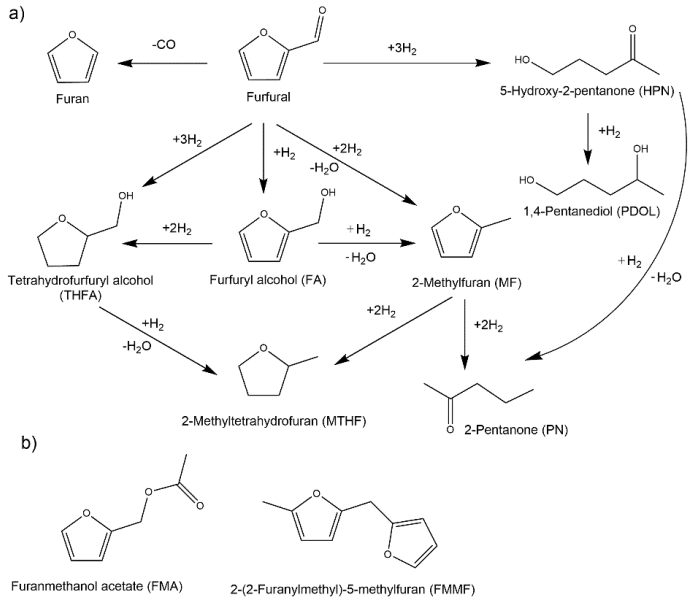

Scheme 2. a) Furfural hydrotreatment reaction network and b) observed condensation products. Reprinted from Publication II with permission from Elsevier B.V., copyright (2020).

2.3.1 2-Methylfuran as a biofuel component

MF has received attention as a valuable product that can be used as a solvent [73]. However, MTHF as a saturated chemical is less reactive and toxic than MF, and thus has even greater potential for solvent applications [73]. The properties of MF also enable its use as a potential biofuel component when blended with gasoline [28]. The heating value of MF (28.5 MJ l^{-1}) is 35% higher than that of EtOH and close to that of gasoline (31.0 MJ l^{-1}) [78]. The high octane number (RON 131) and low water solubility (7 g l^{-1}) of MF have led to increased research on the use of MF as an fuel additive in gasoline [79]. The high octane number can help to resist engine knock and enables higher compression ratios [78]. MF can also alleviate engine cold-start at low temperatures owing to its lower enthalpy of vaporization (389 kJ kg^{-1}) compared with that of ethanol (919 kJ kg^{-1}) [78]. Recently, research related to the combustion of MF together with gasoline has been conducted [78,80].

2.3.2 Catalytic processes for 2-methylfuran production

The majority of studies on furfural hydrotreatment have focused on the production of FA. Recently, the interest in producing MF has led to an increased number of studies on obtaining MF with high yields. Typically, supported metal catalysts are used, which allow furfural adsorption to occur in at least three different adsorption modes: η^1–(O) adsorption mode via the aldehyde function, η^2–(C,O) adsorption mode in which the furan ring adsorbs on the metal from the C atom and from the O atom of the carbonyl group, and η^1–(C) acyl adsorption mode, which is converted from the η^2–(C,O) adsorption mode at high temperatures [81,82]. The selectivity of a catalyst in furfural hydrotreatment can vary depending on the chosen conditions; for example, low reaction temperatures (80–150 °C) with Ni and Pt catalysts typically lead to FA as the main product [83–85], whereas at high temperatures (≥230 °C), the formation of furan [86] and MF [82] is increased.

In addition to the conditions, the chosen metal affects selectivity via the furfural adsorption modes. Cu catalysts produce FA, MF, cyclopentanone, and pentanediols rather than furan or furan ring hydrogenation products (e.g., MTHF and THF) [82]. The selectivity of Cu is attributable to the strong repulsion of the furan ring by the Cu (111) surface, leading to the η^1–(O) adsorption mode and the hydrogenation of the C=O bond [82,87,88]. The hydrogenolysis activity of the C–O bond in FA is less favored by Cu, but the activity can be increased by adding a second oxophilic metal to the catalyst or by increasing the Lewis acidity (e.g., Cu^+ species and selection of the support) of the catalyst [82]. Similarly to Cu, RuO_2 adopts the η^1–(O) adsorption mode, and the combination of RuO_x Lewis acid sites and metallic Ru is needed for improved hydrogenolysis activity toward MF [82]. Unlike Cu and Ru, the interaction of furfural with Ni and Pt is strong, and thus the adsorption of furan ring via the η^2–(C,O) adsorption mode is dominant [82]. This adsorption mode enables the formation of a wide range of products via the furan ring hydrogenation, hydrogenation and hydrogenolysis of the –CHO, and ring opening [82].

Ru, Pt, and Ni catalysts on commercial AC supports have been well studied in furfural hydrotreatment literature: Ru/AC [76,77,89–92], Pt/AC [76,92,93] and Ni/AC [94,95]. However, studies on the effect of AC type (e.g., origin, porosity, and surface properties) on furfural hydrotreatment are limited. The highest reported MF yields in the literature have been obtained with Cu/AC and Cu/SiO_2 catalysts: 95.5% MF yields were reported at 170 °C and 40 bar H_2 after a 4-h reaction in a batch reactor [96] and at 200 °C after a vapor-phase reactor using weight hourly space velocity (WHSV) of 0.5 h^{-1} [97], respectively. Several studies have reported above 90% MF yields with CuNi/AC [98], $CuNi/Al_2O_3$ [99], Ir/AC [100], Co/Al_2O_3 [101], $CuO/Cu_2O{\cdot}SiO_2$ [102], and Cu–Cu_2O/N-reduced graphene oxide nanocomposite [103] catalysts.

In this work, two types of ACs prepared from lignocellulosic biomass residues (Finnish birch and spruce) were characterized and tested as catalyst supports in furfural hydrotreatment to MF, and correlations between catalyst properties and selectivities were provided [I]. In addition, two types of activated carbon foams (ACFs, tannic-acid–based carbon foam and pine-bark-extracts–based carbon foam), in which the mechanical strength can be tailored via thermal treatment at high temperatures [104], were prepared, characterized, and tested as catalyst supports in the same reaction [II]. The use of ACFs as catalyst supports, to the best of the author's knowledge, has not been attempted before. ACFs were expected to provide advantages over ACs owing to their tailorable mechanical strength. The surface properties of the ACF catalysts were modified using acid treatments to increase the selectivity to MF. Moreover, the upgrading of furfural was conducted in liquid phase with 2-propanol as a solvent owing to its compatibility with the furfural production process [89,105] and because the alcohol medium leads to improved selectivity toward hydrogenation products [75–77].

2.4 Production and hydrotreatment of increased carbon-chain-length (>C_6) products

Owing to the limited carbon-chain-length products that can be obtained from lignocellulosic sugars (C_5 and C_6), reactions to increase carbon chains (>C_6) are necessary for renewable jet fuel (C_9–C_{15}) or diesel range (C_{16}–C_{20}) molecules [23]. Routes to increase the carbon chain length of the platform chemicals (e.g. furfural, LA and GVL) include aldol condensation, ketonization and alkene oligomerization, which lead to dimer or heavier structures [106]. Deoxygenation of these heavy molecules to alkanes has received attention recently [23,107]. The present work focuses on the hydrotreatment of LA dimers and its model compound, GNL, with the aim to obtain increased carbon-chain-length (>C_6) products.

2.4.1 Routes to increase carbon chain lengths

Various researchers have studied the conversion of lignocellulosic platform molecules to increased carbon-chain-length products. Crossed aldol condensation of furfural and HMF with acetone and aldol self-condensation of hydrogenated HMF have been studied by the Dumesic research group [108,109]. Other authors have also reported the coupling of these molecules using an organocatalytic approach [110,111]. The hydroxyalkylation–alkylation (HAA) product of MF has been studied as a starting molecule to obtain diesel range hydrocarbons [112–114]. LA intramolecular dehydration and oligomerization to angelica lactone dimer and further HDO to C_7–C_{10} hydrocarbons was studied by Mascal et al. [107]. The Dumesic research group has also studied carbon chain increase reactions starting from GVL, in which butenes were obtained via the pentenoic acid intermediate and were further oligomerized to obtain C_8 hydrocarbons [115]. Furthermore, the ketonization of GVL was studied via ring-opening to pentanoic acid to obtain 5-nonanone [116,117].

2.4.2 Levulinic acid dimers

LA has been mainly used in agriculture, the chemical industry, and the food industry [118]. Owing to its reactive nature, LA (4-oxopentanoic acid) is currently considered as one of the most important platform molecules [8,58]. For example, GVL, angelica lactone, 1,4-pentanediol, and MTHF can be obtained from LA [119]. Recently, the conversion of GVL into fuels has been studied [120] with the main aim of obtaining bio-based oxygenates to be blended with gasoline (e.g., MTHF) [119]. Hydrocarbons obtained from the HDO of GVL have been less desired products owing to their limited carbon chain length.

LA dimers can be obtained via the aldol condensation of LA (Scheme 3a), as described by Blessing and Petrus [121]. Since the first patent application [121], the production of LA dimers has been reported by Käldström et al. [106] using a Pd containing ion-exchange resin catalyst in hydrogenating conditions and by Faba et al. [122] using basic MgZr oxide catalysts in water. Li et al. [123] used the synergetic effect of $ZnCl_2$ and Brønsted acidic trichloroacetic acid to produce LA dimers, and Amarasekara et al. [124] tested various acidic catalysts in the production of LA dimers and found that SiO_2–SO_3H exhibited the highest dimer yield. Moreover, Grilc et al. [125] reported LA dimerization by aldol addition and subsequent dehydrative cyclization to oxo-carboxypentyl-γ-valerolactone during the HDO of LA on a sulfided $NiMo/Al_2O_3$ catalyst. Further processing of LA dimers enables the production of fuel additives, surfactants, plasticizers, hydraulic fluids, and lubricants [122,123,126].

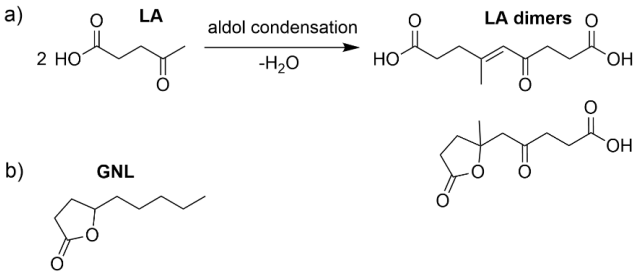

Scheme 3. a) Levulinic acid (LA) dimer formation through aldol condensation and b) γ-nonalactone (GNL) model compound.

The upgrading of LA dimers via HDO was first discussed by van den Brink et al. [127], who reported experiments using a model compound, ethyl levulinate. The main products were GVL, ethyl pentanoate and pentanoic acid with Ni and noble metal catalysts on silica or silica-bound β-zeolite at 250 °C and 80

bar H_2 after a 4-h reaction in a batch reactor. When the silica support was used, only GVL was obtained. The authors also reported the hydrogenation of LA dimers diluted in ethanol using the same catalysts on the silica-bound β-zeolite at 240 °C and 80 bar H_2. After a 75-h reaction, they reported the disappearance of the carbonyl groups present in the LA dimers; however, the types of the obtained products were not reported [127].

In this thesis, LA dimers were upgraded using two approaches. First, GNL (Scheme 3b), being a C_9 compound with two oxygen atoms, was considered a model compound for LA dimers [III]. Furthermore, GNL represents the lactone moieties present in some of the LA dimers (Scheme 3a), and the long sidechain enabled the evaluation of cracking during the HDO reaction. The HDO of GNL was conducted using sulfur-free noble metal catalysts (Ru, Rh, Pt, and Pd) supported on monoclinic ZrO_2 with the aim of comparing different noble metals and studying the removal of oxygen. ZrO_2 was selected as the catalyst support to avoid coking and to ensure sufficient water tolerance and thermal stability [30,128]. To the best of the authors' knowledge, the HDO of GNL has not been previously attempted, although it is analogous to the HDO of GVL. Second, the HDO of LA dimers was demonstrated for the first time with detailed product analysis [IV]. A Ru/ZrO_2 catalyst was used because noble metal catalysts are known to have high activity in C–O hydrogenolysis [30,129]. The aim of the study was to investigate the removal of oxygen and the product distribution.

2.5 Hydrotreatment of 4-propylphenol

Phenol is an industrially important intermediate produced by the cumene process using fossil-based benzene and propylene, where acetone is produced as a side product [130,131]. Phenol is used in the production of bisphenol A, phenol resins, caprolactam, alkylphenols, and adipic acid, etc. [131]; however, 4-propylphenol and other alkylphenols can be directly obtained from lignocellulosic biocrudes. Thus, the production of phenols from renewable and inexpensive lignocellulosic biomass has received attention in recent decades [130,131]. Although various applications for phenols exist, the present work focuses on the HDO of 4-propylphenol—chosen as the model compound for the alkylphenols present in pyrolysis and liquefaction biocrudes—to propylbenzene [V].

The most common upgrading process for pyrolysis and liquefaction biocrudes is hydrotreatment, which is especially challenging for phenolic compounds owing to the strength of the hydroxyl–aryl bond [10]. The reaction mechanisms for the HDO of phenol, which are often proposed in the literature, are presented for 4-propylphenol in Scheme 4; they include hydrogenation–dehydration (HYD), direct deoxygenation (DDO), and tautomerization (TAU). De Souza et al. [132] discussed the reaction mechanisms for the HDO of phenol on Pd catalysts. The DDO mechanism was not considered likely owing to the high dissociation energy of the C–O bond; thus, ring saturation is needed to lower the energy barrier [132]. Typically, DDO has only been proposed for highly oxophilic metals such as Ru and Fe [133,134]. The HYD mechanism requires the support to have acid sites for the dehydration of the hydrogenated intermediate [132,135]. A third mechanism, TAU, has also been proposed. De Souza et al. [132], Barrios et al. [136], and Foster et al. [135] suggested that the phenol species are adsorbed on the support's Lewis acid sites, after which TAU to the 2,4-cyclohexadienone intermediate occurs. Next, the hydrogenation of the carbonyl group to 2,4-cyclohexadienol and further dehydration to benzene takes place [132,135].

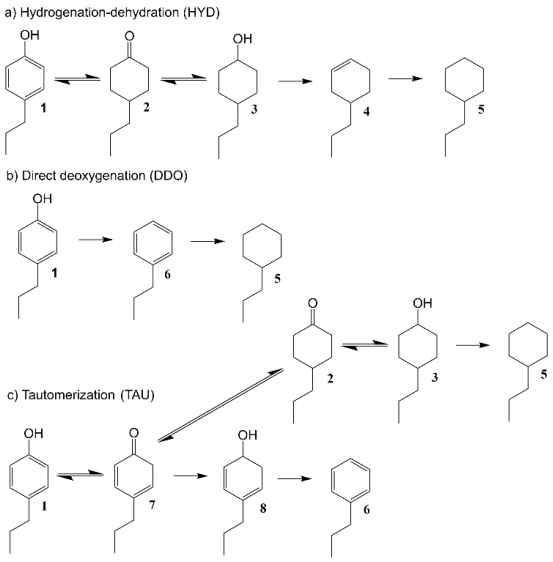

Scheme 4. Proposed mechanisms [132,136–139] for the HDO of 4-propylphenol: a) hydrogenation–dehydration (HYD), b) direct deoxygenation (DDO), and c) tautomerization (TAU). Compounds indicated: (**1**) 4-propylphenol, (**2**) 4-propylcyclohexanone, (**3**) 4-propylcyclohexanol, (**4**) 4-propylcyclohexene, (**5**) propylcyclohexane, (**6**) propylbenzene, (7) 2,4-cyclohexadienone, and (**8**) 2,4-cyclohexadienol. Reprinted from Publication V with permission from Wiley-VCH Verlag GmbH & Co. KGaA, copyright (2020).

2.5.1 Use of bio-based aromatics

Lignin-derived aromatics are an important source of industrial chemicals, pharmaceuticals, and polymers [140]. In general, bio-based aromatic hydrocarbons and cycloalkanes are interesting as potential jet fuel components [141]. Based on the current regulations, conventional jet fuel is composed of 20% of *n*-paraffins, 40% of *i*-paraffins, 20% of cycloalkanes, and 20% of aromatic hydrocarbons [24,142]. Unlike fossil-based jet fuel, renewable jet fuel does not contain any aromatics, which are vital for fuel quality and material compatibility [24,141,142]. Thus, renewable jet fuel has to be blended up to 50% with conventional jet fuel to meet the fuel specifications [24]. For the production of 100% bio-based jet fuel in the future, bio-based aromatics are needed. Low molecular weight alkylbenzenes, such as propylbenzene, have been identified as the most suitable aromatic compounds for renewable jet fuel because their combustion results in less soot formation than other aromatics [24]. Moreover, the production of propylbenzene instead of propylcyclohexane in HDO is beneficial owing to less consumption of hydrogen.

2.5.2 Catalytic processes for the production of bio-based aromatics

Various types of catalysts have been used to study the HDO of phenolic compounds. The HDO of phenols to obtain aromatics with base metal catalysts [143–145] and noble metal catalysts [35,136,137,146–148] as well as to obtain cyclohexane and other non-aromatics with base metal catalysts [138,149] and noble metal catalysts [35,137,147,150–152] has been studied. Moreover, both reducible and irreducible supports have been studied. Reducible metal oxide supports (e.g., TiO_2 and Nb_2O_5) have been found to enhance the deoxygenation activity of noble metal catalysts [136,137,153,154] owing to oxygen vacancies [155,156] and SMSI [136,157,158]. The SMSI promotes HDO because the active metal is partially covered with the support, which brings the dissociated hydrogen from the metal site in close proximity to the

oxide sites that activate the phenolic oxygen [157]. Therefore, reducible metal oxide supports were used in this thesis [V].

In addition to the support and the metal catalyst, the choice of solvent also plays an important role in the HDO of phenolic compounds. The solvent used and the phase distribution of the components in the reaction mixture significantly affect the product selectivities [159–161]. Most studies have focused on vapor-phase HDO to obtain aromatics [135,136,137,148,151,152,154,162–165], which can be integrated with the pyrolysis process [164]. In contrast, studies on liquid-phase HDO have mainly focused on producing cyclic aliphatics [138] or aromatics in aqueous medium [144,146,150,166]. However, the aqueous medium has been found to cause severe catalyst deactivation by leading to an excessive coverage of the noble metal by the support [146]. Thus, liquid-phase HDO with a non-polar organic solvent might be advantageous and could also be integrated with biomass liquefaction or solvolysis processes [69,70]. Some studies have investigated the conversion of alkylphenols to aromatics in liquid phase using organic solvents with MoO_x- and Ru-based catalysts [143,145,167,168].

The most promising study on the HDO of phenols was conducted by Zhang et al. [143], who obtained benzene selectivity of 99.5% with phenol conversion of 98% at 340 °C after a 6-h reaction in a batch reactor (liquid-phase, *n*-octane solvent, and 5 bar H_2 + 30 bar N_2) using a bulk MoO_3 catalyst. Others have reported 60%–80% aromatic product selectivities with unsupported MoO_3 [145] and Pt/TiO_2 [137] catalysts (conversions ≤80%). Ohta et al. [146] and Feng et al. [144] conducted the HDO of 4-propylphenol in aqueous conditions. They reported 85% selectivity to propylbenzene with a $Pt–Re/ZrO_2$ catalyst (300 °C, 1 h and 20 bar H_2) and 54% yield to propylbenzene with a $Re–Ni/ZrO_2$ catalyst (300 °C and 40 bar H_2), respectively. However, both studies were conducted in aqueous medium, which deactivated the catalyst and complicated the product analysis.

In this thesis, the upgrading of phenols from biocrudes was studied using 4-propylphenol as a model compound. Liquid-phase HDO of 4-propylphenol was conducted using an organic solvent (*n*-tetradecane) and sulfur-free Pt catalysts supported on reducible metal oxide supports (Nb_2O_5 and TiO_2) to produce propylbenzene as the main product [V]. The HDO of 4-propyphenol to propylbenzene in organic medium has been reported only once before [169]. Monoclinic ZrO_2, considered as an irreducible support in the used conditions, was used as reference. Moreover, the propyl side chain of the model compound enabled the evaluation of cracking during the HDO reaction.

3. Materials and methods

This chapter describes chemicals, catalysts, characterization methods, reactors, and product analysis methods used in this thesis. In general, two types of catalysts were used: (i) noble and non-noble metals supported on bio-based carbon materials and (ii) noble metals supported on reducible and irreducible metal oxides. The experiments were conducted in three different batch reactors.

3.1 Materials

In total, 98 chemical compounds and catalytic materials were used in this thesis. The compounds, suppliers, and compound purities are listed in Table 1. The compounds were used as received, except furfural, which was purified via distillation to a final molar purity of 99.8%.

Table 1. Chemicals, gases, and catalytic precursors and materials used in the thesis.

Chemical	Compound formula	Supplier	Purity/Composition	Publication
Potassium nitrate	KNO_3	Merck KGaA	≥99%	I
Potassium hydroxide	KOH	Merck KGaA	99%	I
Methylene blue	$C_{16}H_{18}ClN_3S$	Merck KGaA	≥82%	I
Orange II	$C_{16}H_{11}N_2NaO_4S$	Sigma-Aldrich	≥85%	I
Furfural[a]	$C_5H_4O_2$	Sigma-Aldrich	99.8%	I, II
Furfuryl alcohol	$C_5H_6O_2$	Sigma-Aldrich/ Agros Organics	98%	I, II
Furan	C_4H_4O	Sigma-Aldrich	≥99%	I, II
2-Methylfuran	C_5H_6O	Sigma-Aldrich	99%	I, II
Tetrahydrofurfuryl alcohol	$C_5H_{10}O_2$	Sigma-Aldrich	99%	I, II
2-Methyltetrahydrofuran	$C_5H_{10}O$	Sigma-Aldrich	≥99%	I, II
2-Pentanol	$C_5H_{12}O$	Sigma-Aldrich	98%	I, II
Cyclopentanol	$C_5H_{10}O$	Sigma-Aldrich	99%	I, II
2-Pentanone	$C_5H_{10}O$	Sigma-Aldrich	99.5%	I, II
Cyclopentanone	C_5H_8O	Sigma-Aldrich	≥99%	I, II
Vanadium pentoxide	V_2O_5			I, II
2,5-(Bis(5-*tert*-butyl-2-benzoaxazol-2-yl)thiophene	$C_{26}H_{26}N_2O_2S$	Unknown	Unknown	I, II
Methionine	$C_5H_{11}NO_2S$	Unknown	Unknown	I, II
Hydrochloric acid	HCl	Honeywell Fluka	≥37%	I, II
Nitric acid	HNO_3	Honeywell Fluka	≥69%	I, II
Nitric acid	HNO_3	Merck KGaA	65%	I, II
2-Butanol	$C_4H_{10}O$	Sigma-Aldrich	99%	I–IV
2-Propanol	C_3H_8O	Sigma-Aldrich	≥99.5%	I–IV
Tannic acid	$C_{76}H_{52}O_{46}$	Agros Organics	95%	II
p-Toluenesulfonic acid monohydrate	$C_7H_{10}O_4S$	Merck KGaA	99%	II
n-Pentane	C_5H_{12}	Merck KGaA	99.4%	II
Eta 700 solution		Etra Oy	70% EtOH	II
Zinc chloride	$ZnCl_2$	VWR	97%	II
Tween 85 surfactant		Agros Organics	Unknown	II
Hydrochloric acid	HCl	Merck KGaA	32%	II
Sulfuric acid	H_2SO_4	Merck KGaA	96%	II
Hydrofluoric acid	HF	Merck KGaA	40%	II
Boric acid	H_3BO_3	VWR	≥99.8%	II
γ-Nonalactone	$C_9H_{16}O_2$	Sigma-Aldrich	98%	III
3-Octanone	$C_8H_{16}O$	Sigma-Aldrich	≥98%	III
Octanoic acid	$C_8H_{16}O_2$	Sigma-Aldrich	≥99%	III
3-Octanol	$C_8H_{18}O$	Sigma-Aldrich	99%	III

n-Octane	C_8H_{18}	Sigma-Aldrich	Analytical standard	III
Methyl nonanoate	$C_{10}H_{20}O_2$	Sigma-Aldrich	≥97%	III
4-Nonanone	$C_9H_{18}O$	Sigma-Aldrich	"AS IS"	III
1-Nonanol	$C_9H_{20}O$	Sigma-Aldrich	98%	III
n-Nonane	C_9H_{20}	Sigma-Aldrich	Analytical standard	III
Hexanoic acid	$C_6H_{12}O_2$	Sigma-Aldrich	≥99%	III
n-Hexane	C_6H_{14}	Sigma-Aldrich	≥95%	III
Heptanoic acid	$C_7H_{14}O_2$	Sigma-Aldrich	96%	III
n-Heptane	C_7H_{16}	Sigma-Aldrich	99%	III
4-Nonanol	$C_9H_{20}O$	Merck KGaA	≥96.5%	III
2-Heptanone	$C_7H_{14}O$	Merck KGaA	≥98%	III
n-methyl-*n*-trimethylsilylfluoroacetamide	$C_6H_{12}F_3NOSi$	Sigma-Aldrich	≥98.5%	III
Formic acid	CH_2O_2	VWR Chemicals	99%	III, IV
Acetonitrile	C_2H_3N	Riedel-de Haën /VWR	99.9%	III, IV
Nonanoic acid	$C_9H_{18}O_2$	Sigma-Aldrich	98%	III, IV
Apura® two component titrant	MeOH + Iodine	Merck KGaA	Unknown	III–V
Apura® solvent	MeOH + Imidazole	Merck KGaA	Unknown	III–V
Apura® water standard	H_2O + MeOH	Merck KGaA	1% H_2O	III–V
Tetrahydrofuran	C_4H_8O	Sigma-Aldrich	≥99.9%	IV
Tetrahydrofuran-d_8	C_4D_8O	Sigma-Aldrich	99.5 atom.% D	IV
Levulinic acid	$C_5H_8O_3$	Merck KGaA	For synthesis	IV
LA dimer mixture[b]		Neste Oyj	As prepared	IV
Azelaic acid	$C_9H_{16}O_4$	Alfa Aesar	96%	IV
Dodecanedioic acid	$C_{12}H_{22}O_4$	Honeywell Fluka	≥98%	IV
Stearic acid	$C_{18}H_{36}O_2$	Sigma-Aldrich	>99%	IV
4-Propylphenol	$C_9H_{12}O$	Sigma-Aldrich	≥97%	V
n-Tetradecane	$C_{14}H_{30}$	Sigma-Aldrich	≥99%	V
Propylbenzene	C_9H_{12}	Sigma-Aldrich	98%	V
Propylcyclohexane	C_9H_{18}	Sigma-Aldrich	99%	V
4-Propylcyclohexanone	$C_9H_{16}O$	Sigma-Aldrich	≥99%	V
2-Isopropylphenol	$C_9H_{12}O$	Sigma-Aldrich	98%	V
4-Propylcyclohexanol	$C_9H_{18}O$	Tokyo Chemical Industry	>98%	V
NH_3/He	15% NH_3 in He	Oy AGA Ab	5.0/5.0	I
Hydrogen	H_2	Oy AGA Ab	5.0	I–V
Nitrogen	N_2	Oy AGA Ab	5.0	I–V
Helium	He	Oy AGA Ab	4.6	I–V
Argon	Ar	Oy AGA Ab	5.0	I–V
Calibration gas[c]		Oy AGA Ab		I–V
Calibration gas[d]		Oy AGA Ab		I–V
Synthetic air	O_2 + N_2	Oy AGA Ab	5.0	I–V
Carbon monoxide	CO	Linde	4.7	I, III, V
Oxygen	O_2	Oy AGA Ab	5.0	I, III–V
H_2/Ar	2% H_2 in Ar	Oy AGA Ab	5.0/5.0	I, IV, V
NH_3/He	5% NH_3 in He	Oy AGA Ab	5.0/5.0	V
CO_2/He	5% CO_2 in He	Oy AGA Ab	5.0/5.0	V
Nickel nitrate hydrate	$H_{12}N_2NiO_{12}$	ACS	99%–102% Ni	I
Nickel nitrate hexahydrate	$H_{12}N_2NiO_{12}$	Merck KGaA	20.17% Ni	II
Copper nitrate hemi-pentahydrate	$Cu_2H_{10}N_4O_{17}$	Alfa Aesar	27.3% Cu	II
Ruthenium chloride hydrate	$RuCl_3 \cdot nH_2O$	Agros Organics	35%–40% Ru	III
Palladium nitrate solution	N_2O_6Pd	Alfa Aesar	12%–16% Pd	III
Rhodium nitrate solution	N_3O_9Rh	Sigma-Aldrich	10% Rh	III
Platinum nitrate solution	$N_4O_{12}Pt$	Alfa Aesar	15% Pt	I, III, V
Ruthenium nitrosyl nitrate solution	$N_4O_{10}Ru$	Alfa Aesar	≥31.3% Ru	I, IV
1 wt.% Pt/C catalyst (F103R)		Degussa		I
Forest residue (birch)		Unknown, Finland		I
Forest residue (spruce)		Unknown, Finland		I, II
Pine bark		Unknown, Finland		II
Activated carbon Norit RB4C	C	Norit		II
Activated carbon Norit RX3	C	Norit		II
Monoclinic zirconia	ZrO_2	Saint-Gobain NorPro		III–V
Anatase titanium oxide	TiO_2	Alfa Aesar		V
Noibium oxide hydrate	$Nb_2O_5 \cdot nH_2O$	Companhia Brasileira de Metalurgia e Mineração		V

[a] Distilled to a final molar purity of 99.8%. [b] Prepared from LA with 0.7 wt.% Pd/Amberlyst CH28 ion exchange resin catalyst at 120 °C in a fixed-bed reactor under H_2 atmosphere [106]. [c] 40 mol.% nitrogen, 5 mol.% methane, 10 mol.% ethane, 5 mol.% ethene, 10 mol.% propane, 5 mol.% propene, 5 mol.% acetylene, 10 mol.% butane, and 10 mol.% isobutene. [d] 15 vol.% carbon monoxide, 15 vol.% carbon dioxide, 15 vol.% hydrogen, 40 vol.% nitrogen, and 15 vol.% methane.

3.2 Catalyst preparation

3.2.1 Preparation of carbon-based support materials

Carbon-based supports for noble metals (Pt and Ru) and non-noble metals (Ni and bimetallic Cu/Ni) were used in studies on furfural hydrotreatment [I,II]. Wood-based ACs from spruce (AC-S and S3) [I,II] and birch (AC-B) [I] sawdust were prepared via drying, carbonization, and steam activation. The AC prepared for Publication II (S3) was also washed with hot water to remove impurities (e.g., Ca, K, Mg, Na, and Fe). The prepared ACs were crushed and sieved to 1.4–2 mm [I] and 100–425 µm [II] particles. Commercial ACs including steam-activated RB4C and acid-washed RX3 from Norit were used in Publication II as reference materials. Both materials were crushed and sieved to 100–425 µm particles [II].

Two types of ACFs were prepared for Publication II: the first (S1) was prepared from commercial tannic acid and the second (S2) from pine bark extracts. Foaming occurred via polymerization after mixing tannic acid or pine bark extracts with deionized water, FA, and a surfactant. The ACFs were matured in an oven, cut into pieces, and activated with steam (S1) or $ZnCl_2$ (S2). The prepared S2 was refluxed with HCl to remove remaining $ZnCl_2$ and washed with deionized water until neutral. Both prepared ACFs were crushed and sieved to 100–425 µm particles.

The surfaces of the prepared ACFs were modified via acid treatments: A1 (3 M HNO_3) or A2 (6 M H_2SO_4). The treatments were conducted at 100 °C for 2 h (HNO_3) or at 80 °C for 3 h (H_2SO_4). After the acid treatments, the ACFs were washed with deionized water until neutral. The details of support and catalyst preparation can be found in Publications I and II.

3.2.2 Impregnated catalysts on carbon-based support materials

The prepared catalysts supported on bio-based carbon materials are listed in Table 2. Prior to incipient wetness impregnation (IWI) of the metals, all the support materials were dried at 105 °C overnight and the pore volumes of the supports were measured by N_2 physisorption. Next, appropriate amounts of metal precursors (to match the target metal loading in the catalyst) were dissolved in deionized water just sufficient to fill the pore volume of each support. The impregnated catalysts were mixed overnight in a Rotavapor [I] or with a spatula for 4–5 h [II] and dried at 105 °C [I] or 100 °C [II] overnight. Finally, the catalysts were thermally treated at 350 °C for 5 h [I] or at 500 °C for 2 h [II] under N_2 flow.

Table 2. Prepared and tested catalysts on carbon-based support materials (n.a. = not applicable, n.d. = not determined).

Catalyst	Support type	Support activation	Catalyst location in reactor	Catalyst particle size /mm	Determined metal loading /wt.%				S_{BET} /m² g⁻¹	Metal dispersion[a]	Publication
					Pt	Ru	Ni	Cu			
1.5Pt/AC-S	Spruce-based AC	Steam-activated	Basket	1.4–2.0	1.2	n.a.	n.a.	n.a.	850	33%	I
3Pt/AC-S	Spruce-based AC	Steam-activated	Basket	1.4–2.0	2.3	n.a.	n.a.	n.a.	840	37%	I
3Ru/AC-S	Spruce-based AC	Steam-activated	Basket	1.4–2.0	n.a.	2.8	n.a.	n.a.	770	22%	I
3Ni/AC-S	Spruce-based AC	Steam-activated	Basket	1.4–2.0	n.a.	n.a.	2.0	n.a.	910	12%	I
10Ni/AC-S	Spruce-based AC	Steam-activated	Basket	1.4–2.0	n.a.	n.a.	8.9	n.a.	690	7.0%	I

S3_Cu/Ni	Spruce-based AC	Steam-activated	Slurry	0.1–0.425	n.a.	n.a.	4.3	4.3	680	n.d.	II
3Pt/AC-B	Birch-based AC	Steam-activated	Basket	1.4–2.0	3.2	n.a.	n.a.	n.a.	780	19%	I
1.5Ru/AC-B	Birch-based AC	Steam-activated	Basket	1.4–2.0	n.a.	1.7	n.a.	n.a.	870	20%	I
3Ru/AC-B	Birch-based AC	Steam-activated	Basket	1.4–2.0	n.a.	2.9	n.a.	n.a.	880	26%	I
3Ni/AC-B	Birch-based AC	Steam-activated	Basket	1.4–2.0	n.a.	n.a.	2.5	n.a.	990	7.2%	I
Norit_S_Cu/Ni	Commer-cial AC	Steam-activated	Slurry	0.1–0.425	n.a.	n.a.	4.0	3.8	760	n.d.	II
Norit_A_Cu/Ni	Commer-cial AC	Acid-washed	Slurry	0.1–0.425	n.a.	n.a.	4.7	4.3	1150	n.d.	II
S1_Cu/Ni	Carbon foam from tan-nic acid	Steam-activated	Slurry	0.1–0.425	n.a.	n.a.	n.d.	n.d.	n.d.	n.d.	II
S1_A1_Cu/Ni	Carbon foam from tan-nic acid	Steam-activated, HNO_3-washed	Slurry	0.1–0.425	n.a.	n.a.	7.2	7.0	550	n.d.	II
S1_A2_Cu/Ni	Carbon foam from tan-nic acid	Steam-activated, H_2SO_4-washed	Slurry	0.1–0.425	n.a.	n.a.	5.1	5.0	470	n.d.	II
S2_Cu/Ni	Carbon foam from pine bark ex-tracts	Chemi-cally activated	Slurry	0.1–0.425	n.a.	n.a.	n.d.	n.d.	n.d.	n.d.	II
S2_A1_Cu/Ni	Carbon foam from pine bark ex-tracts	Chemi-cally activated, HNO_3-washed	Slurry	0.1–0.425	n.a.	n.a.	6.5	6.6	720	n.d.	II
S2_A2_Cu/Ni	Carbon foam from pine bark ex-tracts	Chemi-cally activated, H_2SO_4-washed	Slurry	0.1–0.425	n.a.	n.a.	5.6	5.7	1150	n.d.	II

[a] From chemisorption.

3.2.3 Impregnated catalysts supported on metal oxides

In the studies on the HDO of GNL, LA dimers, and 4-propylphenol [III–V], noble metal catalysts on irreducible and reducible metal oxide supports were used. ZrO_2 and TiO_2 supports were ground and sieved to 0.25–0.42 mm [III,V] and 0.15–0.3 mm [IV] particles. ZrO_2 was calcined in synthetic air at 600 °C for 10 h and TiO_2 at 500 °C for 7 h. Niobium oxide hydrate powder was thermally treated in synthetic air at 270 °C for 7 h, after which it was pressed into tablets, ground, sieved to 0.25–0.42 mm particles, and calcined in synthetic air at 500 °C for 7 h [V].

Appropriate amounts of noble metal (Pt, Pd, Ru, and Rh) precursors in water solutions were added on the supports via IWI. The pore volumes of the supports were empirically estimated from their water uptake capacity. The impregnated catalysts were first dried at room temperature for 5 h and later at 100 °C overnight. Thermal treatments were conducted in synthetic air at 300 °C [III] or at 350 °C [IV,V] for 3 h. The prepared and tested noble metal catalysts on metal oxide supports are listed in Table 3.

Table 3. Prepared and tested catalysts on metal oxide supports (n.a. = not applicable). All catalysts were used in slurry with the reaction mixture.

Catalyst	Catalyst particle size /mm	Determined metal loading /wt.%				S_{BET} /m^2 g^{-1}	Metal dispersion[a]	Publication
		Ru	Rh	Pd	Pt			
2.7Ru/ZrO_2	0.25–0.42	2.7	n.a.	n.a.	n.a.	80	11%	III
3.6Ru/ZrO_2	0.15–0.30	3.6	n.a.	n.a.	n.a.	70	25%	IV
2.5Rh/ZrO_2	0.25–0.42	n.a.	2.5	n.a.	n.a.	58	87%	III
3.0Pd/ZrO_2	0.25–0.42	n.a.	n.a.	3.0	n.a.	64	21%	III
2.7Pt/ZrO_2	0.25–0.42	n.a.	n.a.	n.a.	2.7	65	37%	III
2.7Pt/ZrO_2	0.25–0.42	n.a.	n.a.	n.a.	2.7	80	57%	V
3.1Pt/Nb_2O_5	0.25–0.42	n.a.	n.a.	n.a.	3.1	85	41%	V
3.2Pt/TiO_2	0.25–0.42	n.a.	n.a.	n.a.	3.2	119	69%	V

[a] From chemisorption.

3.3 Characterization of supports and catalysts

3.3.1 Chemical composition

The total carbon (TC) content of the prepared AC supports in Publication I was measured using a Skalar Primacs MCS instrument, in which the dried samples of AC supports were combusted at 1100 °C in pure oxygen and the formed CO_2 was detected using an infrared (IR) analyzer. The ash content of the AC supports [I] was measured according to the SFS-EN 14775 standard [170].

The elemental compositions (C, H, N, O, and S) of the AC supports [I] and support materials S1 and S2 [II] were investigated using Thermo Scientific Flash 2000 CHNS-O Organic equipment and a Perkin Elmer 2400 Series II CHNS/O device, respectively. Prior to the elemental analysis, the samples (1 mg) were ground and mixed with 10 mg of V_2O_5 to enhance burning at 960 °C. The standard was 2,5-(bis(5-*tert*-butyl-2-benzo-axazol-2-yl) thiophene for oxygen and methionine for the other elements.

The metal content of the prepared catalysts [I,II] was measured using inductively coupled optical emission spectroscopy (ICP–OES). Sample preparation included dissolving 0.10–0.12 g of catalyst in a mixture of 37% HCl and 63% HNO_3 at 200 °C for 10 min. In Publication II, a small amount of HF was added to the mixture, and the catalyst was dissolved again at 200 °C for 10 min. HF was neutralized with H_3BO_3 [II] and all prepared solutions were diluted to 50 ml. The metals in the prepared solutions were analyzed using Perkin Elmer Optima 5300 DV equipment.

The noble metal contents of the prepared catalysts in Publications III–V were analyzed via X-ray fluorescence (XRF) using Rigaku ZSX Primus [III,IV] or PANalytical Axios Max [V] equipment with wavelength dispersive spectrometers. The samples were either ground and pressed into tablets using Boreox® binder [III,IV] or placed into a sample cup on a Mylar® film without any pretreatment [V].

3.3.2 Physisorption and chemisorption

Isothermal (–196 °C) nitrogen adsorption measurement (area of N_2 molecule: ~16.2 Å^2) was performed for the prepared catalysts to obtain the specific surface areas according to the Brunauer–Emmett–Teller (BET) theory [171] and the pore volumes and pore size distributions according to the Barrett–Joyner–Halenda (BJH) theory [172] (mesoporous metal oxide supports, Publications III–V) or density functional theory (DFT) (carbon-based supports, Publications I and II) [173,174]. Micromeritics ASAP 2020 equipment [I,II] or Thermo Fisher Surfer equipment [III–V] was used for the measurements. Prior to the analysis, fresh catalyst samples (0.1–0.3 g) were evacuated at 140–300 °C to remove moisture and adsorbed components. Spent catalysts were washed with EtOH, dried overnight at 100 °C oven, and evacuated at 140 °C [I] and at 120 °C [III,V] for 5 h prior to the analysis.

H_2 or CO chemisorption measurements were used to obtain active metal surface area (A_m), dispersion (D) and average metal particle sizes (d_{met}), as shown in Equations 1–3.

$$A_{\mathrm{m}} = \frac{V_{\mathrm{ads}} \cdot N_{\mathrm{A}} \cdot n \cdot a_{\mathrm{m}}}{V_{\mathrm{mol}} \cdot C_{\mathrm{met}}} \quad (1)$$

Here, V_{ads} is the volume of the irreversibly adsorbed gas, N_{A} is Avogadro's number, n is the stoichiometry of adsorption, a_{m} is the surface area of the metal atom, V_{mol} is the molar volume, and C_{met} is the fraction of metal in the catalyst.

$$D = \frac{V_{\mathrm{ads}} \cdot n \cdot M}{V_{\mathrm{mol}} \cdot C_{\mathrm{met}}} \quad (2)$$

Here, M is the molecular weight of the metal.

$$d_{\mathrm{met}} = \frac{6 \cdot M}{\rho \cdot D \cdot a_{\mathrm{m}} \cdot N_{\mathrm{A}}} \quad (3)$$

Here, ρ is the density of the metal, and metal particles were assumed to be spherical.

Micromeritics ASAP 2020 [I] or Thermo Fisher Surfer [I,III–V] equipment was used for measurements. Prior to the measurements, fresh, thermally treated catalysts or spent catalysts washed with EtOH and dried overnight at 100 °C (0.2–0.5 g) were reduced in H_2 at (250–350 °C) and degassed for 2–3 h. Chemisorption measurements were performed at 25–35 °C for Pt, Pd and Ni catalysts and at 75 °C for Ru catalysts based on the work of Shen et al. [175]. The stoichiometry was assumed to be two for H_2 and one for CO in all measurements [176]. The surface areas of the metal atoms were 8.07, 7.93, 7.58, 6.35, and 6.51 Å^2 for Pt, Pd, Rh, Ru, and Ni, respectively [176]. The densities of the metals were 21.45, 12.02, 12.40, 12.30, and 8.90 g cm^{-3} for Pt, Pd, Rh, Ru, and Ni, respectively [176].

3.3.3 Electron microscopy

Energy-filtered transmission electron microscopy (EFTEM) analysis was used in Publications I–V to study the morphology of the catalyst samples. Either LEO 912 OMEGA at 120 kV [I] or JEOL JEM-2200FS at 200 kV [II–V] equipment with a scan generator was used and was operated in scanning transmission electron microscopy (STEM) mode. The samples were drop-casted onto carbon-coated copper grids from a micro-emulsion, which was prepared by mixing the catalyst with ethanol or acetone in an ultrasonic bath. The elemental compositions of the samples and metal particle sizes were visually estimated from the images using energy-dispersive X-ray spectroscopy (EDS). When applicable, the average metal particle sizes were estimated from the images using Gatan DigitalMicrograph software.

Field-emission scanning electron microscopy (FESEM) analysis with a Zeiss Ultra Plus microscope equipped with EDS was used to visualize the microstructure of the AC-supported catalysts and carbon foams S1 and S2 [I,II].

3.3.4 Temperature programmed methods

Temperature programmed desorption (TPD) of NH_3 to reveal catalyst acidity [I,V] and of CO_2 to reveal catalyst basicity [V] were performed with AutoChem II 2920 equipment. The samples (50 mg) were pretreated in He flow at 500 °C for 30 min [I] or reduced in H_2 at 353 °C for 60 min [V]. After pretreatments, the samples were cooled to 100 °C, followed by the adsorption of ammonia (15% [I] or 5% [V] NH_3/He) for 60 min at 100 °C. Prior to desorption, the samples were flushed with He for 30 min. NH_3 desorption was performed in He flow from 100 to 550 °C [I] or from 100 to 600 °C [V] with a temperature ramp of 10 °C min^{-1}.

For the TPD of CO_2, a reduction procedure similar to that for the TPD of NH_3 [V] was used, after which the samples were cooled to 50 °C and flushed with He for 5 min. The adsorption of 5% CO_2/He was

performed at 50 °C for 60 min, followed by flushing with He for 30 min. CO_2 desorption was conducted in He flow from 50 to 600 °C (temperature ramp of 10 °C min^{-1}). The total acidity and basicity were determined by integrating the areas between the final and starting temperatures (linear baseline) and using the equipment's software to obtain the desorbed gas volumes with the help of calibration.

Temperature programmed reduction (TPR) was used to estimate the reduction temperatures for the fresh catalysts in Publications I, IV, and V. Altamira AMI-200R equipment connected to a thermal conductivity detector (TCD) [I,IV,V] and also to an OmniStar™ mass spectrometer (MS) [IV] was used. The catalyst samples (10–50 mg) were placed inside a U-shaped quartz reactor supported on quartz wool and preheated to 350 °C for 1 h with He flow, after which they were cooled to 30 °C. A cold trap between the sample and the TCD was filled with CO_2 ice to prevent moisture from entering the detector. For the TPR analysis, the samples were heated up to 700 °C with a heating ramp of 5 °C min^{-1} in 2% H_2/Ar [I,V]. The Ru/ZrO_2 catalyst in Publication IV was treated differently to mimic the *in situ* reduction conditions in the batch reactor. The sample was heated up to 350 °C (heating ramp of 10 °C min^{-1}) in 2% H_2/Ar and the temperature was maintained for 2 h. Next, the sample was cooled to 30 °C. The catalyst sample was kept at room temperature overnight in 5 ml min^{-1} He flow and exposed to atmosphere for 20 min before being sealed again. The preheating and TPR procedures were repeated. For comparison, the same TPR procedure was also conducted with fresh catalyst without exposing it to atmosphere [IV].

3.3.5 X-ray methods

X-ray diffraction (XRD) analysis to detect the crystallographic phases of catalysts was performed with PANalytical X'Pert PRO equipment using monochromatic CuKα1 radiation (45 kV, 40 mA) [I–III,V]. Scanning ranges between 4.5° and 120° were used with step sizes of 0.013°–0.026°. The analysis was performed for thermally treated, ground catalyst samples.

X-ray photoelectron spectroscopy (XPS) measurements were performed to analyze the surface groups on carbon-based catalysts [I,II] and to investigate the metal oxidation states [I,II,V]. Thermo Fisher ESCALAB 250Xi [I,II] or Kratos Axis Ultra [V] equipment with a monochromatic AlKα X-ray source was used, and high-resolution scans were performed with 20 eV pass energy. A charge neutralizer/compensator was used to interpret the obtained spectra, and C1s at 284.8 eV was used for energy calibration.

3.3.6 Thermogravimetric analysis

Solid deposits on spent catalysts were analyzed via thermogravimetric analysis (TGA) in Publications III–V using TA Instruments' TGA Q500 equipment. In Publications III and V, the spent, unwashed catalyst samples (10–20 mg) were placed in a sample holder and dried in N_2 up to 250 [III] or 260 °C [V] (temperature ramp of 10 °C min^{-1}) with isothermal holds of 5 or 30 min, respectively. The drying step was needed to evaporate liquid products still present in the spent catalysts. Finally, the samples were cooled close to room temperature and heated up to 900 °C in O_2 [III,V].

Owing to the lack of boiling point information for LA dimers, a more complex TGA procedure was applied in Publication IV (Figure 3). First, the fraction of evaporated liquid dimer product ($f_{v,DIM}$) was determined in the evaporation step (heating up to 300 °C in N_2, Figure 3a). Next, it was assumed that the same fraction of liquid also evaporated during spent catalyst drying (heating up to 300 °C in N_2, Figure 3b). Finally, the combustion of the dried, spent catalyst was conducted up to 900 °C in O_2 (Figure 3c) [IV].

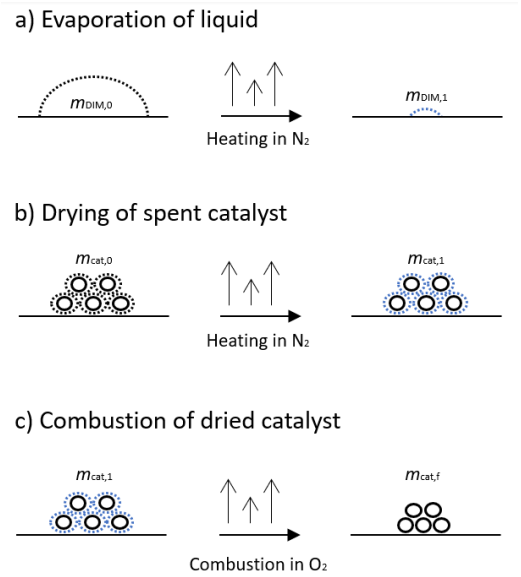

Figure 3. Schematic of the procedure applied for the TGA of the spent catalysts [IV]: a) evaporation step for the liquid product, b) drying of the spent catalyst, and c) combustion of the dried, spent catalyst. Symbol explanations: $m_{DIM,0}$ is the mass of the dimer product in the beginning of the evaporation step, $m_{DIM,1}$ is the mass of the dimer product after the evaporation step, $m_{cat,0}$ is the mass of the soaked, spent catalyst sample, $m_{cat,1}$ is the mass of the spent catalyst after the drying step, and $m_{cat,f}$ is the mass of the catalyst after combustion.

The fraction of evaporated liquid dimer product ($f_{v,DIM}$) and the mass of the liquid product in the spent catalyst ($m_{DIM/C}$) were calculated using Equations 4 and 5, respectively [IV].

$$f_{v,DIM} = \frac{m_{DIM,0} - m_{DIM,1}}{m_{DIM,0}} \quad (4)$$

$$m_{DIM/C} = \frac{m_{cat,0} - m_{cat,1}}{f_{v,DIM}} \quad (5)$$

Here, $m_{DIM,0}$ is the mass of the dimer product in the beginning of the evaporation step, $m_{DIM,1}$ is the mass of the dimer product after the evaporation step, $m_{cat,0}$ is the mass of the soaked, spent catalyst sample, and $m_{cat,1}$ is the mass of the spent catalyst after the drying step. The mass of the solid deposits (m_s) was calculated using Equation 6, where $m_{cat,f}$ is the mass of the catalyst after combustion.

$$m_s = m_{cat,0} - m_{DIM/C} - m_{cat,f} \quad (6)$$

3.3.7 Other methods

The adsorption of dye molecules, methylene blue (MB), and orange II (OR) was measured to study the adsorptive properties of the AC supports in Publication I. Solutions containing 300 mg l^{-1} dye molecules were mixed with each AC sample for 24 h. The solutions were then filtered, and the absorbance values were measured at 664 and 485 nm for MB and OR, respectively, using a Shimadzu UV/Vis 1800 double-beam spectrophotometer. The concentrations of the solutions were obtained from a calibration line.

Point of zero charges (PZC) of the ACs in Publication I were determined as follows [177]. The AC samples were mixed with initial pH solutions (pH 2–12), which were prepared by mixing KOH or HNO_3

solutions with KNO_3 solution. The mixtures were agitated for 72 h at room temperature prior to measuring the pH. The adsorbed amounts of H^+ and OH^- ions were calculated as the difference between the initial and final concentrations.

The compressive strengths (σ) of the prepared ACFs (S1 and S2 with dimensions 1.1 cm × 1.5 cm × 0.4 cm [II]) were determined (Zwick/Roell Z010, 10 kN load cell) prior to and after thermal treatment at 800 °C for 2 h. The loading speed was 0.1 mm s^{-1}, and the measurement was continued until the force decreased by 50% or deformation reached 30%.

3.4 Batch reactor experiments

3.4.1 Hydrotreatment of furfural

Furfural hydrotreatment experiments were conducted in a 50 ml batch reactor (Parker Autoclave Engineers, Figure 4a). The catalyst (0.2 g) was either placed in a Robinson Mahoney type catalyst basket [I] or applied as slurry [II] and reduced at 250 °C and 40 bar H_2 pressure for 2 h. Next, the reactor was cooled to room temperature and the gas was vented. Furfural (1 ml) was mixed with 2-propanol solvent (15 ml) and added to the preheated reactor (210–240 °C) with 40 bar H_2 pressure, followed by continuous stirring at 700–800 rpm. The typical reaction time was 5 h with the catalyst basket, and samples were taken during the experiment after 0, 15, 30, 60, 120, and 300 min using a sampling line [I]. In contrast, the slurry experiments were conducted for 30, 120, and 300 min without any samples taken during the experiments. After the experiments, the reactor was cooled to room temperature using a water bath, after which the gas sample was taken into a previously evacuated gas container. Finally, the liquid product and the spent catalysts were collected.

3.4.2 Hydrotreatment of LA dimers

The HDO of LA dimer model compound, GNL, was performed in a 100 ml batch reactor (Parr, Figure 4b). The experiments were conducted without solvent in slurry with the catalysts. Prior to the experiments, the catalyst (0.6 g) was placed at the bottom of the reactor, dried (N_2 atmosphere at 180 °C for 1 h) and reduced (20 bar H_2 at 290 °C for 1 h). During the reduction, stirring was applied at 200 rpm, after which the gas was vented and the reactor was cooled to room temperature. Next, the reactor was preheated to the desired reaction temperature (220–280 °C) and the feed (23 ml) was added with 60 bar H_2 pressure and 700 rpm stirring. Hydrogen was replenished during the reaction when pressure dropped to 55 bar to maintain an average pressure of 57.5 bar. After the reaction (various reaction times applied), the reactor was cooled to room temperature with a water bath and the gas sample was taken to a previously evacuated gas container. Finally, the reactor was vented, flushed with N_2, and opened to recover the liquid product and spent catalyst.

The HDO of the LA dimer mixture was conducted in a 50 ml batch reactor from Parr using a borosilicate liner (Figure 4c). The experiments were conducted without solvent in slurry with the catalysts. The catalyst (1.0 or 2.0 g) was dried (N_2 atmosphere at 120 °C for 1 h) and reduced (60 bar H_2 at 350 °C for 2 h). During the reduction, stirring at 100 rpm was applied, after which the gas was vented and the reactor was cooled to room temperature and flushed with N_2. Next, the reactor was opened to add the feed (typically around 9.4 g melted at 70 °C) onto the liner, flushed with H_2, and heated to 250 °C. Then, stirring was applied at 400 rpm, and 50 bar H_2 was added to avoid thermal reactions while heating further to the desired reaction temperature. The amount of feed was chosen to have the highest possible volume of H_2 but also to be able to fully stir the liquid. Hydrogen was replenished during the reaction when pressure dropped by 5 bar. After the experiment (typically around 5 h), the reactor was cooled to

room temperature using a water bath, and the gas sample was taken to a previously evacuated gas container. Then, the pressure was released, and the reactor was flushed with N_2 prior to opening and the collection of the liquid product and spent catalyst.

3.4.3 Hydrotreatment of 4-propylphenol

The HDO of 4-propylphenol was performed in slurry in the same reactor used for the GNL experiments (100 ml batch reactor from Parr, Figure 4b). The catalyst (typically around 65 mg, but different amounts were also used to match desired batch residence times) was placed at the bottom of the reactor, dried in N_2 atmosphere at 180 °C for 1 h and reduced in 20 bar H_2 at 353 or 400 °C for 1 h with 200 rpm stirring. After reduction, the reactor was vented and cooled to room temperature. The reactor was preheated to 350 °C prior to adding the feed (580 mg of 4-propylphenol mixed with 27 ml of tetradecane), pressure (20 bar H_2), and stirring (645 rpm). Different reaction times were applied to obtain the desired batch residence times, after which the reactor was cooled to room temperature using a water bath. The gas sample, liquid product, and spent catalyst were collected as described earlier. For reusability tests, the collected spent catalysts were washed with EtOH and dried at 100 °C overnight prior to being used again in the reaction. The experimental procedure for activity tests with the spent catalysts was the same as that described for fresh catalysts.

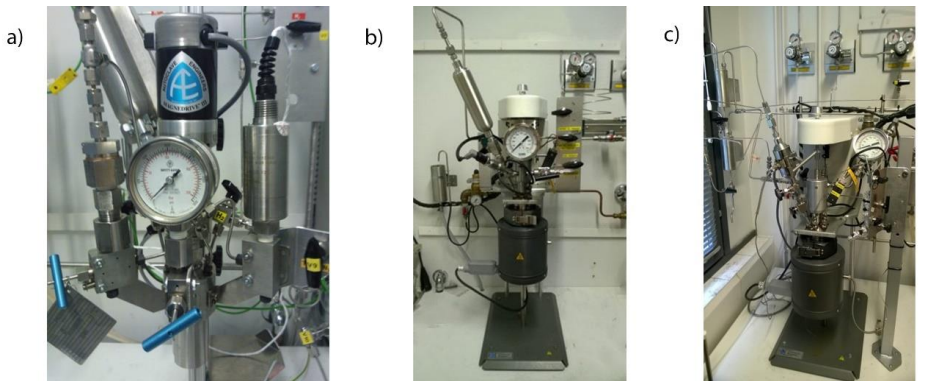

Figure 4. Batch reactors used in this thesis: a) 50 ml batch reactor from Parker Autoclave Engineers (photo by Salla Likander), b) 100 ml batch reactor from Parr (modified; original photo by José Luis González Escobedo), and c) 50 ml batch reactor from Parr (photo by José Luis González Escobedo).

3.5 Analysis of organic phase

3.5.1 Chromatographic methods

The components of the organic liquid products [I–V] were identified using an Agilent gas chromatograph (GC) equipped with MS. The GC–MS (Agilent 7890–5975) was equipped with a Zebron ZB-wax Plus column (60 m × 0.25 mm × 0.25 μm), and the mass spectra were collected with electron impact (EI) ionization of 70 eV and a quadrupole scan range of 30–500 m/z. The used temperature programs are described in Table 4. The National Institute of Standards and Technology (NIST) mass spectral database was used to identify the products. The samples were used as obtained from the reactor, and the detector was turned off during the retention time of the feed to avoid saturation. In Publication IV, GC–MS was also used to estimate the amounts of obtained products, not just for their identification. The products of the HDO of LA dimers (20 wt.%) were diluted with 2-butanol, and 2 wt.% of 2-propanol was added as an internal standard [IV].

Some large peaks (e.g., feed or solvent) were deconvoluted using the NIST automated mass spectral deconvolution and identification system (AMDIS) for diluted samples to reveal any overlapping products. In Publication III, octanoic acid was noticed to overlap with the GNL peak; thus, the amount of octanoic acid was estimated through a calibration with selected ion monitoring (SIM) mode using ions 6.10 and 73.10 *m*/z, which were only found in the mass spectrum of octanoic acid. In Publication V, GC–MS with chemical ionization (CI) at 180 °C (positive polarity, 1.5 ml min^{-1} methane) was also conducted with a Thermo Fisher Trace 1300 ISQ using the same column and method as that for the GC–MS–EI to confirm the identification of product 1-methoxy-4-(1-methylpropyl)-benzene.

In Publication III, the silylation of the product samples was performed to reveal possible non-volatile compounds. Selected samples (20 mg) were mixed with *n*-methyl-*n*-trimethylsilylfluoroacetamide (MSTFA, 1 ml). The solutions were maintained at room temperature overnight prior to analysis using the Thermo Scientific Trace 1300 ISQ GC–MS–EI equipped with an Agilent J&W HP–5 column (60 m × 0.25 mm × 0.25 µm). The split ratios of 1:100 and 1:20 were attempted with a solvent delay.

The liquid samples were quantitatively analyzed using an Agilent or HP 6890 Series GC with a flame ionization detector (FID) and a Zebron ZB-wax Plus column (60 m × 0.25 mm × 0.25 µm) [I–III,V]. The used GC temperature programs are listed in Table 4. Split ratio of 80:1 was used, and internal standards were added for the quantification: 2-butanol [I,II], 2-propanol [III], and 2-isopropylphenol [V]. In Publication III, octanoic acid was observed to overlap with the GNL peak; thus, a GC equipped with Sigma-Aldrich's Supelco SLB111 hyperpolar column (30 m × 0.25 mm × 0.2 µm) was used for the quantification of GNL (without overlaps). However, the column did not separate the hydrocarbons, which were then separated (along with the quantification of other products) by the ZB-wax column described earlier. Most of the product compounds were calibrated; however, not all the product compounds were commercially available. The response factors for components that were not calibrated were estimated according to the effective carbon number method by Scanlon and Willis [178] with the corrections proposed by Jorgensen et al. [179].

High-performance liquid chromatography (HPLC) was applied to detect possible non-volatile condensation products formed during the HDO of GNL as well as to search some compounds that could not be identified with sufficient certainty using the NIST MS library [III]. Moreover, the consumption of LA dimers in the HDO reaction was estimated [IV]. The equipment used was an Agilent 1260 HPLC system coupled to an Agilent 6530 QTOF MS with electrospray ionization (ESI) source and a Luna Omega PS-C18 column (100 × 2.1 mm, 3 µm) [III,IV] or Kinetex Biphenyl column (2.6 µm × 100 mm × 2.1 mm) [III].

The samples from the HDO of GNL [III] were diluted with MilliQ water/acetonitrile (ACN) solution (30/70 wt.%) to a final concentration of approximately 100 ppm. Eluent was 20/80 wt.% MilliQ water/ACN solution with 0.1 wt.% formic acid, and the injection volume was 20 µl. For the total ion current (TIC), the positive mode of electrospray ionization (+ESI) was used in the range of 50–1000 *m*/*z*. Moreover, extract ion chromatograms (EIC) for selected molecular masses were recorded. Agilent MassHunter software with a Find by Formula algorithm was used to obtain the mass spectrum of a compound. The samples from the HDO of LA dimers and the LA dimer feed were diluted with 50/50 wt.% MilliQ water/ACN solution, which also contained 100 ppm of nonanoic acid as a standard. Two solvents were used: 1) MilliQ water with 0.1% formic acid and 2) ACN with 0.1% formic acid. The injection volume was 5 µl, and the mass chromatograms were recorded as TIC with negative mode (–ESI) in the range of 50–1100 *m*/*z*. The individual dimers were detected with EIC for selected molecular masses (214, 216, 202, 200, and 198 amu).

Gel permeation chromatography (GPC) was used to estimate molecular sizes in Publication IV. An Agilent 1100 HPLC system equipped with an ultraviolet (UV) and a refractive index (RI) detectors as

well as a Phenogel 50 Å column at 35 °C (5 µm × 300 × 7.8 mm) was used. THF was used as eluent, and the samples (0.1 g) were dissolved in THF (1 g) prior to analysis. The injection volume was 20 µl, RI detector temperature was 30 °C, and UV detection was performed at a wavelength of 270 nm.

3.5.2 Spectroscopic methods

IR spectroscopy was applied in Publication IV for the qualitative analysis of the LA dimer feed and the liquid products. Perkin Elmer Spectrum Two equipment with an attenuated total reflection (ATR) crystal was used.

^{1}H nuclear magnetic resonance (NMR) spectroscopy (Bruker AVANCE-III 400 MHz spectrometer) was applied in Publication IV to qualitatively analyze the organic products. Samples (1 mg) were dissolved at 22°C in deuterated d_8-THF (1 ml) in 5 mm NMR tubes. In the NMR spectra, a solvent residual signal (3.58 ppm) was used to correct peak positions.

3.5.3 Other methods

The elemental compositions (C, H, and O) of the organic products [III,IV] were analyzed with a Perkin Elmer 2400 Series II elemental analyzer. The obtained compositions were used to draw van Krevelen diagrams, which excluded the presence of dissolved water (from Karl Fisher titration).

In the organic liquid products, dissolved or colloidal water could be present, which was analyzed by a volumetric Karl Fisher titrator (TitroLine 7500 KF, SI Analytics). Prior to analyzing the organic products, the titrant concentration was calibrated with a water standard [III–V].

Table 4. GC and GC–MS temperature programs used to identify and quantify the obtained products.

Sample type	Column	T_{Inlet} /°C	$V_{injection}$ /µl	T_0 /°C	Hold 0 /min	Ramp 1 /°C min^{-1}	T_1 /°C	Hold 1 /min	Ramp 2 / °C min^{-1}	T_2 /°C	Hold 2 /min	Ramp 3 / °C min^{-1}	T_3 /°C	Hold 3 /min	Publi-cation
Liquid organic	Zebron ZB-wax Plus	230	1	40	0	5	100	0	20	230	0				I, II
Liquid organic	Zebron ZB-wax Plus	250	1	60	2	7	160	3	5	200	6				III
Liquid organic	Supelco SLB-IL111	250	1	60	2	7	160	3	5	200	6				III
Liquid organic	Agilent HP-5	280	1	80	1	15	300								III
Liquid organic	Zebron ZB-wax Plus	250	1	60	2	7	160	3	5	200	6	10	250	15	IV
Liquid organic	Zebron ZB-wax Plus	250	1	60	2	7	160	3	5	200	6	10	240	1	V
Liquid aqueous	Zebron ZB-wax Plus	250	0.5	60	2	7	160	3	5	200	6				III
Liquid aqueous	Zebron ZB-wax Plus	250	0.5	60	2	7	160	3	5	200	6	10	250	15	IV
Gaseous	3 columns[a]	200		40	9.5	10	200								I–V

[a] HP-AL/KCL, HP-PLOT/Q, and HP Molesieve.

3.6 Analysis of aqueous phase

In Publications III and IV, the possibly formed aqueous phase was separated from the organic liquid product using a separating funnel and was qualitatively analyzed using the GC–MS equipment described earlier. The temperature programs are presented in Table 4, and the quadrupole scan range was 18–500 m/z. The pH values of the aqueous phases were obtained with a pH paper [IV]. Total water was calculated as the sum of aqueous phase (if any) and the water dissolved in the organic phase.

3.7 Analysis of gas product

In all experiments [I–V], the samples taken from the gaseous phases were analyzed using an Agilent 6890 GC having an FID and a thermal conductivity detector (TCD). The FID was connected to an HP-AL/KCL column (50 m × 0.32 mm × 8 µm) and the TCD to an HP-PLOT/Q (30 m × 0.53 mm × 40 µm) and to an HP Molesieve (30 m × 0.53 mm × 25 µm) columns. The hydrocarbons were analyzed using the FID, and CO, CO_2, H_2, and N_2 were analyzed using the TCD. The GC was calibrated using two calibration gas mixtures from Oy AGA Ab. The GC temperature program is presented in Table 4.

From the gas phase analysis, the molar fractions of the components in the samples were obtained. To determine the molar and mass-based amounts of the gases, ideal gas law was applied with the temperature and absolute pressure in the reactor at the time of sampling.

3.8 Calculations

Furfural conversion was calculated using Equation 4, and product selectivities and yields were calculated using Equations 5 and 6, respectively.

$$X = \frac{C_{\mathrm{F},0} - C_{\mathrm{F,t}}}{C_{\mathrm{F},0}} \tag{4}$$

$$S_{\mathrm{i}} = \frac{C_{\mathrm{i,t}}}{C_{\mathrm{F},0} - C_{\mathrm{F,t}}} \tag{5}$$

$$Y_{\mathrm{i}} = \frac{C_{\mathrm{i,t}}}{C_{\mathrm{F},0}} \tag{6}$$

Here $C_{\mathrm{F},0}$ is the furfural concentration (mmol g^{-1}) in the feed, $C_{\mathrm{F,t}}$ is the furfural concentration at reaction time t, and $C_{\mathrm{i,t}}$ is the concentration of a product i at reaction time t [I,II]. To facilitate comparison among experiments, batch residence time τ_{b} (g_{cat} min g_{feed}^{-1}, Equation 7) was applied in Publications II, IV, and V instead of simple reaction time or contact time, t_{c} (reaction time in terms of metal loading, min wt.%)

$$\tau_{\mathrm{b}} = \frac{m_{\mathrm{cat}} t}{m_{\mathrm{f}}}, \tag{7}$$

where m_{cat} is the mass of the catalyst added to the reactor, m_{f} is the mass of the feed, and t is the reaction time.

GNL conversion was calculated with Equation 8 [III]

$$X = \frac{n_{\mathrm{GNL},0} - n_{\mathrm{GNL,t}}}{n_{\mathrm{GNL},0}}, \tag{8}$$

where $n_{GNL,0}$ is the amount of GNL (mol) in the beginning and $n_{GNL,t}$ is the amount of GNL at reaction time *t*. Products yields (mol.%) were calculated with Equation 9

$$Y_i = \frac{|v_{GNL}|n_i}{v_i \cdot n_{GNL,0}}, \quad (9)$$

where *v* indicates stoichiometric factors ($v_{GNL} = -1$) and *i* indicates an HDO product. The stoichiometric factors for the products were calculated with Equation 10

$$v_i = \frac{x_{GNL}}{x_i}, \quad (10)$$

where *x* is defined by the general formula $C_xH_yO_z$, indicating the number of carbon atoms in the molecule. The product selectivities (wt.%) were calculated with Equation 11. Instead of molar units, the selectivities were calculated as mass-based because some products were not identified and their molar amounts remained unknown. The total amount of products, $\sum_n m_i$, was calculated from the mass balance closure

$$S_i = \frac{m_i}{\sum_n m_i}. \quad (11)$$

Finally, the turnover frequencies (*TOF*) were calculated with Equation 12

$$TOF = \frac{r_{GNL}}{\Gamma}, \quad (12)$$

where r_{GNL} is the initial reaction rate (mol g_{cat}^{-1} s^{-1}) and Γ is the molar amount of surface metal sites per gram of catalyst (mol g_{cat}^{-1}), assumed to be equal to the irreversible chemisorption capacity of the catalyst [III].

The semi-quantitative relative changes of LA dimers were estimated with Equation 13 using HPLC analysis [IV]. Each sample was analyzed thrice, and the final estimation was an average of the three measurements.

$$X = \frac{P_i - P_{i0}}{P_{i0}} \quad (13)$$

Here, P_i is the mass fraction of dimer *i* in the product mixture and P_{i0} is the mass fraction of dimer *i* in the LA dimer feed. The semi-quantitative yields (wt.%) of the volatile components determined via GC–MS analysis were calculated using Equation 14.

$$Y = \frac{m_i}{m_f} \quad (14)$$

Here, m_i is the mass of component *i* in the product mixture and m_f is the mass of feed added in the reactor. Batch residence time was calculated using Equation 7 owing to the different amounts of feed added in the reactor in each experiment [IV].

The molar conversion of 4-propylphenol was calculated similarly to GNL using Equation 8 and the initial *TOF*s using Equation 12. The molar selectivity was determined using Equation 15 [V]

$$S_i = \frac{|v_A|n_i}{v_i(n_{A,0} - n_{A,f})}, \quad (15)$$

where n_i is the molar amount of a product, ν_A is the stoichiometric factor of 4-propylphenol (– 1) and ν_i is the stoichiometric factor of the product calculated by Equation 10. For certain products (benzene, toluene, ethylbenzene, cyclohexane, methylcyclohexane, phenol, and 2-ethylphenol), the stoichiometric factor was assumed to be 1. The molar yields of products were calculated with Equation 16. Mass-based selectivity and yield were calculated analogously without stoichiometric factors. The batch residence time was calculated with Equation 7 [V].

$$Y_i = \frac{|\nu_A| n_i}{\nu_i n_{A,0}} \tag{16}$$

4. Characterization of the prepared catalysts

This chapter describes the characterization of the prepared fresh catalysts on carbon-based supports and the noble metal catalysts on oxide supports. Some textural characteristics of the support materials are discussed. Few catalysts were also characterized after the experiments, and the characterization of spent catalysts is presented.

4.1 Characterization of the carbon-based supports and catalysts

Furfural hydrotreatment has typically been conducted with copper chromite catalyst; however, less harmful metals, such as noble metals and Ni, have recently attracted attention [28] and were also selected for this thesis [I]. In addition, the bimetallic combinations of Cu and Ni have been found to be beneficial particularly in MF production [98,99,180]; thus, Cu/Ni catalysts were prepared and tested in this thesis [II]. ACs were selected as catalyst supports [I,II] owing to their large surface areas, highly porous structures, chemical stability, and surface functionality [46,47]. Commercial AC-based catalysts have also been successfully applied for furfural hydrotreatment in several studies [76,89,90,92,95]. Moreover, activated bio-based carbon foams were tested as catalyst supports in this thesis [II].

The chemical compositions of the thermally treated spruce- and birch-based AC supports (AC-S and AC-B, respectively) and the ACFs (S1 prepared from tannic acid and S2 prepared from pine bark extracts) were determined by elemental analysis. For the ACs, also TC and ash contents were measured. The AC-S support had higher TC content, whereas AC-B had higher ash content, indicating a higher amount of inorganic materials. In general, the ash contents of the prepared supports were low compared with commercial ACs that can have up to 15% of ash [46]. Based on the elemental analysis, AC-B had higher O content then AC-S, whereas the contents of H and N were similar and no S was detected in the supports. Compared with ACs, ACFs had more heteroatoms. Moreover, foam S1 had less C and more heteroatoms than S2 [II].

Figure 5 presents the FESEM images of the porous ACFs: S1 (a) and S2 (b) [II]. One of the main advantages of ACFs over ACs is their tailorable mechanical strength [104]. The compressive strengths of matured carbon foam precursors (no thermal treatment) and thermally treated ACF supports are presented in Table 5. A clear difference in strengths was observed between the matured and thermally treated supports. The strength of S1 almost tripled and that of S2 doubled after thermal treatment [II]. Moreover, both the matured precursor to S2 and thermally treated S2 were stronger than that of S1. S2 had higher compressive strength than S1 owing to the more complex composition of the raw material. The exact composition of the pine bark extract was unknown, but S2 certainly had more cross-linking molecules, such as lignin and sugars, than S1 (made from tannic acid), thus making S2 more rigid during the polymerization reaction. The structures of the supports are presented in Figure 5. No clear visual difference was observed between the mechanical strengths of the two ACF supports after the furfural

hydrotreatment experiments. However, the ACF-based catalysts, in general, had significantly less catalyst dust after the experiments compared with AC-based catalysts (by visual observation), which qualitatively confirmed the higher mechanical strength of the ACF-based catalysts.

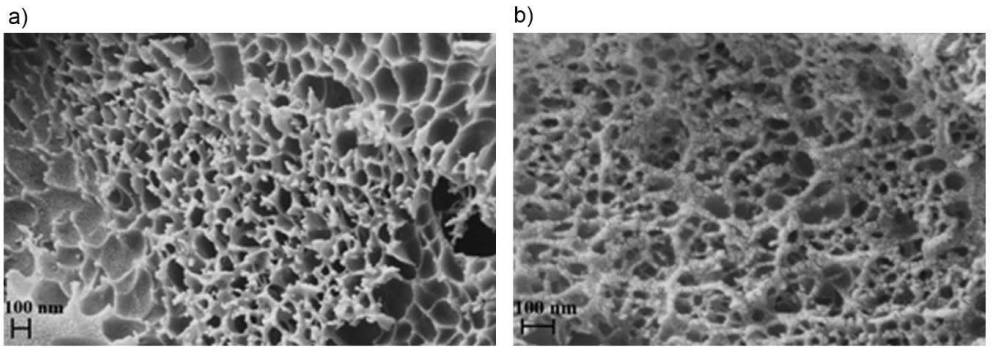

Figure 5. FESEM images of the ACF supports: a) S1 and b) S2. Reprinted from Publication II with permission from Elsevier B.V., copyright (2020).

Table 5. Compressive strengths of matured and thermally treated ACFs (S1 and S2). Reprinted from Publication II with permission from Elsevier B.V., copyright (2020).

	Matured		Thermally treated	
	Precursor to S1	Precursor to S2	Support S1	Support S2
Average compression strength /MPa	0.040	1.15	0.142	2.29

Metal loadings and levels of impurities were determined by ICP–OES. Both AC-S and AC-B supports prepared in Publication I contained K, Ca, and Mg as impurities, but AC-B also contained Na. In general, AC-B had more impurities than AC-S [I]. The metal loadings of Pt, Ru, and Ni were close to the nominal values (Table 6); however, the Ni and Pt loadings on AC-S were slightly lower than expected. In the case of Cu/Ni catalysts, the metal loadings were close to the nominal values except for the catalysts on HNO_3-washed supports, for which both Cu and Ni contents were higher than expected [II]. In addition to Cu and Ni, Zn and S contents were measured, as these impurities might have accumulated from the pretreatment processes. In most cases, Zn content was low and randomly divided among the samples, indicating contamination in the reactors used for thermal treatment rather than accumulating from the $ZnCl_2$ treatment (chemical activation for S2) [II]. The S content was below the detection limit of the analysis (<2 wt.%) in most of the samples, except for the S2_A2_Cu/Ni catalyst (treated with sulfuric acid) that had 2.2 wt.% S [II].

Physisorption analysis of the AC-S, S3 (spruce-based AC) and AC-B supports revealed high BET surface areas (between 900 and 1000 $m^2\ g^{-1}$), which were comparable with the BET surface areas of commercial ACs used in this thesis (Norit_S and Norit_A, Table 6) [I,II]. Because the catalytic reactions take place on the material's surface, high surface areas are preferred. Unlike the highly microporous commercial AC supports, the wood-based ACs had quite even distribution between micropores and mesopores. After Pt, Ru, or Ni impregnation, the surface areas decreased by 15%–31%. The BET surface areas for the ACF supports were 600 $m^2\ g^{-1}$ for the microporous S1 and as high as 1400 $m^2\ g^{-1}$ for the S2

support, which had both micropores and mesopores [II]. The acid treatments mostly decreased the surface areas and pore volumes of the ACF supports, and after Cu/Ni impregnation, the surface areas typically decreased or remained similar compared with the parent materials.

H_2 or CO chemisorptions were conducted for the thermally treated, reduced AC-based catalysts [I]. Higher metal dispersions were obtained on the noble metal catalysts compared with the Ni catalysts. The best dispersion (37%) was obtained on 3 wt.% Pt/AC-S, whereas the highest dispersion among the Ru catalysts was 26% (3 wt.% Ru/AC-B) [I]. These were comparable to commercial 1 wt.% Pt/AC catalyst (Degussa type F103R), which had 28% Pt dispersion. The calculated average particle sizes (from the chemisorption measurements) were high (≥8.4 nm) for the Ni catalysts, whereas the noble metal catalysts had average particle sizes of around 3–4 nm [I]. Small metal particles and high dispersion are usually preferred to maximize the available metal surface area for a chemical reaction.

Table 6. Textural properties of prepared, thermally treated carbon-based catalysts and supports [I,II] and the spent catalysts after experiments, H_2O wash and drying (n.a. = not applicable, n.d. = not determined) [I].

Catalyst	Metal loading /wt.%				S_{BET} /m^2 g^{-1}	DFT pore volume /cm^3 g^{-1}	DFT average pore diameter /nm	DFT micropores	DFT mesopores	Metal SA /m^2 g^{-1}	Dispersion /%	Average particle size /nm
	Pt	Ru	Ni	Cu								
AC-S	n.a.	n.a.	n.a.	n.a.	1010	0.62	2.8	45%	55%	n.a.	n.a.	n.a.
AC-B	n.a.	n.a.	n.a.	n.a.	1050	0.64	2.9	45%	55%	n.a.	n.a.	n.a.
1.5Pt/AC-S[a]	1.2	n.a.	n.a.	n.a.	850	0.46	2.5	54%	46%	1.1	33	3.1
3Pt/AC-S[a]	2.3	n.a.	n.a.	n.a.	840	0.44	2.6	55%	43%	2.4	37	2.7
3Pt/AC-B[a]	3.2	n.a.	n.a.	n.a.	780	0.47	2.8	47%	53%	1.6	19	4.8
1.5Ru/AC-B[b]	n.a.	1.7	n.a.	n.a.	870	0.51	2.8	47%	53%	1.8	20	4.6
3Ru/AC-S[b]	n.a.	2.8	n.a.	n.a.	770	0.40	2.4	58%	43%	3.3	22	4.1
3Ru/AC-B[b]	n.a.	2.9	n.a.	n.a.	880	0.53	2.8	47%	53%	4.3	26	3.4
3Ni/AC-S[c]	n.a.	n.a.	2.0	n.a.	910	0.55	2.8	47%	53%	1.6	12	8.4
3Ni/AC-B[c]	n.a.	n.a.	2.5	n.a.	990	0.58	2.7	47%	52%	1.2	7.2	14
10Ni/AC-S[c]	n.a.	n.a.	8.9	n.a.	690	0.34	2.3	62%	38%	3.0	7.0	15
Spent 3Pt/AC-S	2.1	n.a.	n.a.	n.a.	500	0.37	3.3	36%	64%	n.d.	n.d.	n.d.
Spent 3Ru/AC-B	n.a.	0.84	n.a.	n.a.	270	0.22	3.7	27%	73%	n.d.	n.d.	n.d.
Spent 3Ni/AC-S	n.a.	n.a.	1.7	n.a.	110	0.14	5.2	7%	86%	n.d.	n.d.	n.d.
S1	n.a.	n.a.	n.a.	n.a.	560	0.20	<1.5	96%	4%	n.a.	n.a.	n.a.
S2	n.a.	n.a.	n.a.	n.a.	1360	0.76	2.2	45%	55%	n.a.	n.a.	n.a.
S3	n.a.	n.a.	n.a.	n.a.	890	0.51	2.0	50%	50%	n.a.	n.a.	n.a.
Norit_S	n.a.	n.a.	n.a.	n.a.	960	0.34	1.5	94%	6%	n.a.	n.a.	n.a.
Norit_A	n.a.	n.a.	n.a.	n.a.	1380	0.51	1.6	89%	11%	n.a.	n.a.	n.a.
S1_A1	n.a.	n.a.	n.a.	n.a.	330	0.12	<1.5	93%	4%	n.a.	n.a.	n.a.
S1_A2	n.a.	n.a.	n.a.	n.a.	380	0.13	<1.5	96%	45%	n.a.	n.a.	n.a.
S2_A1	n.a.	n.a.	n.a.	n.a.	910	0.44	1.8	57%	43%	n.a.	n.a.	n.a.
S2_A2	n.a.	n.a.	n.a.	n.a.	1400	0.78	2.2	45%	55%	n.a.	n.a.	n.a.
S1_A1_Cu/Ni	n.a.	n.a.	7.2	7.0	550	0.19	<1.5	95%	5%	n.d.	n.d.	n.d.
S1_A2_Cu/Ni	n.a.	n.a.	5.1	5.0	470	0.17	<1.5	95%	5%	n.d.	n.d.	n.d.
S2_A1_Cu/Ni	n.a.	n.a.	6.5	6.6	720	0.31	1.9	69%	31%	n.d.	n.d.	n.d.
S2_A2_Cu/Ni	n.a.	n.a.	5.6	5.7	1150	0.61	2.1	50%	50%	n.d.	n.d.	n.d.
S3_Cu/Ni	n.a.	n.a.	4.3	4.3	680	0.39	2.0	49%	51%	n.d.	n.d.	n.d.
Norit_S_Cu/Ni	n.a.	n.a.	4.0	3.8	760	0.27	1.5	93%	7%	n.d.	n.d.	n.d.
Norit_A_Cu/Ni	n.a.	n.a.	4.3	4.7	1150	0.42	1.5	90%	10%	n.d.	n.d.	n.d.

[a] Reduction at 250 °C for 2 h and CO chemisorption at 35 °C. [b] Reduction at 350 °C for 2 h and H_2 chemisorption at 75 °C. [c] Reduction at 350 °C for 2 h and H_2 chemisorption at 35 °C [I].

The morphologies of the thermally treated, unreduced catalysts are presented in the STEM images (Figure 6). The size of Pt particles on AC supports (Figure 6a–c) was 5–10 nm in the 3 wt.% catalysts and slightly larger in the 1.5 wt.% Pt catalyst. Ru particles were observed to be smaller than 5 nm in size and more evenly distributed than Pt particles (Figure 6d–f). In the Ni catalysts, the Ni particle size was observed to be around 10 nm (Figure 6g–i), but larger NiCa clusters (≥20 nm) were noticed on AC-B (Figure 6h) [I]. Compared with the particle sizes calculated from the chemisorption measurements, the most variation was observed in the Pt catalysts, which according to chemisorption measurements, seemed to have better dispersion and smaller particle sizes than visually observed from the STEM images. In all the ACF-supported Cu/Ni catalysts (Figure 6j–m), metal particles (ca. 10–40 nm) were quite homogeneously distributed; however, some larger Cu particles were detected (up to 250 nm). Both Ni

and Cu particles seemed to be smaller on S2 than on S1. Moreover, washing with H_2SO_4 resulted in larger particles than the washing with HNO_3. The higher O content of the HNO_3-washed supports (based on XPS analysis) might facilitate better metal dispersion and thus smaller particle size [181]. In general, similar Cu/Ni metal particle sizes were observed with the reference catalysts [II].

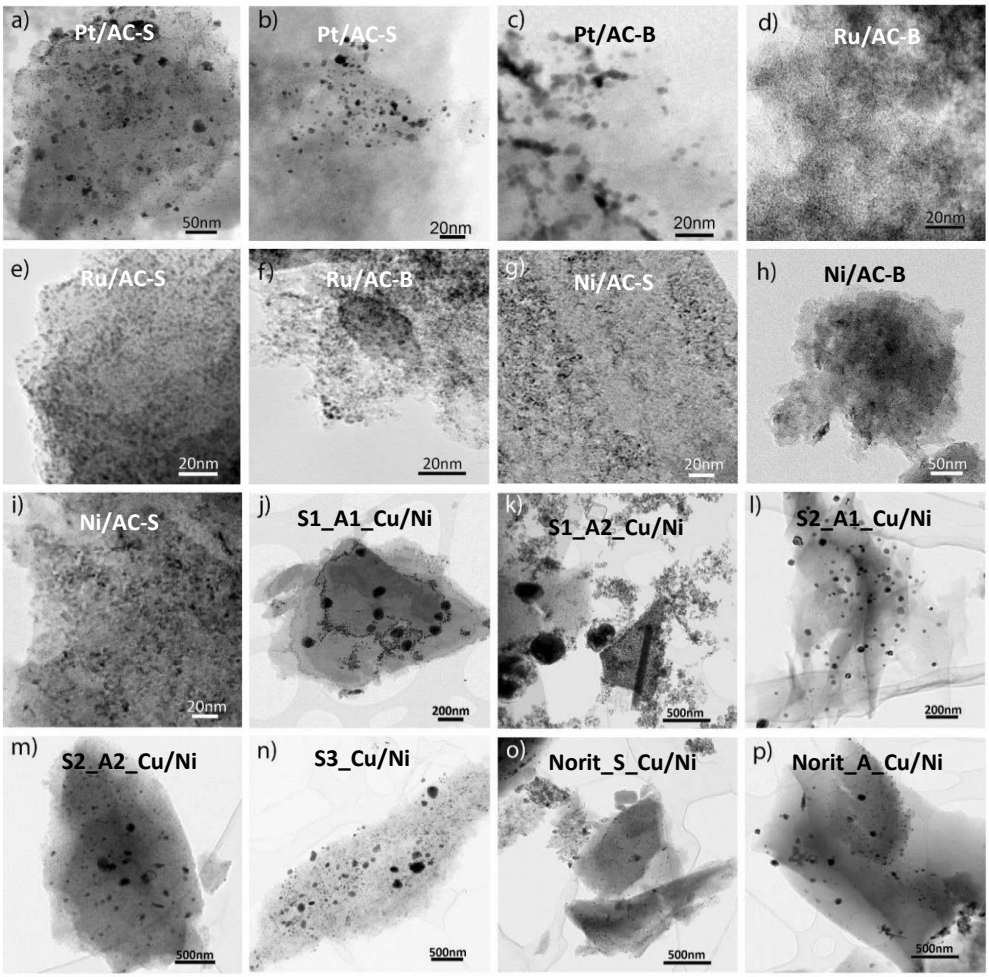

Figure 6. Bright-field STEM images of fresh, thermally treated Pt, Ru, and Ni catalysts on wood-based AC supports: a) 1.5Pt/AC-S, b) 3Pt/AC-S, c) 3Pt/AC-B, d) 1.5Ru/AC-B, e) 3Ru/AC-S, f) 3Ru/AC-B, g) 3Ni/AC-S, h) 3Ni/AC-B, and i) 10Ni/AC-S [I]. Bright-field STEM images of fresh, thermally treated Cu/Ni catalysts on carbon-based supports: j) S1_A1_Cu/Ni, k) S1_A2_Cu/Ni, l) S2_A1_Cu/Ni, m) S2_A2_Cu/Ni, n) S3_Cu/Ni, o) Norit_S_Cu/Ni, and p) Norit_A_Cu/Ni. Modified from Publications I and II.

XPS was used to characterize the surface functionalities of the AC and ACF supports and the oxidation states of the active metals (after thermal treatment, unreduced) [I,II]. The carbon-containing groups were deconvoluted into five peaks according to their binding energy (BE): sp^3 C–C (284.8 eV), sp^2 C–C (285 eV), carbon species in alcohol or ether groups (286.3–287.0 eV), carbon in carbonyl groups (287.5–288.1 eV), carbon in carboxyl or ester groups (289.3–290.0 eV), and shake-up satellites from π–π* transitions in aromatic rings (291.2–292.1 eV). Based on the C1s scans, AC-S, AC-B, S1, and S2 mainly comprised C–C bonds, to some extent oxygen-containing functional groups, and small amounts of aromatic carbons (from π–π* transitions) [I,II]. Commercial supports and S3 seemed to be similar to the support

S1. Both acid wash treatments (HNO_3 and H_2SO_4) increased the amount of oxygen functionalities on the surfaces compared with unwashed S1 and S2 [II]. Moreover, the HNO_3 treatment increased the oxygen functionalities on the surfaces of both ACFs more than the H_2SO_4 treatment; it also increased the amount of nitrogen-containing surface groups, especially nitrates.

In the prepared catalysts (after thermal treatment, unreduced), Pt was present in zero-valent state and Ru was present in both metallic and oxidized states (RuO_2) [I]. On the AC and ACF supports, Ni was present as different oxides (NiO, $Ni(OH)_2$, or NiOOH), whereas metallic Ni was not detected. This was in line with the results of XRD analysis, which confirmed the presence of metallic Pt and Ru but not Ni in the unreduced AC-supported catalysts [I]. Unlike XPS analysis, XRD also revealed some Pt oxides (Pt_3O_4) present in the catalysts. On the ACF supports, both metallic and oxidized Cu (CuO and Cu_2O) were detected [II]. The presence of both Cu and Cu^+ are often preferred in the catalyst as it has been proposed that metallic Cu can activate H_2 and the Cu^+ species act as electrophilic sites polarizing the C=O bond [182].

TPR and ammonia TPD measurements were conducted for the AC-supported catalysts [I]. No acidity was detected on the supports or on the prepared catalysts based on ammonia TPD measurements [I]. Figure 7 presents the TPR profiles of the 3 wt.% metal catalysts on AC-S (a) and AC-B (b). Hydrogen consumption was detected at around 600 °C for both supports, but after the addition of Pt, a broad peak from 450 to 650 °C occurred instead owing to hydrogen spillover and the reduction of the support. No reduction peaks at lower temperatures attributed to Pt reduction were detected. Ru catalysts had small peaks around 90 °C owing to the reduction of Ru oxides, and the reduction of the functional groups of the AC as well as hydrogen spillover occurred around 475 °C [I]. With Ni catalysts, the shoulders at low temperature (around 240 and 350 °C) were attributable to the reduction of NiO species with little interaction with the support, whereas the peak around 475 °C was related to the reduction of NiO with strong interaction with the support [I].

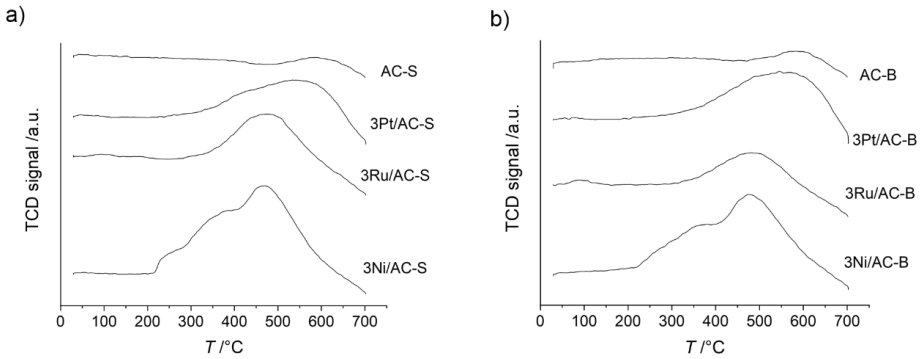

Figure 7. TPR profiles of a) AC-S and b) AC-B and the corresponding 3 wt.% Pt, Ru, and Ni catalysts (a.u. = arbitrary unit). Reprinted from Publication I with permission from Wiley-VCH Verlag GmbH & Co. KGaA, copyright (2018).

The selected spent catalysts (3 wt.% Pt/AC-S, 3 wt.% Ru/AC-B and 3 wt.% Ni/AC-S) were characterized after being used in the furfural hydrotreatment experiments at 230 °C [I]. The metal contents of the catalysts decreased after the experiments (Table 6); in particular, the metal content of the Ru catalyst decreased by around 70% owing to leaching. In contrast, the metal contents of the other catalysts were close to the fresh catalysts (decrease of 0.2–0.3 wt.% units). The most severe deactivation in terms of decreased pore volume after the experiments was observed for the Ni catalyst, which lost 95% of its micropores and 58% of its mesopores. For the Ru and Pt catalysts, the total pore volumes decreased by

59% and 25%, respectively. The BET surface areas of the Pt, Ru, and Ni catalysts also decreased by 40%, 69%, and 88%, respectively. The deactivation observed from the physisorption measurements could be attributable to the partial collapse of the bulk material and coke formation inside the pores [I]. Fast deactivation is a general concern with carbon-supported catalysts, and carbon methanation or oxidation to CO have been reported to be responsible for the sintering of the metal particles [183–185]. The metal particle sizes estimated from the STEM images of the spent catalysts were close to those of the fresh catalysts, except for the spent Ni catalyst, which also had larger aggregates (>20 nm). Overall, the spent catalyst characterization revealed that the Pt catalyst experienced the least deactivation.

The prepared carbon-based catalysts were characterized using multiple methods. In conclusion, the ACFs were thought to have advantages over ACs in terms of the mechanical strength, which was supported by visual evidence from the catalytic experiments. A difference between the heteroatom content of the ACF- and AC-supported catalysts was also observed; the ACFs had higher heteroatom content. However, no differences in the Cu/Ni particle sizes were observed between the ACF-supported catalysts and reference catalysts. Compared with noble metals, the particles of Cu and Ni were larger. In general, the XPS and XRD results revealed oxidized Ni species in the unreduced catalysts. Moreover, the TPR measurements showed that the reduction of Ni required higher temperatures than those used in *in situ* reduction before the experiments (250 °C) or used prior to the chemisorption measurements (350 °C). In summary, the Ni catalysts were partially oxidized, and the large particle sizes calculated from chemisorption measurements could also indicate that the metal sites were not available. Furthermore, the full reduction of the carbon supports needed higher temperatures than those used. Thus, some of the detected oxygen-containing surface groups likely existed during the reaction.

4.2 Characterization of the noble metal catalysts on oxide supports

In addition to Pt and Ru catalysts, Rh and Pd catalysts were studied in HDO reactions in this thesis owing to their known ability to remove oxygen [30,186]. A major difference between noble metal catalysts and conventional HDO catalysts (sulfided NiMo and CoMo) is that for the noble metals, no sulfiding agent addition to the feed is needed [27]. Monoclinic ZrO_2 was selected as a catalyst support to prevent excess coke formation (attributed to more acidic supports) and to obtain high water tolerance and thermal stability [30,128]. In Publication V, Nb_2O_5 and TiO_2 were studied as reducible metal oxide supports, which have been reported to enhance the deoxygenation of phenols [136,137,154]. ZrO_2 was considered to be irreducible in the used conditions.

The textural properties of the noble metal catalysts on metal oxide supports were determined using several methods described in Section 3.3 [III–V]. XRD measurements on unreduced Nb_2O_5, TiO_2, and ZrO_2 supports (after thermal treatment) showed the presence of pseudo-hexagonal TT, anatase, and monoclinic phases, respectively. The metal loadings of the prepared catalysts (close to 3 wt.%) were determined using XRF and are presented in Table 7, along with the measured BET surface areas, pore volumes, and mean pore diameters (from physisorption) as well as the metal dispersion and average particle sizes (from chemisorption and STEM). The ZrO_2 support presented the lowest surface area and the highest mean pore diameter among the supports, whereas the TiO_2 support had the highest surface area. No clear trends were observed after metal impregnation, and both higher and lower surface areas and pore volumes were obtained for the catalysts compared with their supports.

Considerable variation among the catalysts was observed in terms of metal dispersion [III–V]; calculated dispersion for the prepared catalysts was in the range of 11%–87%. The lowest dispersion was calculated for 2.7 wt.% Ru/ZrO_2 catalyst, which was prepared from the $RuCl_3$ precursor and likely remained

partly chlorinated after calcination and reduction [III]. The chlorides might have occluded chemisorption sites, thus resulting in low dispersion. The other Ru catalyst (3.6 wt.% Ru/ZrO_2), prepared from the Ru nitrosylnitrate precursor, presented significantly higher dispersion and lower average particle size in the same measurement conditions. The highest dispersion (87%) was obtained for 2.5 wt.% Rh/ZrO_2 catalyst, whereas the different Pt catalysts had dispersions between 37% and 69%.

The average metal particle sizes of the catalysts were obtained via chemisorption measurements and STEM images [III–V]. In most cases, the particle sizes observed in the STEM images were similar to or lower than those calculated from chemisorption. However, for 2.7 wt.% Ru/ZrO_2 catalyst ($RuCl_3$ precursor), the average particle size calculated from chemisorption (8.0 nm) was significantly higher than that from the STEM images (1.5 nm) [III], and the STEM particle size was thought to be more reliable owing to the presence of chlorides. No peaks related to noble metals were observed in the XRD analysis, and the diffractograms of the catalysts were similar to those of the corresponding supports. Thus, the metal particles were likely small in size (XRD detection limit: ~3 nm) [187], which supports the particle sizes obtained via STEM rather than those calculated from chemisorption. The STEM images of the prepared noble metal catalysts are presented in Figure 8.

Table 7. Textural properties of prepared, thermally treated noble metal catalysts on metal oxide supports [III–V] and spent catalysts after experiments, ethanol wash, and drying (n.a. = not applicable, n.d. = not determined) [III,V].

Catalyst	Determined metal loading /wt.%				S_{BET} /m^2 g^{-1}	BJH pore volume /cm^3 g^{-1}	BJH mean pore diameter /nm	Metal dispersion	Chemisorption average particle size /nm	STEM average particle size /nm
	Ru	Rh	Pd	Pt						
ZrO_2[a]	n.a.	n.a.	n.a.	n.a.	64–67	0.18–0.27	11–13	n.a.	n.a.	n.a.
TiO_2	n.a.	n.a.	n.a.	n.a.	125	0.25	8.6	n.a.	n.a.	n.a.
Nb_2O_5	n.a.	n.a.	n.a.	n.a.	74	0.12	6.9	n.a.	n.a.	n.a.
3.6Ru/ZrO_2[b]	3.6	n.a.	n.a.	n.a.	70	0.21	11	25%	3.7	n.d.
2.7Ru/ZrO_2[b]	2.7	n.a.	n.a.	n.a.	80	0.32	10	11%	8.0	1.5
2.5Rh/ZrO_2[c]	n.a.	2.5	n.a.	n.a.	58	0.23	11	87%	1.2	2.0
3.0Pd/ZrO_2[c]	n.a.	n.a.	3.0	n.a.	64	0.26	11	21%	5.3	2.9
2.7Pt/ZrO_2[c]	n.a.	n.a.	n.a.	2.7	65	0.22	13	37%	2.7	1.9
2.7Pt/ZrO_2[c]	n.a.	n.a.	n.a.	2.7	80	0.19	12	57%	1.8	1.9
3.2Pt/TiO_2[c]	n.a.	n.a.	n.a.	3.2	119	0.22	8.5	69%	1.5	1.3
3.1Pt/Nb_2O_5[c]	n.a.	n.a.	n.a.	3.1	85	0.10	5.3	41%	2.5	1.4
Spent[d] Ru/ZrO_2	n.d.	n.d.	n.d.	n.d.	70	0.25	8	19%	4.8	1.8
Spent[d] Rh/ZrO_2	n.d.	n.d.	n.d.	n.d.	54	0.22	9	15%	7.4	4.8
Spent[d] Pd/ZrO_2	n.d.	n.d.	n.d.	n.d.	60	0.25	10	7.0%	16	5.4
Spent[d] Pt/ZrO_2	n.d.	n.d.	n.d.	n.d.	71	0.28	10	23%	4.5	3.8
Spent[e] Pt/ZrO_2	n.a.	n.a.	n.a.	1.8	68	0.19	11	23%	4.6	2.9
Spent[e] Pt/TiO_2	n.a.	n.a.	n.a.	2.5	69	0.16	12	48%	2.1	2.1
Spent[e] Pt/Nb_2O_5	n.a.	n.a.	n.a.	2.2	61	0.10	6.5	13%	7.8	2.7

[a] Several measurements, taken from Publications III–V. [b] Reduction at 290 °C for 3 h and H_2 chemisorption at 25, 35 or 75 °C. [c] Reduction at 290 °C for 3 h and CO chemisorption at 25 or 35 °C. [d] After experiment at 280 °C with 30%–40% GNL conversion [III]. [e] After experiments with τ_b of 4–5 g_{cat} min $g_{reactant}^{-1}$ [V].

TPR profiles of the catalysts were studied in Publications IV and V. In the case of the HDO of LA dimers, the TPR profiles of the 3.6 wt.% Ru/ZrO_2 catalyst were obtained to explore the effect of exposing the catalyst to atmosphere after reduction to load the feed (see Section 3.3.4) [IV]. The TPR profiles of fresh and reduced Ru/ZrO_2 (a) with and (b) without exposure to air are presented and in Figure 9. The TPR profile of fresh Ru/ZrO_2 showed a large peak (from 100 to 170 °C) attributable to the reduction of RuO_x species. In the TPR profiles of reduced Ru/ZrO_2, almost no difference was observed between the catalyst exposed to air and the catalyst not exposed to air; thus, the *in situ* reduction protocol of the Ru catalyst in the LA dimer experiments was sufficient, despite the opening of the reactor after reduction (to add the feed) [IV].

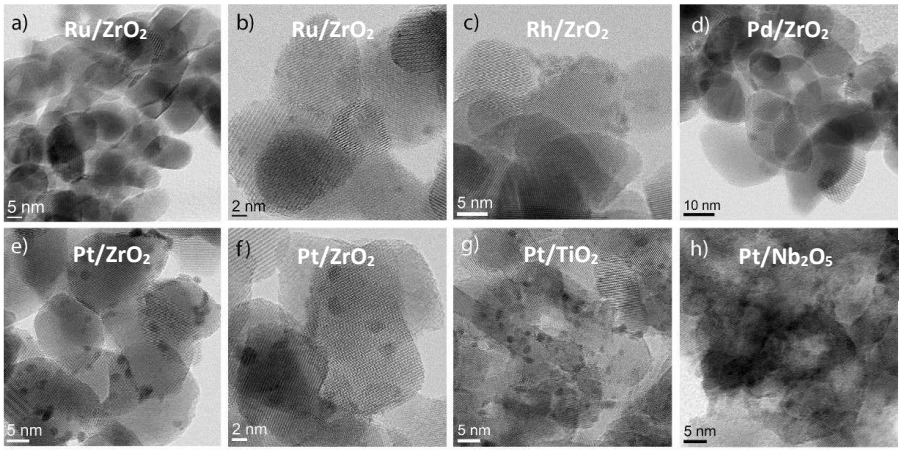

Figure 8. Bright-field STEM images of fresh, thermally treated noble metal catalysts: a) 3.6Ru/ZrO_2, b) 2.7Ru/ZrO_2, c) 2.5Rh/ZrO_2, d) 3.0Pd/ZrO_2, e) 2.7Pt/ZrO_2 [III], f) 2.7Pt/ZrO_2 [V], g) 3.2Pt/TiO_2, and h) 3.1Pt/Nb_2O_5. Note the differences in scales. Images a–d modified from Publications III–V and images f–h previously unpublished.

The TPR measurements of the catalysts used in the HDO of the 4-propylphenol were performed to investigate the reduction tendency of the supports (ZrO_2, TiO_2, and Nb_2O_5) [V]. Small peaks below 150 °C were observed with all the catalysts (Figure 9c–e), attributable to the reduction of PtO_x species. The XPS analysis suggested the presence of Pt^{2+} in $Pt(OH)_2$ and Pt^{4+} in PtO_2 on zirconia (70%/30%) and on niobia (50%/50 %) surfaces, whereas Pt^0 and Pt^{2+} in $Pt(OH)_2$ existed on titania (50% / 50%) [V]. As expected, no reduction peaks associated with ZrO_2 reduction were observed. In the case of reducible supports, the reduction of the supports was visible at 400–550 °C (TiO_2) and from 400 °C onward (Nb_2O_5). The reduction shifted to lower temperatures after the addition of Pt. Thus, 350 (actual 353 °C) and 400 °C were selected as catalyst reduction temperatures in Publication V to obtain partially reduced supports.

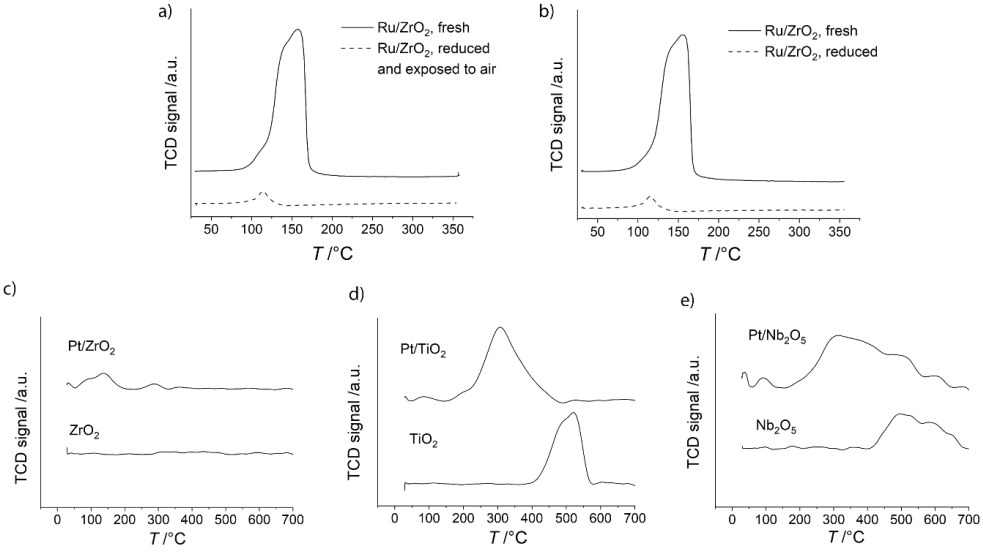

Figure 9. TPR profiles (measured with Altamira AMI–200R) of fresh, thermally treated 3.6 wt.% Ru/ZrO_2 catalyst before and after reduction at 350 °C and the TPR profiles of fresh, thermally treated Pt catalysts and supports (a.u. = arbitrary unit): a) 3.6Ru/ZrO_2 catalyst exposed to air for 20 min after reduction, b) 3.6Ru/ZrO_2 catalyst not exposed to air after reduction, c) 2.7Pt/ZrO_2, d) 3.2Pt/TiO_2, and e) 3.1Pt/Nb_2O_5. Modified from Publications IV and V.

Spent catalysts were tested the second time in the reaction in Publication V; however, some characterization was performed for all the spent catalysts. For example, TGA was applied to determine the amount of solid deposits accumulated on the catalysts during the HDO experiments [III–V]. In the case of the catalysts used in the HDO of GNL (Ru, Rh, Pd, and Pt on ZrO_2), around 2% of the mass of the dry catalysts was combustible below 900 °C [III]. For the 3.6 wt.% Ru/ZrO_2 catalyst used in the LA dimer experiments, approximately 4%–5% of the mass of the dry catalysts was combustible [IV]. For the catalysts used in the HDO of 4-propylphenol, the majority of the combustion occurred below 450 °C, and around 2% of the dry mass was combustible in the case of 2.7 wt.% Pt/ZrO_2 and 3.1 wt.% Pt/Nb_2O_5 and almost 3% in the case of 3.2 wt.% Pt/TiO_2 [V].

In Publications III and V, the spent catalysts were also characterized based on physisorption, chemisorption, and STEM measurements (Table 7). The surface areas of the spent catalysts significantly decreased compared with the fresh, thermally treated catalysts. In Publication III, the average decrease of surface area was around 10%. The pore volumes decreased by 4%–40% and metal dispersion by 40%–80%. The only exception was the spent Ru/ZrO_2 catalyst, which showed a 72% increase in metal dispersion [III]. This increase may be attributable to the removal of chloride during the reaction. The decrease in the surface areas of the spent catalysts after the HDO of 4-propylphenol [V] was severe (15%–50%). Spent TiO_2 catalyst had severe loss of pores, which could be attributable to carbonaceous deposits and the collapse of the pore structure [V]. The decrease in metal dispersion likely occurred owing to metal agglomeration during the experiments, which was also evidenced by the increase in the metal particle sizes measured from the STEM images (Table 7). In addition, the deactivation of the metal sites owing to the covering of solid deposits, the support (owing to SMSI), or impurities might render them unavailable for chemisorption, leading to the calculation of low dispersion and large particle sizes.

In conclusion, major differences among the noble metal catalysts were noticed in terms of the surface area of their supports, metal dispersion, and reduction tendencies of the supports. The highest Pt dispersion was obtained on TiO_2 support, which provided the highest surface area among the supports. In general, metal dispersions were high for all catalysts except Ru/ZrO_2 owing to the presence of chlorides. As expected, ZrO_2 support was irreducible in the used conditions. However, the reduction of Nb_2O_5 and TiO_2 was observed in the TPR measurements; thus, the effect of reduction temperature on the performance of the reducible catalysts was studied in the HDO of 4-propylphenol.

5. Hydrotreatment of furfural

Furfural hydrotreatment is a complex reaction where various products can be targeted (Scheme 2). In this thesis, the target compound was MF, which can be used as a biofuel component. First, the production of MF was studied with Ni and noble metal (Pt and Ru) catalysts on wood-based AC supports prepared form spruce and birch. Moreover, the effects of reaction temperature and metal loading on MF production were studied. Second, bimetallic Cu/Ni catalysts on bio-based ACFs were studied in the same reaction. Two different ACFs and their post-treatments were used to maximize the MF yield.

5.1 2-Methylfuran production using catalysts supported on wood-based activated carbons

The prepared, nominally 3 wt.%, Ni, Pt, and Ru catalysts on birch- (AC-B) and spruce-based (AC-S) ACs were studied at 230 °C and 40 bar H_2 during 300 min reaction time by taking samples during the reaction [I]. All the catalysts were active, as over 97% furfural conversions were obtained. The initial reaction rates (furfural consumption during the first 15 min of reaction time per metal loading) were always higher for catalysts on AC-S.

The achieved MF yields as a function of contact time (min wt.%) are presented in Figure 10. With Ni and Pt, the AC-S supported catalysts produced higher MF yields, whereas with Ru, the AC-B supported catalyst reached higher MF yield [I]. In addition to MF, FA, THFA, MTHF, furan, PN and furanmethanol acetate (FMA) were produced. Some trends among the catalyst were noticed: a ring-opening reaction to PN was more abundant on the AC-S-based catalysts, the decarboxylation to furan was slightly higher with the noble metal catalysts (especially those supported on AC-B) than with the Ni catalysts, and the formation of THFA was higher with the Ni catalysts than with the noble metal catalysts [I]. The detailed product distributions of all the experiments conducted at 230 °C are presented in Table 8.

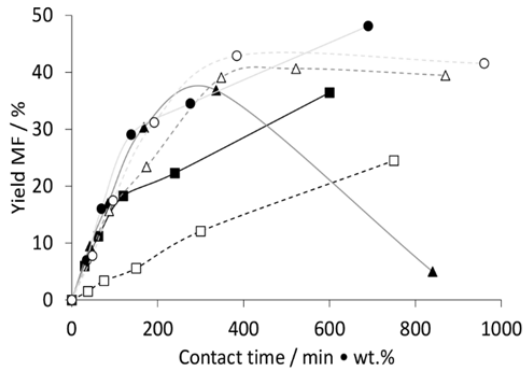

Figure 10. 2-Methylfuran yield as a function of contact time with various catalysts at 230 °C and 40 bar H_2: ● = 3Pt/AC-S, ○ = 3Pt/AC-B, ▲ = 3Ru/AC-S, Δ = 3Ru/AC-B, ■ = 3Ni/AC-S, and □ = 3Ni/AC-B. Reprinted from Publication I with permission from Wiley-VCH Verlag GmbH & Co. KGaA, copyright (2018).

Table 8. Furfural conversion at the highest observed MF yield, corresponding reaction time, and product yields at 230 °C and 40 bar H_2. Modified from Publication I.

Catalyst	X /%	t /min	τ /g_{cat} min $g_{reactant}^{-1}$	Y_{MF} /%	Y_{FA} /%	Y_{THFA} /%	Y_{MTHF} /%	Y_{Furan} /%	Y_{FMA} /%	Y_{PN} /%
1.5Pt/AC-S	99	300	62	47	5.7	0.9	0.0	2.1	0.4	0.3
3Pt/AC-S	100	300	62	48	3.8	1.1	0.0	2.5	0.0	0.5
3Pt/AC-B	98	120	24	43	6.3	0.8	0.0	5.4	1.7	0.1
1.5Ru/AC-B	99	300	62	35	17	1.8	0.0	3.5	2.0	0.0
3Ru/AC-S	99	120	24	37	9.3	2.7	0.9	2.7	0.7	0.8
3Ru/AC-B	100	180	37	41	2.4	1.5	0.0	2.8	0.7	0.2
3Ni/AC-S	97	300	59	36	2.5	3.7	0.0	2.2	0.8	0.1
3Ni/AC-B	99	300	59	25	22	5.7	0.6	2.0	0.7	0.0
10Ni/AC-S	100	300	62	37	9.1	6.2	1.6	1.5	0.1	0.5

Compared with the 3 wt.% noble metal catalysts, the 3 wt.% Ni catalysts had lower actual metal loading and dispersion (Table 6) [I]. In particular, 3 wt.% Ni/AC-B catalyst had low dispersion (Table 6), leading to decreased activity and low MF yield. With three catalysts (Figure 10), the MF yield decreased after its observed maximum, indicating that the potential maximum MF yield was attained and that MF was further hydrogenated to other products. In particular, with 3 wt.% Ru/AC-S catalyst, the MF yield rapidly decreased as MTHF, THFA, PN, condensation products, and alcohols including mainly POL but also pentanediols were produced [I]. With both Pt catalysts, relatively similar activity toward MF was noticed (Figure 10). Among all the experiments conducted at 230 °C, the highest obtained MF yield was achieved with 3 wt.% Pt/AC-S catalyst (48%), which also had the highest metal dispersion (37%) and the smallest particle size (2.7 nm) [I].

The effect of reaction temperature (210, 230, and 240°C, Figure 11) on MF production was also investigated [I]. In these studies, the best support material for each metal in terms of MF production (AC-S for Ni and Pt, and AC-B for Ru) was selected based on the experiment conducted at 230 °C (Figure 10). With the Ni catalyst, the highest MF yield (36%) was almost the same at all temperatures [I]. The severe deactivation of the Ni catalyst could explain why the higher reaction temperature (240 °C) did not result in higher MF yield, assuming that the deactivation occurred soon after the start of the reaction [I]. However, the potential maximum yield was perhaps not reached at all the studied temperatures, as significant amounts of FA were detected from the final samples. With the noble metal catalysts, the higher reaction temperature (240 °C) resulted in higher observed MF yields with shorter reaction times (120 min): 49% for 3 wt.% Ru/AC-B and 50% for 3 wt.% Pt/AC-S. Moreover, the increase in temperature from 230 to 240 °C had a more significant impact on the MF yield than the increase from 210 to 230 °C, and the produced MF started to further hydrogenate to other products [I].

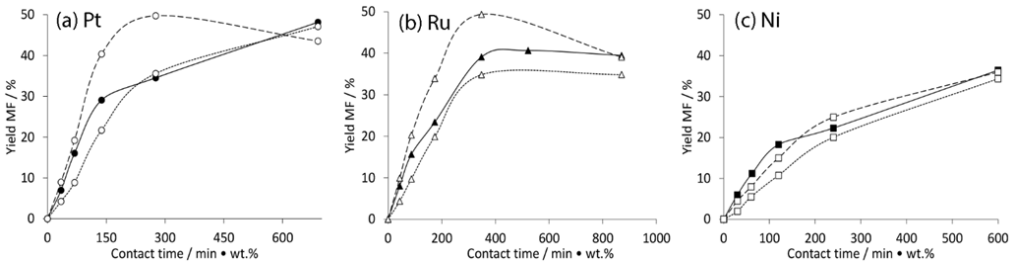

Figure 11. 2-Methylfuran yield as a function of contact time at various temperatures: (a) 3Pt/AC-S; ● (solid) = 230 °C, ○ (dashed) = 240 °C, and ○ (dotted) = 210 °C, (b) 3Ru/AC-B; ▲ (solid) = 230 °C, Δ (dashed) = 240°C, and Δ (dotted) = 210°C, and (c) 3Ni/AC-S; ■ (solid) = 230 °C, □ (dashed) = 240 °C, and □ (dotted) = 210 °C. Reprinted from Publication I with permission from Wiley-VCH Verlag GmbH & Co. KGaA, copyright (2018).

Different metal loadings (1.5 and 3 wt.% Pt/AC-S, 1.5 and 3 wt.% Ru/AC-B, and 3 and 10 wt.% Ni/AC-S) were also investigated for MF production at 230 °C. The 10 wt.% Ni/AC-S catalyst achieved an MF yield (37%) similar to the 3 wt.% Ni/AC-S catalyst, which might be because of the large metal particle size (15 nm) and poor dispersion (7%) of the 10 wt.% Ni/AC-S catalyst [I]. The 1.5 wt.% Ru/AC-B catalyst probably did not achieve the potential maximum MF yield, as 17% FA yield was still observed after the 300 min reaction time. Unlike Ru, 1.5 wt.% Pt/AC-S catalyst achieved similar maximum MF yield as the 3 wt.% Pt/AC-S catalyst, and the properties of the two catalysts were also similar based on characterization [I].

5.2 2-Methylfuran production using catalysts supported on bio-based carbon foams

The hydrotreatment of furfural to MF was studied with bimetallic 5/5 wt.% Cu/Ni catalysts on two types of bio-based ACFs (S1 and S2) as well as on acid-washed ACFs (S1_A1, S1_A2, S2_A1, and S2_A2) [II]. The prepared and tested catalysts in this study are listed in Table 2. S1 was prepared from commercial tannic acid mixture, and S2 was prepared from pine bark extracts. The surfaces of the prepared ACFs were modified with acids A1 (HNO_3) or A2 (H_2SO_4). The combination of Cu and Ni was selected based on high MF yields obtained with similar catalysts in the literature [98,99]. In addition to the ACF supports, 5/5 wt.% Cu/Ni catalysts were prepared on two commercial AC supports (Norit_S and Norit_A) and on bio-based AC from spruce (S3) for reference purposes.

Figure 12 presents furfural conversion as a function of batch residence time (τ) for the ACF-supported catalysts (a), acid-washed ACF-supported catalysts (b), and reference catalysts (c). S1_Cu/Ni catalyst was more active than S2_Cu/Ni catalyst, as 100 % furfural conversion was reached after 300 min reaction time [II]. The higher activity of S1_Cu/Ni catalyst was surprising because the surface area of support S1 was significantly lower (Table 6) than that of support S2. For comparison, the activities of Cu/Ni catalysts on reference materials (Figure 12c) were similar to those of S1_Cu/Ni catalyst [II].

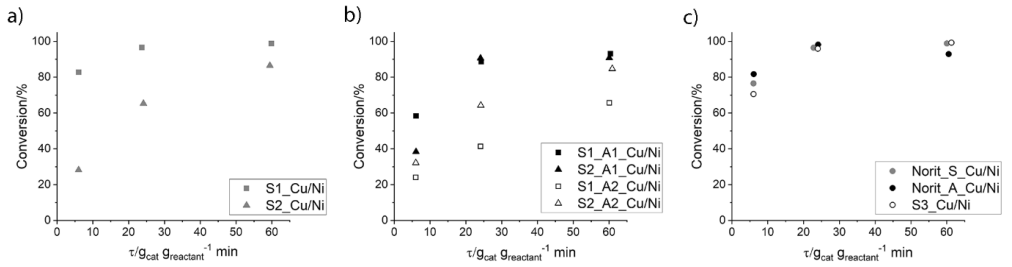

Figure 12. Furfural conversion as a function of batch residence time (τ): a) Cu/Ni catalysts on ACFs, b) Cu/Ni catalysts on acid-washed ACFs, and c) Cu/Ni catalysts on reference materials. Reprinted from Publication II with permission from Elsevier B.V., copyright (2020).

The selectivity of the ACF-supported catalysts to MF as a function of furfural conversion is presented in Figure 13, which shows that the selectivity of both ACF-supported catalysts to MF (Figure 13a, <30%) was not at the desired level [II]. Acid wash was performed for S1 and S2 to modify their surface properties. After HNO_3 wash, the activity of S1-supported catalyst (S1_A1_Cu/Ni) decreased in the beginning of the reaction but eventually, 100% furfural conversion was achieved (Figure 12b). For S2, the HNO_3 wash increased the catalytic activity throughout the batch residence time range and full conversion was reached. Interestingly, the acid wash with H_2SO_4 significantly decreased the activity of the S1-supported catalyst, whereas with S2, the H_2SO_4 wash did not affect catalytic activity. Compared with the reference

materials, only Cu/Ni on HNO_3-washed supports reached similar conversion levels with longer reaction times.

The MF selectivity of S2_Cu/Ni catalyst was higher than that of S1_Cu/Ni catalyst (Figure 13a) with comparable conversion levels. The acid-washed ACF-supported catalysts had higher selectivities to MF than the pure ACF-supported catalysts. S2_A1_Cu/Ni catalyst had the highest selectivity to MF (52%) at 90% conversion level, whereas S1_A1_Cu/Ni catalyst reached 40% MF selectivity with similar conversion level. The two H_2SO_4-washed catalysts provided similar MF selectivities of ~30% at ~60% conversion level even though the metal particles on S2_A2 were observed to be smaller than those on S1_A2 and previously, small metal particles have promoted the production of MF [I]. Compared with the reference catalysts, only S2_A1_Cu/Ni catalyst reached an almost similar MF selectivity at >90% conversion level [II].

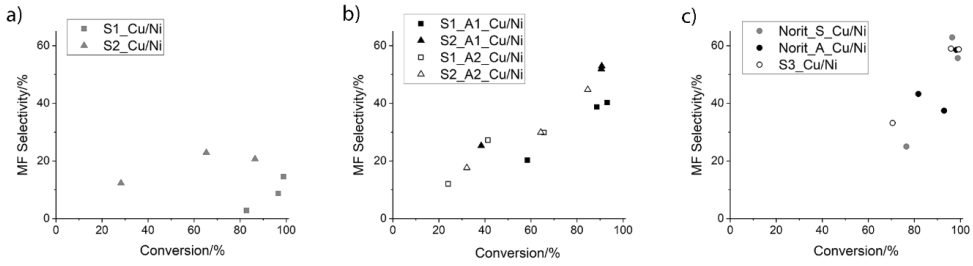

Figure 13. MF selectivity as a function of furfural conversion: a) Cu/Ni catalysts on ACFs, b) Cu/Ni catalysts on acid-washed ACFs, and c) Cu/Ni catalysts on reference materials. Reprinted from Publication II with permission from Elsevier B.V., copyright (2020).

The product distributions of all the tested catalysts at the highest observed MF yields are presented in Table 9 [II]. High FA yield (with S1_Cu/Ni, S1_A1_Cu/Ni, and S1_A2_Cu/Ni) indicates that potential maximum MF yields were not yet reached. The highest MF yield (61%) was obtained with the Norit_S_Cu/Ni catalyst having commercial steam-activated carbon support. The other reference catalysts, Norit_A_Cu/Ni and S3_Cu/Ni, reached similar MF yields of 57% and 58%, respectively. High MF yield of 48% was also obtained with the HNO_3-washed S2_A1_Cu/Ni catalyst. After the acid wash, the ACF supports had a higher amount of oxygen-containing surface groups, as detected by XPS [II], which might affect the adsorption properties of ACs [188]. Without acid wash, the S1- and S2-supported catalysts led to the production of significant amounts of THFA or MTHF. With all the ACF-supported catalysts (except S1_Cu/Ni), significant amounts of FMA were produced. However, FMA was only a minor side product when the reference catalysts were used.

Table 9. Furfural conversion at the highest observed MF yield, the corresponding reaction time, and the main side-product yields at 230 °C and 40 bar H_2. Reprinted from Publication II with permission from Elsevier B.V., copyright (2020).

Catalyst	X /%	t /min	τ /g_{cat} min $g_{reactant}^{-1}$	Y_{FA} /%	Y_{MF} /%	Y_{THFA} /%	Y_{MTHF} /%	Y_{Furan} /%	Y_{FMA} /%
S1_Cu/Ni	99	300	60	71	14	18	0.0	4.9	0.1
S2_Cu/Ni	86	300	60	5.1	18	6.6	17	0.0	6.3
S1_A1_Cu/Ni	93	300	60	16	37	6.6	3.4	3.8	4.2
S2_A1_Cu/Ni	91	300	60	3.6	48	3.3	2.9	0.7	5.3
S1_A2_Cu/Ni	66	300	60	13	20	1.7	1.9	0.2	5.6
S2_A2_Cu/Ni	85	300	61	5.5	38	1.3	2.3	0.1	6.1
Norit_S_Cu/Ni	96	120	23	8.0	61	7.2	2.2	4.1	0.2
Norit_A_Cu/Ni	98	120	24	1.1	57	3.2	10	5.1	0.3
S3_Cu/Ni	99	300	61	2.9	58	8.1	3.0	4.5	0.0

5.3 Comparison of the obtained results to literature

The feasibility of using wood-based ACs from spruce and birch sawdust as catalyst support in furfural hydrotreatment was studied [I]. Noble metal catalysts were superior to Ni catalysts on the wood-based ACs for the production of MF. Reasons could be poor Ni dispersion, large Ni particles, insufficient reduction temperature (250 °C) for Ni, as evident by the TPR analysis, and the severe deactivation of the Ni catalysts. In general, the observed spent catalyst deactivation was in the order Pt < Ru < Ni. In the literature, higher MF yields than in this work have been reported for Ni catalysts supported on ACs [95]. However, in this work, 1.5 wt.% and 3 wt.% Pt/AC-S catalysts had higher MF yields than, and 3 wt.% Ru/AC-B had similar MF yield to, commercial catalysts with higher metal loadings: 40% MF yield in liquid phase at 175 °C with a 5 wt.% Pt/C catalyst [76], and 51% MF yield in liquid phase at 180 °C with a 5 wt.% Ru/C catalyst [89].

To increase the mechanical strength of the carbon-based support materials, bio-based ACFs from tannic acid and pine bark extracts were prepared [II]. Bimetallic Cu/Ni catalysts were prepared and tested in furfural hydrotreatment [II] based on studies reporting high MF yields with bimetallic Cu/Ni catalysts: 92% with 10 wt.% Ni–10 wt.% Cu/Al_2O_3 at 210 °C after 7 h reaction time with formic acid as hydrogen donor [99] and 91% with 10 wt.% Ni–10 wt.% Cu/AC at 200 °C after 8 h reaction time with formic acid as hydrogen donor [98]. The MF yield obtained with the HNO_3-washed S2_A1_Cu/Ni catalyst (48%) was similar to that obtained with the noble metal catalysts in Publication I. However, an even higher MF yield (58%) was obtained with Cu/Ni catalyst supported on spruce-based AC (S3_Cu/Ni) [II]. The support prepared from pine bark extracts led to higher mesoporosity, and the HNO_3 wash led to more active catalysts compared with H_2SO_4 wash. Compared with the state-of-the-art studies with bimetallic Cu/Ni catalysts [98,99], the MF yields in this work were lower, but so were the used metal amounts (approximately 5 wt.% each). Moreover, longer reaction times (>300 min) might have produced higher MF yields, as all the ACF-supported catalysts had some FA remaining in the product mixtures.

In conclusion, the AC support materials studied in this thesis present potential to be used as bio-based substitutes for charcoal-based ACs, and the ACFs showed potential for catalytic purposes. Further tailoring of the ACF-supported catalysts is, however, needed to increase their selectivity toward MF.

6. Hydrodeoxygenation of levulinic acid dimers

LA is a platform molecule, which has the potential to be used for the production of increased carbon-chain-length products (>C_6). In this thesis, the hydrotreatment of LA dimers was first studied via GNL as a model compound representing the lactone moieties in the dimers. Various noble metal catalysts (Pt, Pd, Ru, and Rh) on monoclinic ZrO_2 were tested, and the product distributions were compared. With Ru catalyst, also the effect of reaction temperature on product distribution was studied. Finally, the HDO of industrially produced LA dimer mixture was studied with Ru/ZrO_2 catalyst, which was chosen owing to its selectivity toward hydrocarbons observed in the HDO of GNL.

6.1 Hydrodeoxygenation of γ-nonalactone model compound using noble metal catalysts

The activity of the 3 wt.% noble metal catalysts was tested in the HDO of GNL at 280 °C and 57.5 bar (average) H_2 with reaction times varying from 15 to 300 min [III]. Figure 14a presents GNL conversion as a function of reaction time achieved using the four catalysts. The highest conversion was obtained with the Rh catalyst after 300 min reaction time. However, when initial activity was calculated per active surface metal site (from chemisorption), the order of TOFs was 1, 0.7, 0.5, and 0.2 s^{-1} for Ru, Pd, Pt, and Rh, respectively [III]. The Ru catalyst had the lowest amount of surface atoms, which was thought to be attributable to the residual Cl species (from catalyst preparation) occluding the chemisorption sites.

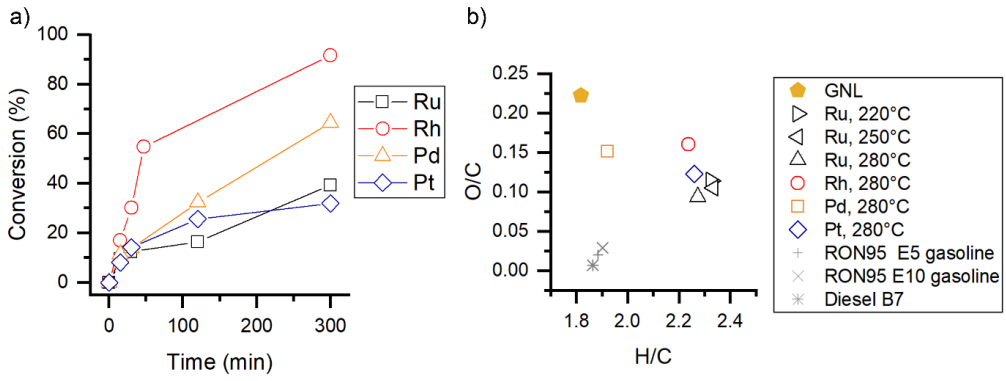

Figure 14. a) GNL conversion as a function of reaction time at 280 °C and b) van Krevelen diagram for the organic liquid product mixtures obtained with the catalysts at 220–280 °C compared with the reactant (GNL) and standard fuels [189]. In the reactions at 280 °C, the reported products were obtained at 30%–40% GNL conversion. The values exclude unconverted GNL and water. Modified from Publication III.

Based on the experimental results, van Krevelen diagrams were applied to assess the oxygen removal activity of the catalysts. Figure 14b presents the diagrams for the organic liquid products at comparable conversion levels (30%–40%) obtained at 280 °C, excluding unreacted GNL and water. All the catalysts removed oxygen to some extent, based on the oxygen content in the GNL feed, but the oxygen levels remained above standard fuel specifications [III]. The lowest O/C ratio was obtained with the Ru catalyst. The H/C ratios increased with all the catalysts, whereas Pd resulted in the lowest H/C ratio among the catalysts.

The grouped product selectivities (by functional groups) of the catalysts at 280 °C with comparable conversion levels (30%–40%) are presented in Figure 15, including all liquid, gaseous, and solid (from TGA analysis) products. The highest selectivity to liquid hydrocarbons (24%) was obtained with the Ru catalyst [III]. The Ru catalyst also produced gaseous hydrocarbons, mainly methane, and lactones with less than five carbon sidechains. Another major product group with Ru was ketones, which were obtained with 20% selectivity [III]. Compared with Ru, the other metals had higher selectivity to acids: 28%, 43%, and 80% with Pt, Rh, and Pd, respectively [III]. In addition to acids, the Rh catalyst produced alcohols and ketones, whereas Pt and Pd produced esters. More 2-pentyl tetrahydrofuran (PTHF) was produced (8%) with Pt than with the other catalysts, and the selectivity of Pt toward liquid hydrocarbons was the second highest (9%) [III]. The selectivities of Rh (30%) and Pt (20%) to unaccounted products remained high, despite using multiple analytical methods.

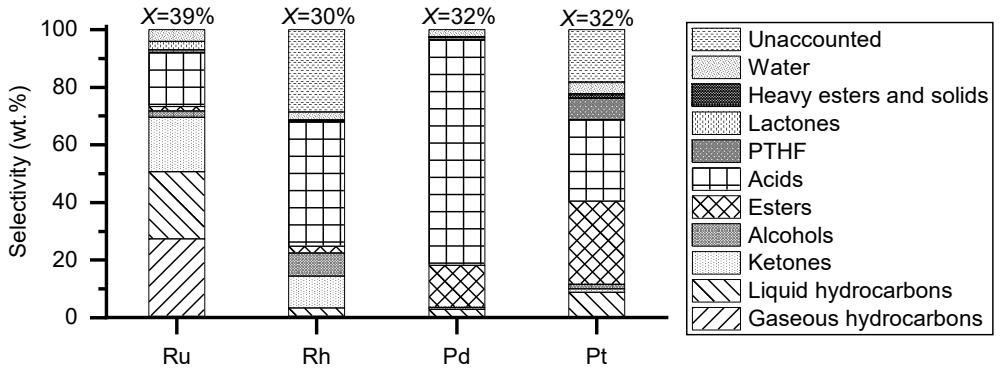

Figure 15. Grouped product selectivities of the noble metal catalysts. GNL conversion (*X*) is marked on top of the bars. Reaction conditions: 0.6 g catalyst, ~3 wt.% metal loading, 23 mL GNL (pure), 280 °C, and 57.5 bar H_2. The results were obtained after 300, 30, 120, and 300 min reaction time for Ru, Rh, Pd, and Pt catalysts, respectively. Reprinted from Publication III with permission from Springer Nature, copyright (2019).

Owing to the high selectivity of Ru toward hydrocarbons at 280 °C, Ru was also studied at 220 and 250 °C [III]. At 220 °C, GNL conversion of 25% was obtained after 300 min reaction time, which was the lowest conversion observed. However, similar conversions (37%–39%) were obtained at 250 and 280 °C, which could be attributable to experimental errors or catalyst deactivation [III]. Some deoxygenation and hydrogen uptake was obtained at all the tested temperatures (Figure 14b) compared with the GNL feed. The higher reaction temperature decreased the selectivity of Ru to alcohols and PTHF, whereas the amount of gaseous and liquid hydrocarbons, ketones, and acids increased [III]. Because the amounts of PTHF and ketones changed to opposite directions when increasing the reaction temperatures, it was possible that 4-nonanone formed from PTHF. In the literature, the formation of PN has been observed during MTHF hydrotreatment [190].

The organic liquid products obtained in the HDO of GNL with the noble metal catalysts are summarized in Figure 16. The carbon numbers of the obtained liquid products generally varied from C_4 to C_9.

Among the hydrocarbons, *n*-octane was the most abundant product with all the catalysts (share of total liquid hydrocarbons: 64%–96%) [III]. Pt was the only catalyst that produced a significant amount of *n*-nonane (16%) [III]. The most abundant alcohol was 3-octanol with Ru and Rh and nonanols with Pd, whereas Pt produced both. The position of the hydroxyl group in nonanols varied between C_1 and C_4 (carboxyl and gamma carbons of the parent lactone) [III]. The formation of secondary alcohols has been proposed to occur via the decarbonylation or deoxygenation of a ring-opening surface intermediate [191] or 4-hydroxynonanal intermediate [192]. With Ru, the decarbonylation route is energetically favorable [191,193]. Pt and Pd also produced 1,4-nonanediol by lactone ring opening without oxygen removal, which can further react to form PTHF, 4-nonanol [194], or 1-nonanol [192]. The most abundant acid was nonanoic acid, and the most abundant esters were nonyl nonanoates, except with Rh that produced nonanoates of lower alcohols. The most abundant ketones were 3-octanone (Ru, Rh, and Pd) and 4-nonanone (Pt and Pd) [III]. Moreover, LC–MS analysis revealed a diester, 4-nonanoyloxynonyl nonanoate ($C_{27}H_{52}O_4$), which was formed with Pt and Pd catalysts via the reaction between 1,4-nonanediol and two nonanoic acid molecules [III]. The most abundant component in the gas phase was methane, which was formed in the methanation of CO, especially with Ru. The produced water was mainly dissolved in the organic phase, and only Ru and Rh had separate aqueous phases at 39% and 91% conversion levels, respectively.

Most of the products (e.g., acids and ketones) accumulated during the progress of the reaction. The formation of an acid from a lactone has been reported to occur in the presence of a bifunctional catalyst via an alkenoic acid intermediate [195]; however, no alkenoic acids were observed in this study with ZrO_2. Unlike acids, alcohols typically decreased toward the end of the reaction, which is typical for the reaction intermediates. Particularly with Pd, alcohols were consumed in esterification, whereas the amount of hydrocarbons remained low. The formation of nonyl nonanoate consumed two molecules of GNL, and oxygen was removed as water. Moreover, the formation of PTHF removed oxygen. Together, these two reactions explained the low O/C ratio of the product obtained with Pt even though hydrocarbons were not the main products [III]. Although ketones could be hydrogenated to their corresponding alcohol, studies have shown the inability of Rh and Ru in hydrogenating the ketone group [196,197].

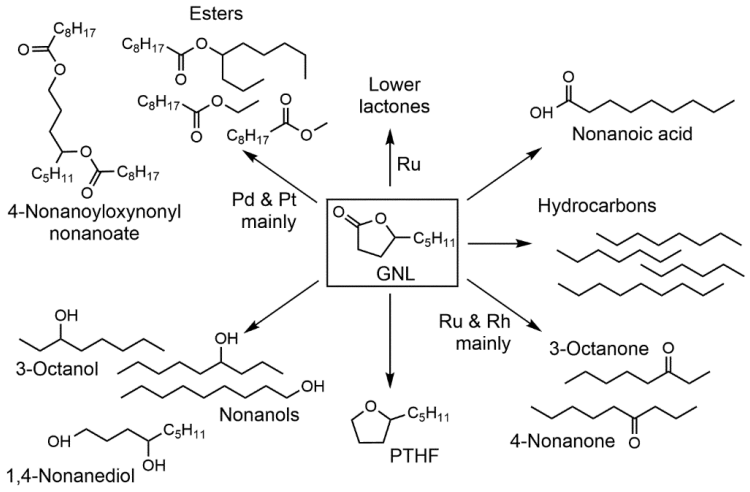

Figure 16. Summary of the products obtained in the HDO of GNL with noble metal catalysts supported on ZrO_2. Reprinted from Publication III with permission from Springer Nature, copyright (2019).

6.2 Hydrodeoxygenation of LA dimers using a Ru/ZrO_2 catalyst

The HDO of LA dimers was conducted in a batch reactor with 3.6 wt.% Ru/ZrO_2 catalyst between 250 and 300 °C and thermally at 250 °C, and the batch residence times (τ_b) were 0.6 or 1.1 g_{cat} h g_{feed}^{-1} [IV]. The identified LA dimers (in the feed mixture) are presented in Scheme 5. Owing to the hydrogenation conditions used to produce the dimers, several hydrogenated and deoxygenated dimers were observed with HPLC. Six main components were identified based on their molecular weights: **216** (70 area-%), **214** (10 area-% including both isomers), **202** (4 area-%), **200** (10 area-%), and **198** (6 area-%) [IV]. Various other isomers of the dimers and some unreacted LA could also have existed.

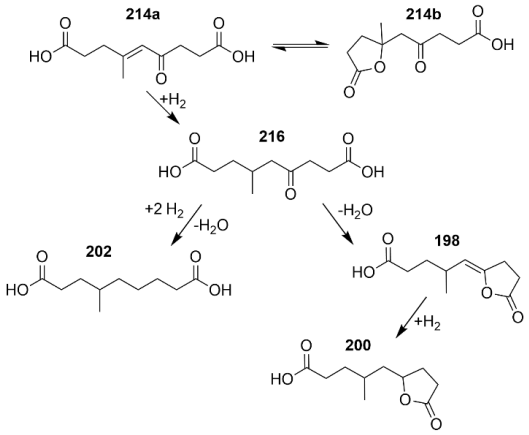

Scheme 5. Identified LA dimers in the feed mixture with corresponding molecular weights and reactions among them. Modified from Publication IV.

Figure 17a presents the relative changes of the individual LA dimers after the experiments. A positive change indicated a net increase in the amount of the dimer after the reaction whereas a negative change indicated a net consumption of the dimer. The net consumption was observed especially with the reactive dimers **214a**, **214b**, and **216** (containing a double bond and/or a ketone group) that experienced relative changes of over –90% in the catalytic experiments [IV]. Dimers **214a**, **214b**, and **216** particularly converted to the less reactive dimers **200** and **202**. Dimer **198** was also mainly consumed in the catalytic experiments but was produced in the thermal experiment. Dimers **214a**, **214b**, and **216** were not fully converted in the thermal experiment. In Figure 17b, the H/C and O/C ratios of the products obtained by the HDO of LA dimers are compared with those of the feed. Oxygen was removed in all the experiments, but full deoxygenation was not yet achieved. The decreased H/C ratios compared with the feed also indicated more unsaturation in the obtained products, especially at 300 °C. No significant differences to the relative changes of the individual dimers or to their position in the van Krevelen diagram were observed in the high batch residence time (1.1 g_{cat} h g_{feed}^{-1}) experiment.

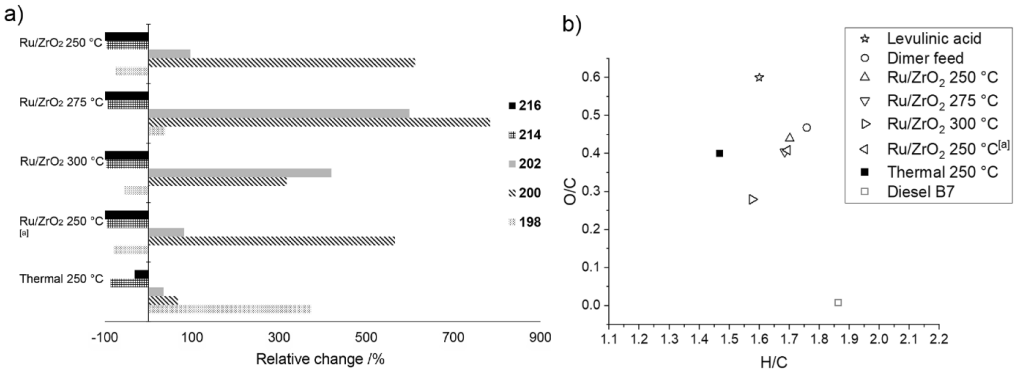

Figure 17. a) Relative changes of the LA dimers obtained with 3.6 wt.% Ru/ZrO_2 catalyst and thermally. Dimer **214** includes both isomers **214a** and **214b** (Scheme 5). b) van Krevelen diagram of the molar H/C and O/C ratios of the dimer feed and the organic liquid product mixtures compared with LA and standard diesel [189]. [a] τ_b = 1.1 g_{cat} h g_{feed}^{-1}. Modified from Publication IV.

The sizes of the molecules present in the organic product mixtures were investigated via GPC analysis [IV]. Three standard acid molecules—stearic acid (SA, 284 amu), azelaic acid (AA, 188 amu), and LA (116 amu)—were used to guide the interpretation of the chromatograms presented in Figure 18. Two detectors, RI and UV (270 nm) were used; from the used standards, only LA exhibited UV absorbance owing to the C=O chromophore. Figure 18a and b present the chromatograms recorded with the RI detector. The LA dimer feed presented two major peaks at 9.0 and 9.5 min, and the former peak (molecular mass close to that of AA) decreased especially in the catalytic experiments. The peak likely contained dimer **216**, which was the most abundant and one of the most reactive components in the feed. The second peak at 9.5 min increased in the experiments, which indicated the formation of dimers **200** and **202**. In addition to the peaks associated with the dimers, both lighter and heavier products were detected in the experiments. The possible chromophores were determined using the UV detector (Figure 18c and d) because the used wavelength was especially suitable for detecting aromatics and conjugated systems, whereas only weak absorption of carbonyl derivatives was expected [198]. The formation of UV chromophores different from the feed was observed at 7.0–9.5 min, especially at a high reaction temperature. Several peaks were obtained in the same region (7.0–9.5 min) in the thermal experiment, but also a strong peak was obtained after 10 min [IV].

The compositions of the organic liquid products were also analyzed using IR and ^{1}H NMR [IV]. IR spectra revealed the consumption of the acid groups because the O–H band attributed to the carboxylic acid decreased in the catalytic experiments. O–H stretching from alcohols or water with H-bonding was present in all the products. Only at 300 °C, a peak attributed to free O–H stretching from alcohols or water emerged, indicating less oxygen in the product. The consumption of C=O bond stretching was also observed, indicating the consumption of acid and ketone groups present in the feed, which was confirmed by ^{1}H NMR analysis [IV]. The formation of aromatics was not clear in the IR analysis results but was evident in the GPC UV analysis results, which clearly showed the formation of non-oxygen-containing chromophore (high absorption of ν = 270 nm) especially at 300 °C (Figure 18) [IV]. In the ^{1}H NMR analysis, the chemical shifts of aromatic protons were detected only at high reaction temperatures (≥275 °C) with the Ru catalyst [IV].

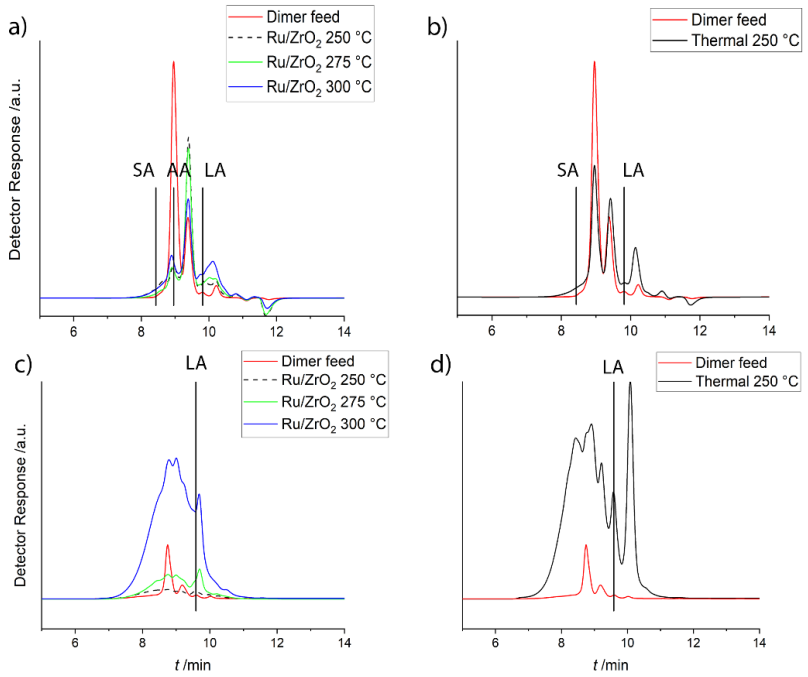

Figure 18. Gel permeation chromatography (GPC) chromatograms of the LA dimer feed and the products obtained with Ru/ZrO_2 catalyst a) and thermally b) at various temperatures with refractive index (RI) detector (equal scaling). GPC chromatograms of the dimer feed and the products obtained with Ru/ZrO_2 catalyst c) and thermally d) at various temperatures with UV detector (270 nm, equal scaling). SA: stearic acid (284 amu), AA: azelaic acid (188 amu), LA: levulinic acid (116 amu). Reprinted from Publication IV with permission from MDPI, copyright (2020).

The main volatile product groups (boiling point below 250 °C) were semi-quantitatively estimated from the conducted GC–MS analyses [IV]. Most of the volatile products were oxygenates, such as ketones, acids, and esters. The most common compounds among the groups of esters, acids, and hydrocarbons are presented in Scheme 6 with the corresponding parent dimers. An increasing trend in the production of all types of aliphatic hydrocarbons (including olefins and cyclic) was observed as a function of increasing reaction temperature. Aromatics were detected with the Ru catalyst at temperatures higher than 250 °C, which supports the similar findings obtained via GPC UV and ^{1}H NMR analyses [IV]. The presence of olefins and aromatics helps to explain the decreasing H/C ratios, particularly at higher temperatures (Figure 17b). In the thermal experiment, ketones were mainly produced. The high UV absorbance in the thermal experiment (Figure 18) may be attributable to non-aromatic chromophores, such as conjugated systems, as no aromatics were detected by GC–MS or ^{1}H NMR [IV].

HDO was preferred at a low reaction temperature (O removed as H_2O); at higher temperatures, decarboxylation became more dominant and a higher amount of CO_2 was detected in the gas phase [IV]. Decarboxylation could also explain the formation of many of the major volatile products catalytically or thermally obtained (Scheme 6). GVL was formed in the presence of Ru catalyst from the unconverted LA in the feed because no pentanoic acid was detected (Reaction 3.1, Scheme 6) [IV]. The products in brackets (Reactions 2 and 3.2, Scheme 6) were suggested by the MS spectral database with poor match factors; thus, similar compounds were proposed based on the decarboxylation of the parent dimers [IV]. With Ru catalyst, the most abundant volatile aromatic compound was 5-hydroxy-2,3,4-trimethylacetophenone. The formations of 1,2,3-trimethylcyclopentene (TMCP) and 1-oxaspiro(4,5)decan-2-one (OSD) were speculated to occur only thermally (alongside the catalyzed reactions with Ru), as the

amounts were higher in the thermal experiment at 250 °C compared with the catalytic experiment with Ru at the same temperature [IV]. Moreover, dimer **198** was produced in the thermal experiment (Figure 17a), indicating a thermal tendency for intramolecular cyclization.

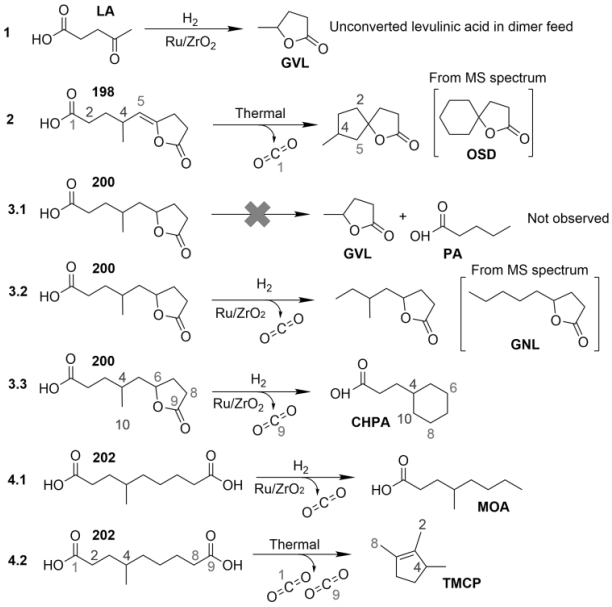

Scheme 6. Suggested formation of selected volatile products. LA: levulinic acid, GVL: γ-valerolactone, OSD: 1-oxaspiro(4,5)decan-2-one, PA: pentanoic acid, GNL: γ-nonalactone, CHPA: cyclohexanepropanoic acid, MOA: 4-methyloctanoic acid, and TMCP: 1,2,3-trimethylcyclopentene. Reprinted from Publication IV with permission from MDPI, copyright (2020).

6.3 Comparison of the obtained results to literature

In the literature, noble metal catalysts have been studied in HDO experiments to obtain increased carbon-chain-length products; for example, Mascal et al. [107] obtained 88% total hydrocarbon yield (C_7–C_{10}, aliphatic and branched) from angelica lactone dimer using Ir–ReO_x/SiO_2 catalyst at 220 °C. Even higher diesel range hydrocarbon yield (94%) was reported by Li et al. [112], who obtained branched and linear hydrocarbons as well as cycloparaffins from the HDO of HAA product of MF (C_{15}) using an acidic Pt/ZrP catalyst at 350 °C. In addition, Corma et al. [113] reported 93% diesel range hydrocarbon yield (including cyclics and aromatics) from the hydrogenation of the HAA product of MF (C_{15}) using a Pt/C catalyst at 350 °C. Hydrocarbons up to C_{15} have also been produced from the crossed aldol condensation products of furfural and HMF with acetone using a Pt/SiO_2-Al_2O_3 catalyst [108].

The mentioned hydrocarbon yields in the literature are higher than those obtained in this thesis: 24% hydrocarbon selectivity (linear and branched) with 39% conversion level from the HDO of GNL using a 3 wt.% Ru/ZrO_2 catalyst [III]. Other noble metal catalysts were also tested (Rh, Pd, and Pt), but Ru was the most active toward hydrocarbons [III]. In the HDO of LA dimers, the 3.6 wt.% Ru/ZrO_2 catalyst was not as active toward hydrocarbons, as most of the obtained products were oxygenates. The HDO of LA dimers also yielded various cyclic products [IV], which have been reported by other authors as well [112,113]. All the above-mentioned studies from the literature used feed molecules with either lactone or furan structures, but the LA dimers had, in the worst case, acid, ketone, and lactone structures in the same molecule, thus increasing the complexity. Although the complex nature of the feed most likely affected the HDO, and full deoxygenation was not reached, Ru/ZrO_2 catalyst could be further developed

to enable one-pot synthesis of hydrocarbons from LA dimers. For example, the addition of a reducible promotor (e.g., Re) to a noble metal catalyst increases its activity in C–O bond hydrogenolysis [107].

7. Hydrodeoxygenation of phenols

Lignocellulose-derived pyrolysis and liquefaction biocrudes are sources of bio-based phenolic compounds. The phenols can be converted to aromatics, which are important components, for example, in jet fuel. In this thesis, liquid-phase HDO of phenols was investigated using a model compound, 4-propylphenol, with Pt catalysts and an organic solvent. Moreover, the effect of reducible catalyst support materials (Nb_2O_5 and TiO_2) on product distribution was investigated and compared with an irreducible ZrO_2 support.

7.1 Hydrodeoxygenation of 4-propylphenol to propylbenzene using noble metal catalysts

The HDO of 4-propylphenol (Scheme 4) was studied at 350 °C and 20 bar H_2 pressure at different batch residence times (τ_B) [V]. Figure 19 contains details of the activity and selectivity of 3 wt.% Pt catalysts to the main products (propylbenzene and propylcyclohexane). High temperature was needed to promote the formation of the target product, propylbenzene [199]. Full conversions were obtained with all the catalysts at batch residence times of 4–5 g_{cat} min $g_{reactant}^{-1}$, but the differences in activities were observed at low batch residence time (0.25 g_{cat} min $g_{reactant}^{-1}$), as conversions of 15%, 36%, and 44% were reached with Pt/ZrO_2, Pt/TiO_2, and Pt/Nb_2O_5, respectively [V]. Because the initial TOFs were 1.4 s^{-1} for Pt/ZrO_2, 2.1 s^{-1} for Pt/TiO_2, and 4.1 s^{-1} for Pt/Nb_2O_5, the niobia-supported catalyst was the most active catalyst [V]. In addition, the pure supports (without Pt, τ_B of 3.7–4.0 g_{cat} min $g_{reactant}^{-1}$) resulted in 4-propylphenol conversions of 12% (ZrO_2), 25% (TiO_2), and 43% (Nb_2O_5), indicating the higher activity of Nb_2O_5 compared with the other supports.

In general, propylbenzene selectivities of 60%–70% were reached at τ_B of 4–5 g_{cat} min $g_{reactant}^{-1}$ with all the catalysts [V]. The highest observed propylbenzene selectivity of 77% was obtained with the Pt/Nb_2O_5 catalyst (τ_B of 4.0 g_{cat} min $g_{reactant}^{-1}$ with 98% conversion); however, after τ_B of 5 g_{cat} min $g_{reactant}^{-1}$, the propylbenzene selectivity decreased whereas the selectivity of propylcyclohexane increased [V]. Compared with the Pt catalysts, the pure supports favored different main products, such as 1-methoxy-4-(1-methylpropyl)-benzene [V], hereafter referred to as aromatic oxygenate. The aromatic oxygenate selectivities were 33.6% with Nb_2O_5, 39.3% with TiO_2, and 11.5% with ZrO_2 [V]. Moreover, 4-propylcyclohexanol (≤15% selectivity) was observed mainly with Nb_2O_5 and TiO_2 supports [V].

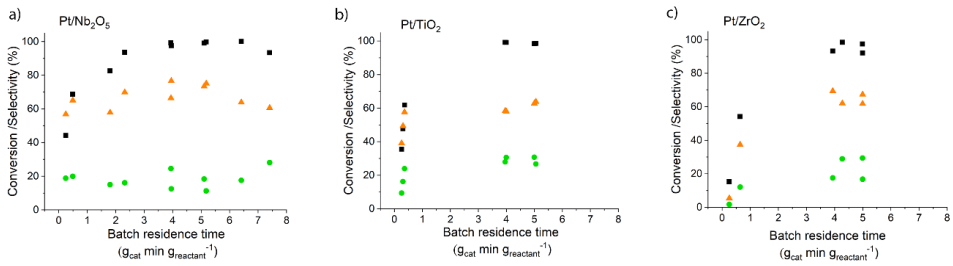

Figure 19. Conversion of 4-propylphenol (■) and the molar selectivities to propylbenzene (▲) and propylcyclohexane (●) of a) Pt/Nb_2O_5, b) Pt/TiO_2, and c) Pt/ZrO_2 catalysts as a function of batch residence time. Reaction conditions: ~3% metal loading, 580 mg 4-propylphenol in 27 ml tetradecane, 350 °C, and 20 bar H_2. Modified from Publication V.

The selectivities of 3 wt.% Pt catalysts were also compared at intermediate conversion levels (44%–54%) under the same conditions presented in Figure 20 [V]. The main product was propylbenzene with all the catalysts, but Pt/ZrO_2 had the lowest selectivity to it. Pt/ZrO_2 was, in general, less active in HDO, as it provided higher amounts of 4-propylcyclohexanone, 4-propylcyclohexanol, and 4-propylcyclohexene compared with the other catalysts. Because toluene was detected in the liquid phase and ethane in the gas phase, minor cracking of the propyl sidechain likely occurred.

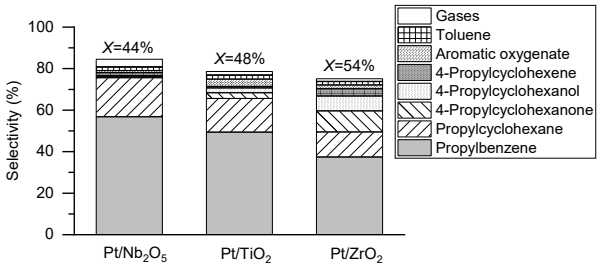

Figure 20. Comparison of molar product selectivities of Pt/Nb_2O_5, Pt/TiO_2, and Pt/ZrO_2 catalysts with comparable conversions (44%–54%) obtained at batch residence times of 0.25, 0.31, and 0.64 g_{cat} min $g_{reatant}^{-1}$, respectively. Reaction conditions: ~3% metal loading, 580 mg 4-propylphenol in 27 ml tetradecane, 350 °C, and 20 bar H_2. Reprinted from Publication V with permission from Wiley-VCH Verlag GmbH & Co. KGaA, copyright (2020).

The effect of reduction temperature on product distribution was studied using 3 wt.% Pt catalysts on reducible supports (Nb_2O_5 and TiO_2) [V]. Two reduction temperatures were applied—353 and 400 °C—based on TPR measurements [V], which were higher than the reaction temperature used (350 °C). Figure 21 and Figure 22 present the results for Pt/Nb_2O_5 and Pt/TiO_2, respectively. Close to 100% conversion was obtained with both catalysts at high batch residence times (~4.0 g_{cat} min $g_{reactant}^{-1}$) [V]. In case of the Pt/Nb_2O_5 catalyst, the higher reduction temperature (400 °C) resulted in higher selectivity to propylcyclohexane than to propylbenzene, which was remarkable among the Pt catalyst experiments because propylbenzene was almost always the most abundant product [V]. However, no significant differences in product distribution were observed at low batch residence times (~0.26 g_{cat} min $g_{reactant}^{-1}$). In the case of the Pt/TiO_2 catalyst, slightly less propylbenzene and slightly more propylcyclohexane were obtained at both batch residence times after reduction at 400 °C compared with those obtained after reduction at 353 °C. At low batch residence time, the Pt/TiO_2 catalyst had ~10% selectivity to the aromatic oxygenate [V]. The effect of reduction temperature (100–500 °C) on the activity of Pt or Pd catalysts supported on Nb_2O_5 has been reported by other authors [136,157]. Owing to the extent of metal

surface coverage with NbO_x species, reduction temperatures higher than 350 °C seemed to be less beneficial for Nb_2O_5-supported noble metal catalysts.

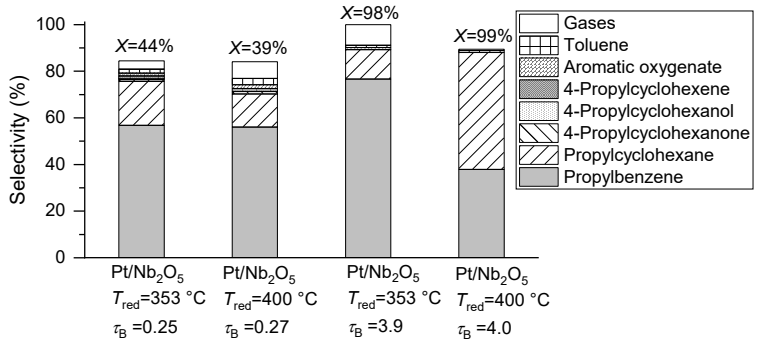

Figure 21. The effect of catalyst reduction temperature (353 or 400 °C) on the molar product selectivities of Pt/Nb_2O_5 catalyst at different batch residence times (τ_B = ~0.26 or 4.0 g_{cat} min $g_{reactant}^{-1}$). Reaction conditions: ~3% metal loading, 580 mg 4-propylphenol in 27 ml tetradecane, 350 °C, and 20 bar H_2. Reprinted from Publication V with permission from Wiley-VCH Verlag GmbH & Co. KGaA, copyright (2020).

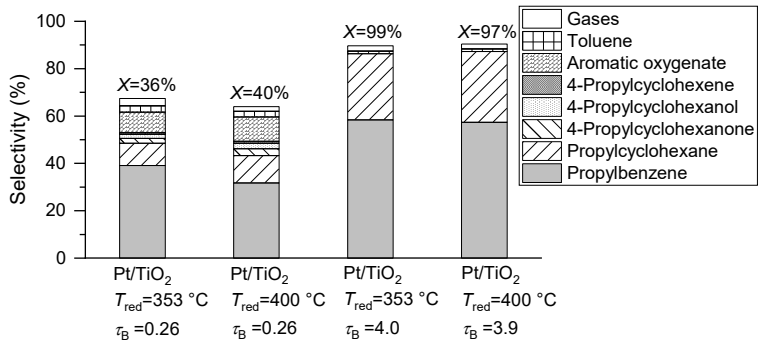

Figure 22. The effect of catalyst reduction temperature (353 or 400 °C) on the molar product selectivities of Pt/TiO_2 catalyst at different batch residence times (τ_B = ~0.26 or 4.0 g_{cat} min $g_{reactant}^{-1}$). Reaction conditions: ~3% metal loading, 580 mg 4-propylphenol in 27 ml tetradecane, 350 °C, and 20 bar H_2. Reprinted from Publication V with permission from Wiley-VCH Verlag GmbH & Co. KGaA, copyright (2020).

Spent catalysts were reused in the HDO of 4-propylphenol after they were recovered, washed with EtOH, and dried [V]. For the spent Pt/Nb_2O_5, Pt/TiO_2, and Pt/ZrO_2 catalysts, residence times of 0.49, 0.36, and 0.64 g_{cat} min $g_{reactant}^{-1}$, respectively, were applied to obtain comparable 50%–70% conversion levels of fresh catalysts. Significant decrease in the conversion levels of spent catalysts was observed (50% with Pt/Nb_2O_5, 44% with Pt/TiO_2, and 46% with Pt/ZrO_2) compared with the fresh catalysts with the same batch residence times [V]. Moreover, the selectivities to deoxygenated products decreased, whereas the selectivity to the aromatic oxygenate increased. In the spent catalysts, the observed deactivation can at least partly be attributable to the lower Pt loading (owing to leaching) and decreased metal dispersion.

7.2 Comparison of the obtained results to literature

One of the highest reported aromatic product selectivities in the literature is 99.5% (benzene) from phenol (98% conversion) using MoO_3 catalyst at 340 °C and 5 bar H_2 + 30 bar N_2 in paraffinic solvent [143]. Other studies have reported 4-propylphenol HDO in aqueous conditions to produce propylbenzene: 65%–85% propylbenzene selectivities at 300 °C and 20 bar H_2 using Pt/ZrO_2 and Pt–Re/ZrO_2 catalysts [146] and 54% propylbenzene yield with Re–Ni/ZrO_2 catalyst at 300 °C and 40 bar H_2 [144]. However, the aqueous medium complicated the product analysis owing to the presence of two liquid phases. Only one other study on the HDO of 4-propylphenol to propylbenzene in an organic medium was conducted by Ohta et al. [169], who used ionic liquids to modify the Pt catalyst surface and obtained 76% aromatic product yield at 110 °C. The best result reported in this thesis, 77% propylbenzene selectivity (98% conversion) with the Pt/Nb_2O_5 catalyst at 350 °C and 20 bar H_2 [V] is among the best results reported in the liquid-phase HDO of phenols. In line with prior studies [143,145], a decrease in the selectivity to the aromatic product after prolonged reaction times was observed (Figure 19a).

In conclusion, increased catalytic activity toward deoxygenation was obtained with the reducible supports (Nb_2O_5 and TiO_2) compared with ZrO_2; this finding is in line with other studies [137]. The activity enhancement may be attributable to the partial reduction of the supports, leading to oxophilic surface species. No correlation was found between the acidity or basicity of the catalysts and their activity in the HDO of 4-propylphenol, which was also consistent with the literature [136,154]. The tested catalysts suffered from deactivation, which has also been reported in other studies of noble metal catalysts on different oxide supports [35,154]. In this work, deactivation led to lower conversion levels and changes in the product distributions. In the literature, carbon deposition, metal sintering, loss of Lewis acid sites, and decrease in the number of oxophilic sites owing to strong adsorption of reaction intermediates have been reported to cause deactivation of the catalysts [35,154].

8. Conclusions

Lignocellulose can be considered as a potential raw material to produce second-generation renewable liquid fuels and chemicals. Owing to its complex structure, lignocellulose can be processed into several platform chemicals, including furfural, LA, and phenols, which can be further hydrotreated into valuable products. In this thesis, the hydrotreatment of lignocellulose-derived molecules to obtain biofuel components and renewable chemicals was studied in batch reactors.

Furfural can be further hydrotreated to MF, which is a potential biofuel component in gasoline. First, the hydrotreatment of furfural was conducted using Pt, Ru, and Ni catalysts supported on wood-based (spruce and birch sawdust) ACs. Both AC supports were active, and close to 50% MF yields were obtained using the noble metal catalysts. Although small differences were found between the support materials (e.g., oxygen content), neither one was found to be superior to the other. Factors affecting the MF selectivity were metal dispersion and particle size in addition to the reaction temperature. Second, furfural hydrotreatment was studied with Cu/Ni catalysts on bio-based ACFs from tannic acid and pine bark extracts. The suitability of the ACF materials as catalyst supports was evaluated by comparing them to spruce-based AC and two commercial AC supports. The tailorable porosity and potentially increased mechanical stability compared with ACs make ACFs interesting for catalytic purposes. The selectivity of the ACF-supported catalysts to MF was increased by nitric acid or sulfuric acid treatments, which increased the oxygen-containing surface groups on the supports. The highest MF yield of 48% was obtained using the Cu/Ni catalyst on HNO_3-treated pine-bark-extract–based support. However, even higher yields (58%–61%) were obtained with the AC-supported catalysts. Further research is suggested to combine the high activity and selectivity of the AC-supported catalysts and the mechanical stability of the ACF-supported catalysts. Moreover, attention should be focused on the environmental impact of the chemicals used for the preparation of different porosities of the ACFs.

LA is an interesting platform chemical, which can be converted into dimers via aldol condensation. Owing to the recent interest to obtain increased carbon-chain-length ($>C_6$) products from lignocellulosic sugars, the hydrotreatment of LA dimers was attempted in this thesis. First, the hydrotreatment of LA dimers was studied with a model compound, GNL, using Pt, Pd, Ru, and Rh catalysts supported on monoclinic ZrO_2. The initial conversion of the catalysts correlated with the amount of detected surface metal atoms (Rh >> Ru), whereas the highest selectivity (24%) to C_8 and C_9 hydrocarbons was obtained with the Ru catalyst. Significant differences were observed in the product distributions: Pt was selective to acids and esters, Pd mainly to acids, Rh to acids, and Ru to liquid and gaseous hydrocarbons. Second, the hydrotreatment of LA dimers was demonstrated using a Ru/ZrO_2 catalyst. The double bonds and ketone moieties were removed or intramolecularly lactonized in the catalytic experiments, which was evidenced by the saturation of the dimers. Deoxygenation and the formation of volatile products and aromatics increased with increasing reaction temperature. The volatile products mainly comprised acids, esters, and ketones as well as linear, branched, and cyclic hydrocarbons. Further catalyst and process development are needed to increase oxygen removal while avoiding oligomerization.

Pyrolysis and liquefaction biocrudes are versatile sources of chemicals and are especially rich in phenolic compounds. Phenols can be further hydrotreated to bio-based aromatics, which are important, for example, in renewable jet fuel. The hydrotreatment of a model compound, 4-propylphenol, was studied with Pt catalysts on reducible TiO_2 and Nb_2O_5 supports as well as on irreducible ZrO_2. The highest propylbenzene selectivity of 77% at 98% conversion level was obtained with the Pt/Nb_2O_5 catalyst. The Pt/Nb_2O_5 catalyst was also the most active among the tested catalysts, and compared with ZrO_2, the superior activity of the Nb_2O_5- and TiO_2-supported catalysts was thought to be attributable to the oxophilic sites created during catalyst reduction. Catalyst deactivation was observed, and the conversion levels of the spent catalysts decreased ~50% compared with the fresh catalyst. Thus, although promising yields were obtained with the Pt/Nb_2O_5 catalyst, further optimization is needed to decrease catalyst deactivation.

This thesis presented the conversion of versatile lignocellulosic platform molecules into value-added chemicals using alternative hydrotreatment catalysts. Some insights were reported for the first time, highlighting the potential of lignocellulose for use as a raw material in the chemical industry.

References

[1] J. Rogelj, D. Shindell, K. Jiang, S. Fifita, P. Forster, V. Ginzburg, C. Handa, H. Kheshgi, S. Kobayashi, E. Kriegler, L. Mundaca, R. Séférian, M.V. Vilariño, Mitigation pathways compatible with 1.5 °C in the context of sustainable development, in: Global Warming of 1.5 °C, 2018. https://www.ipcc.ch/site/assets/uploads/sites/2/2019/02/SR15_Chapter2_Low_Res.pdf. [Accessed:05.12.2020].

[2] Anon., International Energy Outlook 2019 with projections to 2050, (2019). https://www.iea.org/reports/world-energy-outlook-2019. [Accessed: 20.09.2020].

[3] C.L. Williams, R.M. Emerson, J.S. Tumuluru, Biomass compositional analysis for conversion to renewable fuels and chemicals, in: J.S. Tumuluru (Ed.), Biomass Vol. Estim. Valorization Energy, InTech, Rijeka, Croatia, 2017: pp. 251–270.

[4] S.N. Naik, V.V. Goud, P.K. Rout, A.K. Dalai, Production of first and second generation biofuels: a comprehensive review, Renew. Sustain. Energy Rev. 14 (2010) 578–597.

[5] H. Chen, J. Liu, X. Chang, D. Chen, Y. Xue, P. Liu, H. Lin, S. Han, A review on the pretreatment of lignocellulose for high-value chemicals, Fuel Process. Technol. 160 (2017) 196–206.

[6] T. Stedile, L. Ender, H.F. Meier, E.L. Simionatto, V.R. Wiggers, Comparison between physical properties and chemical composition of bio-oils derived from lignocellulose and triglyceride sources, Renew. Sustain. Energy Rev. 50 (2015) 92–108.

[7] S. Morales-Delarosa, and J.M. Campos-Martin, Catalytic processes and catalyst development in biorefining, in: K. Waldron (Ed.), Adv. Biorefineries Biomass Waste Supply Chain Exploit., Woodhead Publishing Limited, Cambridge, UK, 2014: pp. 152–198.

[8] T. Werpy, G. Petersen, Top Value Added Chemicals from Biomass Volume I — Results of Screening for Potential Candidates from Sugars and Synthesis Gas, 2004. 76 p.

[9] M. Dusselier, M. Mascal, B.F. Sels, Top chemical opportunities from carbohydrate biomass: a chemist's view of the biorefinery, in: K. Nicholas (Ed.), Sel. Catal. Renew. Feed. Chem., Springer, 2014: pp. 1–40.

[10] H. Wang, J. Male, Y. Wang, Recent advances in hydrotreating of pyrolysis bio-oil and its oxygen-containing model compounds, ACS Catal. 3 (2013) 1047–1070.

[11] R.G. dos Santos, A.C. Alencar, Biomass-derived syngas production via gasification process and its catalytic conversion into fuels by Fischer Tropsch synthesis: a review, Int. J. Hydrogen Energy 45 (2020) 18114–18132.

[12] M. Shahabuddin, M.T. Alam, B.B. Krishna, T. Bhaskar, G. Perkins, A review on the production of renewable aviation fuels from the gasification of biomass and residual wastes, Bioresour. Technol. 312 (2020) 123596.

[13] T. Su, D. Zhao, M. Khodadadi, C. Len, Lignocellulosic biomass for bioethanol: recent advances, technology trends, and barriers to industrial development, Curr. Opin. Green Sustain. Chem. 24 (2020) 56–60.

[14] P. Zhu, O.Y. Abdelaziz, C.P. Hulteberg, A. Riisager, New synthetic approaches to biofuels from lignocellulosic biomass, Curr. Opin. Green Sustain. Chem. 21 (2020) 16–21.

[15] W. Yin, M.V. Alekseeva, R.H. Venderbosch, V.A. Yakovlev, H.J. Heeres, Catalytic hydrotreatment of the pyrolytic sugar and pyrolytic lignin fractions of fast pyrolysis liquids using nickel based catalysts, Energies 13 (2020) 285.

[16] M.B. Figueirêdo, P.J. Deuss, R.H. Venderbosch, H.J. Heeres, Catalytic hydrotreatment of pyrolytic lignins from different sources to biobased chemicals: identification of feed-product relations, Biomass Bioenergy 134 (2020) 105484.

[17] J.C. Serrano-Ruiz, and J.A. Dumesic, Catalytic routes for the conversion of biomass into liquid hydrocarbon transportation fuels, Energy Environ. Sci. 4 (2011) 83–99.

[18] J.E. Tibaquirá, J.I. Huertas, S. Ospina, L.F. Quirama, J.E. Niño, The effect of using ethanol-gasoline blends on the mechanical, energy and environmental performance of in-use vehicles, Energies 11 (2018) 1–17.

[19] S. Srivastava, and J. Hancsók, Fuels and Fuel-Additives, John Wiley & Sons, Inc., New Jersey, US, 2014. 364 p.

[20] R. Lødeng, L. Hannevold, H. Bergem, M. Stöcker, Catalytic hydrotreatment of bio-oils for high-quality fuel production, in: K. Triantafyllidis, A. Lappas, M. Stöcker (Eds.), Role Catal. Sustain. Prod. Bio-Fuels Bio-Chemicals, 1st ed., Elsevier Science, 2013: pp. 351–396.

[21] S.M. Sadrameli, Thermal/catalytic cracking of liquid hydrocarbons for the production of olefins: a state-of-the-art review II: catalytic cracking review, Fuel 173 (2016) 285–297.

[22] I. Kuznecova, J. Gusca, Property based ranking of CO and CO_2 methanation catalysts, Energy Procedia 128

(2017) 255–260.
[23] J.Q. Bond, A.A. Upadhye, H. Olcay, G.A. Tompsett, J. Jae, R. Xing, D.M. Alonso, D. Wang, T. Zhang, R. Kumar, A. Foster, S.M. Sen, C.T. Maravelias, R. Malina, S.R.H. Barrett, R. Lobo, C.E. Wyman, J.A. Dumesic, G.W. Huber, Production of renewable jet fuel range alkanes and commodity chemicals from integrated catalytic processing of biomass, Energy Environ. Sci. 7 (2014) 1500–1523.
[24] F. Cheng, and C.E. Brewer, Producing jet fuel from biomass lignin: potential pathways to alkyl-benzenes and cycloalkanes, Renew. Sustain. Energy Rev. 72 (2017) 673–722.
[25] M. Breysse, P. Afanasiev, C. Geantet, M. Vrinat, Overview of support effects in hydrotreating catalysts, Catal. Today 86 (2003) 5–16.
[26] M. Mohammad, T.K. Hari, Z. Yaakob, Y.C. Sharma, K. Sopian, Overview on the production of paraffin based-biofuels via catalytic hydrodeoxygenation, Renew. Sustain. Energy Rev. 22 (2013) 121–132.
[27] A. Gutierrez, E.M. Turpeinen, T.R. Viljava, O. Krause, Hydrodeoxygenation of model compounds on sulfided CoMo/γ-Al_2O_3 and NiMo/γ-Al_2O_3 catalysts; role of sulfur-containing groups in reaction networks, Catal. Today 285 (2017) 125–134.
[28] K. Yan, G. Wu, T. Lafleur, C. Jarvis, Production, properties and catalytic hydrogenation of furfural to fuel additives and value-added chemicals, Renew. Sustain. Energy Rev. 38 (2014) 663–676.
[29] F. Dong, Y. Zhu, H. Zheng, Y. Zhu, X. Li, Y. Li, Cr-free Cu-catalysts for the selective hydrogenation of biomass-derived furfural to 2-methylfuran: the synergistic effect of metal and acid sites, J. Mol. Catal. A Chem. 398 (2015) 140–148.
[30] Y. Bie, A. Gutierrez, T.R. Viljava, J.M. Kanervo, J. Lehtonen, Hydrodeoxygenation of methyl heptanoate over noble metal catalysts: catalyst screening and reaction network, Ind. Eng. Chem. Res. 52 (2013) 11544–11551.
[31] A. Gutierrez, R.K. Kaila, M.L. Honkela, R. Slioor, A.O.I. Krause, Hydrodeoxygenation of guaiacol on noble metal catalysts, Catal. Today 147 (2009) 239–246.
[32] P. Rylander, Catalytic Hydrogenation over Platinum Metals, 1st ed., Academic Press, 1967. 564 p.
[33] C.M. Lok, Structure and performance of selective hydrogenation catalysts, in: S.D. Jackson (Ed.), Hydrog. Catal. Process., De Gruyter, Berlin, Germany, 2018: pp. 1–18.
[34] Anon., Fourth list of critical raw materials for the EU of 2020, (2020). https://ec.europa.eu/growth/sectors/raw-materials/specific-interest/critical_en. [Accessed: 04.03.2021].
[35] C.A. Teles, R.C. Rabelo-Neto, G. Jacobs, B.H. Davis, D.E. Resasco, F.B. Noronha, Hydrodeoxygenation of phenol over zirconia-supported catalysts: the effect of metal type on reaction mechanism and catalyst deactivation, ChemCatChem 9 (2017) 2850–2863.
[36] M.S. Scurrell, Heterogeneous catalysis on metal oxides, Annu. Reports Prog. Chem. Sect. A Phys. Inorg. Chem. 70 (1973) 87–122.
[37] E. Laurent, B. Delmon, Influence of water in the deactivation of a sulfided NiMo/gamma-Al_2O_3 catalyst during hydrodeoxygenation, J. Catal. 146 (1994) 281–285.
[38] T. Okuhara, Water-tolerant solid acid catalysts, Chem. Rev. 102 (2002) 3641–3666.
[39] A.R. Puigdollers, P. Schlexer, S. Tosoni, G. Pacchioni, Increasing oxide reducibility: the role of metal/oxide interfaces in the formation of oxygen vacancies, ACS Catal. 7 (2017) 6493–6513.
[40] S.J. Tauster, Strong metal-support interactions, Acc. Chem. Res. 20 (1987) 389–394.
[41] A. Mohammad-Khah, R. Ansari, Activated charcoal: preparation, characterization and applications: a review article, Int. J. ChemTech Res. 1 (2009) 859–864.
[42] A. Ahmadpour, D.D. Do, The preparation of active carbons from coal by chemical and physical activation, Carbon 34 (1996) 471–479.
[43] E. Kordouli, C. Kordulis, A. Lycourghiotis, R. Cole, P.T. Vasudevan, B. Pawelec, J.L.G. Fierro, HDO activity of carbon-supported Rh, Ni and Mo-Ni catalysts, Mol. Catal. 441 (2017) 209–220.
[44] M. Badawi, J.F. Paul, S. Cristol, E. Payen, Y. Romero, F. Richard, S. Brunet, D. Lambert, X. Portier, A. Popov, E. Kondratieva, J.M. Goupil, J. El Fallah, J.P. Gilson, L. Mariey, A. Travert, F. Maugé, Effect of water on the stability of Mo and CoMo hydrodeoxygenation catalysts: a combined experimental and DFT study, J. Catal. 282 (2011) 155–164.
[45] E. Lam, J.H.T. Luong, Carbon materials as catalyst supports and catalysts in the transformation of biomass to fuels and chemicals, ACS Catal. 4 (2014) 3393–3410.
[46] F. Rodríguez-Reinoso, The role of carbon materials in heterogeneous catalysis, Carbon 36 (1998) 159–175.
[47] P. Serp, and B. Machado, Nanostructured Carbon Materials for Catalysis, The Royal Society of Chemistry, Cambridge, UK, 2015. pp. 1-45.
[48] J.L. Figueiredo, M.F.R. Pereira, The role of surface chemistry in catalysis with carbons, Catal. Today 150 (2010) 2–7.
[49] C.R. Correa, and A. Kruse, Biobased functional carbon materials: production, characterization, and applications - a review, Materials 11 (2018) 1568.
[50] L. Prati, D. Bergna, A. Villa, P. Spontoni, C.L. Bianchi, T. Hu, H. Romar, U. Lassi, Carbons from second

generation biomass as sustainable supports for catalytic systems, Catal. Today 301 (2018) 239–243.
[51] R. Lahti, D. Bergna, H. Romar, T. Hu, A. Comazzi, C. Pirola, C.L. Bianchi, U. Lassi, Characterization of cobalt catalysts on biomass-derived carbon supports, Top. Catal. 60 (2017) 1415–1428.
[52] G.V. Plaksin, O.N. Baklanova, A.V. Lavrenov, V.A. Likholobov, Carbon materials from the Sibunit family and methods for controlling their properties, Solid Fuel Chem. 48 (2014) 349–355.
[53] A. Amaya, N. Medero, N. Tancredi, H. Silva, C. Deiana, Activated carbon briquettes from biomass materials, Bioresour. Technol. 98 (2007) 1635–1641.
[54] T. Varila, H. Romar, U. Lassi, Catalytic effect of transition metals (copper, iron, and nickel) on the foaming and properties of sugar-based carbon foams, Top. Catal. 62 (2019) 764–772.
[55] A.K. Kumar, and S. Sharma, Recent updates on different methods of pretreatment of lignocellulosic feedstocks: a review, Bioresour. Bioprocess. 4 (2017).
[56] Y. Sun, J. Cheng, Hydrolysis of lignocellulosic materials for ethanol production: a review, Bioresour. Technol. 83 (2002) 1–11.
[57] J.N. Chheda, G.W. Huber, J.A. Dumesic, Liquid-phase catalytic processing of biomass-derived oxygenated hydrocarbons to fuels and chemicals, Angew. Chemie - Int. Ed. 46 (2007) 7164–7183.
[58] M.J. Climent, A. Corma, S. Iborra, Conversion of biomass platform molecules into fuel additives and liquid hydrocarbon fuels, Green Chem. 16 (2014) 516–547.
[59] X. Tang, X. Zeng, Z. Li, L. Hu, Y. Sun, S. Liu, T. Lei, L. Lin, Production of γ-valerolactone from lignocellulosic biomass for sustainable fuels and chemicals supply, Renew. Sustain. Energy Rev. 40 (2014) 608–620.
[60] M. Dashtban, A. Gilbert, P. Fatehi, Production of furfural: overview and challenges, J-For. 2 (2012) 44–53.
[61] R. Karinen, K. Vilonen, M. Niemelä, Biorefining: heterogeneously catalyzed reactions of carbohydrates for the production of furfural and hydroxymethylfurfural, ChemSusChem 4 (2011) 1002–1016.
[62] D.J. Hayes, S.W. Fitzpatrick, M.H.B. Hayes, J.R.H. Ross, The Biofine process - production of levulinic acid, furfural, and formic acid from lignocellulosic feedstocks, in: B. Kamm, P.R. Gruber, M. Kamm (Eds.), Biorefineries - Ind. Process. Prod. Status Quo Futur. Dir., John Wiley & Sons, Inc., Weinheim, Germany, 2006: pp. 139–163.
[63] R. Mariscal, P. Maireles-Torres, M. Ojeda, I. Sádaba, M. López Granados, Furfural: a renewable and versatile platform molecule for the synthesis of chemicals and fuels, Energy Environ. Sci. 9 (2016) 1144–1189.
[64] S. Xu, N. Wu, H. Yuan, Y. Chen, D. Pan, Y. Wu, J. Fan, L. Gao, G. Xiao, An effective and stable HfP/SiO_2 catalyst for the production of furfural from xylan, Catal. Lett. 150 (2020) 1121–1127.
[65] A. Mukherjee, M.J. Dumont, V. Raghavan, Review: sustainable production of hydroxymethylfurfural and levulinic acid: challenges and opportunities, Biomass Bioenergy 72 (2015) 143–183.
[66] D.S. Bajwa, G. Pourhashem, A.H. Ullah, S.G. Bajwa, A concise review of current lignin production, applications, products and their environment impact, Ind. Crops Prod. 139 (2019) 111526.
[67] Q. Bu, H. Lei, A.H. Zacher, L. Wang, S. Ren, J. Liang, Y. Wei, Y. Liu, J. Tang, Q. Zhang, R. Ruan, A review of catalytic hydrodeoxygenation of lignin-derived phenols from biomass pyrolysis, Bioresour. Technol. 124 (2012) 470–477.
[68] L. Fele Žilnik, and A. Jazbinšek, Recovery of renewable phenolic fraction from pyrolysis oil, Sep. Purif. Technol. 86 (2012) 157–170.
[69] J.P. Lange, Lignocellulose liquefaction to biocrude: a tutorial review, ChemSusChem 11 (2018) 997–1014.
[70] J.Y. Kim, H.W. Lee, S.M. Lee, J. Jae, Y.K. Park, Overview of the recent advances in lignocellulose liquefaction for producing biofuels, bio-based materials and chemicals, Bioresour. Technol. 279 (2019) 373–384.
[71] J.A. Ramirez, R.J. Brown, T.J. Rainey, A review of hydrothermal liquefaction bio-crude properties and prospects for upgrading to transportation fuels, Energies 8 (2015) 6765–6794.
[72] A.V. Bridgwater, Review of fast pyrolysis of biomass and product upgrading, Biomass Bioenergy 38 (2012) 68–94.
[73] R.H. Kottke, Furan derivatives, in: Kirk-Othmer Encycl. Chem. Technol., John Wiley & Sons, Inc., 2000: pp. 259–286.
[74] Rodiansono, M. Dewi Astuti, T. Hara, N. Ichikuni, S. Shimazu, One-pot selective conversion of C_5-furan into 1,4-pentanediol over bulk Ni-Sn alloy catalysts in an ethanol/H_2O solvent mixture, Green Chem. 21 (2019) 2307–2315.
[75] M. Hronec, and K. Fulajtarová, Selective transformation of furfural to cyclopentanone, Catal. Commun. 24 (2012) 100–104.
[76] M. Hronec, K. Fulajtarová, T. Liptaj, Effect of catalyst and solvent on the furan ring rearrangement to cyclopentanone, Appl. Catal. A Gen. 437–438 (2012) 104–111.
[77] V.V. Ordomsky, J.C. Schouten, J. van der Schaaf, T.A. Nijhuis, Biphasic single-reactor process for dehydration of xylose and hydrogenation of produced furfural, Appl. Catal. A Gen. 451 (2013) 6–13.
[78] H. Wei, D. Gao, L. Zhou, D. Feng, C. Chen, Z. Pei, Experimental analysis on spray development of 2-

methylfuran-gasoline blends using multi-hole DI injector, Fuel 164 (2016) 245–253.
[79] S. Sitthisa, W. An, D.E. Resasco, Selective conversion of furfural to methylfuran over silica-supported NiFe bimetallic catalysts, J. Catal. 284 (2011) 90–101.
[80] H. Wei, D. Feng, G. Shu, M. Pan, Y. Guo, D. Gao, W. Li, Experimental investigation on the combustion and emissions characteristics of 2-methylfuran gasoline blend fuel in spark-ignition engine, Appl. Energy 132 (2014) 317–324.
[81] K. Xiong, W. Wan, J.G. Chen, Reaction pathways of furfural, furfuryl alcohol and 2-methylfuran on Cu(111) and NiCu bimetallic surfaces, Surf. Sci. 652 (2016) 91–97.
[82] S. Chen, R. Wojcieszak, F. Dumeignil, E. Marceau, S. Royer, How catalysts and experimental conditions determine the selective hydroconversion of furfural and 5-hydroxymethylfurfural, Chem. Rev. 118 (2018) 11023–11117.
[83] H. Li, H. Luo, L. Zhuang, W. Dai, M. Qiao, Liquid phase hydrogenation of furfural to furfuryl alcohol over the Fe-promoted Ni-B amorphous alloy catalysts, J. Mol. Catal. A Chem. 203 (2003) 267–275.
[84] J. Kijeński, P. Winiarek, T. Paryjczak, A. Lewicki, A. Mikolajska, Platinum deposited on monolayer supports in selective hydrogenation of furfural to furfuryl alcohol, Appl. Catal. A Gen. 233 (2002) 171–182.
[85] B.J. Liaw, S.J. Chiang, S.W. Chen, Y.Z. Chen, Preparation and catalysis of amorphous CoNiB and polymer-stabilized CoNiB catalysts for hydrogenation of unsaturated aldehydes, Appl. Catal. A Gen. 346 (2008) 179–188.
[86] S. Sitthisa, and D.E. Resasco, Hydrodeoxygenation of furfural over supported metal catalysts: a comparative study of Cu, Pd and Ni, Catal. Lett. 141 (2011) 784–791.
[87] S. Sitthisa, T. Sooknoi, Y. Ma, P.B. Balbuena, D.E. Resasco, Kinetics and mechanism of hydrogenation of furfural on Cu/SiO_2 catalysts, J. Catal. 277 (2011) 1–13.
[88] H.Y. Zheng, Y.L. Zhu, B.T. Teng, Z.Q. Bai, C.H. Zhang, H.W. Xiang, Y.W. Li, Towards understanding the reaction pathway in vapour phase hydrogenation of furfural to 2-methylfuran, J. Mol. Catal. A Chem. 246 (2006) 18–23.
[89] P. Panagiotopoulou, and D.G. Vlachos, Liquid phase catalytic transfer hydrogenation of furfural over a Ru/C catalyst, Appl. Catal. A Gen. 480 (2014) 17–24.
[90] P. Panagiotopoulou, N. Martin, D.G. Vlachos, Effect of hydrogen donor on liquid phase catalytic transfer hydrogenation of furfural over a $Ru/RuO_2/C$ catalyst, J. Mol. Catal. A Chem. 392 (2014) 223–228.
[91] J.J. Musci, A.B. Merlo, M.L. Casella, Aqueous phase hydrogenation of furfural using carbon-supported Ru and RuSn catalysts, Catal. Today 296 (2017) 43–50.
[92] N.S. Biradar, A.A. Hengne, S.N. Birajdar, R. Swami, C.V. Rode, Tailoring the product distribution with batch and continuous process options in catalytic hydrogenation of furfural, Org. Process Res. Dev. 18 (2014) 1434–1442.
[93] P.D. Vaidya, and V.V. Mahajani, Kinetics of liquid-phase hydrogenation of furfuraldehyde to furfuryl alcohol over a Pt/C catalyst, Ind. Eng. Chem. Res. 42 (2003) 3881–3885.
[94] S.K. Jaatinen, R.S. Karinen, J.S. Lehtonen, Liquid phase furfural hydrotreatment to 2-methylfuran on carbon supported nickel catalyst - effect of process conditions, ChemistrySelect 1 (2016) 5363–5373.
[95] S.K. Jaatinen, R.S. Karinen, J.S. Lehtonen, Liquid phase furfural hydrotreatment to 2-methylfuran with carbon supported copper, nickel, and iron catalysts, ChemistrySelect 2 (2017) 51–60.
[96] W. Gong, C. Chen, H. Zhang, G. Wang, H. Zhao, Efficient synthesis of 2-methylfuran from bio-derived furfural over supported copper catalyst: the synergistic effect of CuO_x and Cu, ChemistrySelect 2 (2017) 9984–9991.
[97] F. Dong, G. Ding, H. Zheng, X. Xiang, L. Chen, Y. Zhu, Y. Li, Highly dispersed Cu nanoparticles as an efficient catalyst for the synthesis of the biofuel 2-methylfuran, Catal. Sci. Technol. 6 (2016) 767–779.
[98] Z. Fu, Z. Wang, W. Lin, W. Song, Conversion of furan derivatives for preparation of biofuels over Ni–Cu/C catalyst, Energy Sources, Part A Recover. Util. Environ. Eff. 39 (2017) 1176–1181.
[99] Z. Fu, Z. Wang, W. Lin, W. Song, S. Li, High efficient conversion of furfural to 2-methylfuran over Ni-Cu/Al_2O_3 catalyst with formic acid as a hydrogen donor, Appl. Catal. A Gen. 547 (2017) 248–255.
[100] N.S. Date, A.M. Hengne, K.W. Huang, R.C. Chikate, C.V. Rode, Single pot selective hydrogenation of furfural to 2-methylfuran over carbon supported iridium catalysts, Green Chem. 20 (2018) 2027–2037.
[101] P. Liu, L. Sun, X. Jia, C. Zhang, W. Zhang, Y. Song, H. Wang, C. Li, Efficient one-pot conversion of furfural into 2-methyltetrahydrofuran using non-precious metal catalysts, Mol. Catal. 490 (2020) 110951.
[102] B. Li, L. Li, H. Sun, C. Zhao, Selective deoxygenation of aqueous furfural to 2-methylfuran over $Cu0/Cu_2O{\cdot}SiO_2$ sites via a copper phyllosilicate precursor without extraneous gas, ACS Sustain. Chem. Eng. 6 (2018) 12096–12103.
[103] W. Geng, W. Li, L. Liu, J. Liu, L. Liu, X. Kong, Facile assembly of Cu-Cu_2O/N-reduced graphene oxide nanocomposites for efficient synthesis of 2-methylfuran, Fuel 259 (2020) 116267.
[104] T. Varila, H. Romar, T. Luukkonen, U. Lassi, Physical activation and characterization of tannin-based foams enforced with boric acid and zinc chloride, AIMS Mater. Sci. 6 (2019) 301–314.

[105] V. Choudhary, A.B. Pinar, S.I. Sandler, D.G. Vlachos, R.F. Lobo, Xylose isomerization to xylulose and its dehydration to furfural in aqueous media, ACS Catal. 1 (2011) 1724–1728.
[106] M. Käldström, M. Lindblad, K. Lamminpää, S. Wallenius, S. Toppinen, Carbon chain length increase reactions of platform molecules derived from C_5 and C_6 sugars, Ind. Eng. Chem. Res. 56 (2017) 13356–13366.
[107] M. Mascal, S. Dutta, I. Gandarias, Hydrodeoxygenation of the angelica lactone dimer, a cellulose-based feedstock: simple, high-yield synthesis of branched C_7-C_{10} gasoline-like hydrocarbons, Angew. Chemie - Int. Ed. 53 (2014) 1854–1857.
[108] G.W. Huber, J.N. Chheda, C.J. Barrett, J.A. Dumesic, Production of liquid alkanes by aqueous-phase processing of biomass-derived carbohydrates, Science 308 (2005) 1446–1450.
[109] R.M. West, Z.Y. Liu, M. Peter, J.A. Dumesic, Liquid alkanes with targeted molecular weights from biomass-derived carbohydrates, ChemSusChem 1 (2008) 417–424.
[110] J. Wilson, and E.Y.X. Chen, Organocatalytic cross-coupling of biofuranics to multifunctional difuranic C_{11} building blocks, ACS Sustain. Chem. Eng. 4 (2016) 4927–4936.
[111] H. Zang, and E.Y.X. Chen, Organocatalytic upgrading of furfural and 5-hydroxymethyl furfural to C_{10} and C_{12} furoins with quantitative yield and atom-efficiency, Int. J. Mol. Sci. 16 (2015) 7143–7158.
[112] G. Li, N. Li, Z. Wang, C. Li, A. Wang, X. Wang, Y. Cong, T. Zhang, Synthesis of high-quality diesel with furfural and 2-methylfuran from hemicellulose, ChemSusChem 5 (2012) 1958–1966.
[113] A. Corma, O. de la Torre, M. Renz, Production of high quality diesel from cellulose and hemicellulose by the Sylvan process: catalysts and process variables, Energy Environ. Sci. 5 (2012) 6328–6344.
[114] R.Q. Raguindin, M.N. Gebresillase, S.J. Han, J.G. Seo, Hydroxyalkylation/alkylation of 2-methylfuran and furfural over niobic acid catalysts for the synthesis of high carbon transport fuel precursors, Sustain. Energy Fuels 4 (2020) 3018–3028.
[115] J.Q. Bond, D.M. Alonso, D. Wang, R.M. West, J.A Dumesic, Integrated catalytic conversion of γ-valerolactone to liquid alkenes for transportation fuels, Science (2010) 1110–1114.
[116] J.C. Serrano-Ruiz, D. Wang, J.A. Dumesic, Catalytic upgrading of levulinic acid to 5-nonanone, Green Chem. 12 (2010) 574–577.
[117] J.C. Serrano-Ruiz, D.J. Braden, R.M. West, J.A. Dumesic, Conversion of cellulose to hydrocarbon fuels by progressive removal of oxygen, Appl. Catal. B Environ. 100 (2010) 184–189.
[118] K. Yan, C. Jarvis, J. Gu, Y. Yan, Production and catalytic transformation of levulinic acid: a platform for speciality chemicals and fuels, Renew. Sustain. Energy Rev. 51 (2015) 986–997.
[119] J.J. Bozell, L. Moens, D.C. Elliott, Y. Wang, G.G. Neuenscwander, S.W. Fitzpatrick, R.J. Bilski, J.L. Jarnefeld, Production of levulinic acid and use as a platform chemical for derived products, Resour. Conserv. Recycl. 28 (2000) 227–239.
[120] K. Yan, Y. Yang, J. Chai, Y. Lu, Catalytic reactions of gamma-valerolactone: a platform to fuels and value-added chemicals, Appl. Catal. B Environ. 179 (2015) 292–304.
[121] R.W. Blessing, and L. Petrus, A catalytic process for the dimerization of levulinic acid and the preparation of diesters from these dimers obtainable by such process, WO 2006/056591 A1, 2006.
[122] L. Faba, E. Díaz, S. Ordóñez, Base-catalyzed condensation of levulinic acid: a new biorefinery upgrading approach, ChemCatChem 8 (2016) 1490–1494.
[123] Z. Li, J. Zhang, M.M. Nielsen, H. Wang, C. Chen, J. Xu, Y. Wang, T. Deng, X. Hou, Efficient C–C bond formation between two levulinic acid molecules to produce C_{10} compounds with the cooperation effect of Lewis and Brønsted acids, ACS Sustain. Chem. Eng. 6 (2018) 5708–5711.
[124] A.S. Amarasekara, B. Wiredu, T.L. Grady, R.G. Obregon, D. Margetić, Solid acid catalyzed aldol dimerization of levulinic acid for the preparation of C_{10} renewable fuel and chemical feedstocks, Catal. Commun. 124 (2019) 6–11.
[125] M. Grilc, and B. Likozar, Levulinic acid hydrodeoxygenation, decarboxylation and oligmerization over $NiMo/Al_2O_3$ catalyst to bio-based value-added chemicals: modelling of mass transfer, thermodynamics and micro-kinetics, Chem. Eng. J. 330 (2017) 383–397.
[126] B. Cornils, and P. Lappe, Dicarboxylic acids, aliphatic, in: Ullmann's Encycl. Ind. Chem., Wiley-VCH Verlag GmbH & Co. KGaA, Weinheim, Germany, 2014: pp. 1–18.
[127] P.J. van den Brink, K.L. von Hebel, J.-P. Lange, L. Petrus, A process for the hydrogenation of a lactone or of a carboxylic acid or an ester having a gamma-carbonyl group, WO2006067171, 2006.
[128] K.T. Jung, and A.T. Bell, The effects of synthesis and pretreatment conditions on the bulk structure and surface properties of zirconia, J. Mol. Catal. A Chem. 163 (2000) 27–42.
[129] M. Chia, Y.J. Pagán-Torres, D. Hibbitts, Q. Tan, H.N. Pham, A.K. Datye, M. Neurock, R.J. Davis, J.A. Dumesic, Selective hydrogenolysis of polyols and cyclic ethers over bifunctional surface sites on rhodium-rhenium catalysts, J. Am. Chem. Soc. 133 (2011) 12675–12689.
[130] X. Huang, J.M. Ludenhoff, M. Dirks, X. Ouyang, M.D. Boot, E.J.M. Hensen, Selective production of biobased phenol from lignocellulose-derived alkylmethoxyphenols, ACS Catal. 8 (2018) 11184–11190.

[131] Y. Zhang, H. Lei, Z. Yang, K. Qian, E. Villota, Renewable high-purity mono-phenol production from catalytic microwave-induced pyrolysis of cellulose over biomass-derived activated carbon catalyst, ACS Sustain. Chem. Eng. 6 (2018) 5349–5357.
[132] P.M. de Souza, R.C. Rabelo-Neto, L.E.P. Borges, G. Jacobs, B.H. Davis, T. Sooknoi, D.E. Resasco, F.B. Noronha, Role of keto intermediates in the hydrodeoxygenation of phenol over Pd on oxophilic supports, ACS Catal. 5 (2015) 1318–1329.
[133] Q. Tan, G. Wang, L. Nie, A. Dinse, C. Buda, J. Shabaker, D.E. Resasco, Different product distributions and mechanistic aspects of the hydrodeoxygenation of *m*-cresol over platinum and ruthenium catalysts, ACS Catal. 5 (2015) 6271–6283.
[134] A.J.R. Hensley, Y. Wang, J.S. McEwen, Phenol deoxygenation mechanisms on Fe(110) and Pd(111), ACS Catal. 5 (2015) 523–536.
[135] A.J. Foster, P.T.M. Do, R.F. Lobo, The synergy of the support acid function and the metal function in the catalytic hydrodeoxygenation of *m*-cresol, Top. Catal. 55 (2012) 118–128.
[136] A.M. Barrios, C.A. Teles, P.M. de Souza, R.C. Rabelo-Neto, G. Jacobs, B.H. Davis, L.E.P. Borges, F.B. Noronha, Hydrodeoxygenation of phenol over niobia supported Pd catalyst, Catal. Today 302 (2018) 115–124.
[137] M.B. Griffin, G.A. Ferguson, D.A. Ruddy, M.J. Biddy, G.T. Beckham, J.A. Schaidle, Role of the support and reaction conditions on the vapor-phase deoxygenation of *m*-cresol over Pt/C and Pt/TiO_2 catalysts, ACS Catal. 6 (2016) 2715–2727.
[138] I.T. Ghampson, C. Sepúlveda, A.B. Dongil, G. Pecchi, R. García, J.L.G. Fierro, N. Escalona, Phenol hydrodeoxygenation: effect of support and Re promoter on the reactivity of Co catalysts, Catal. Sci. Technol. 6 (2016) 7289–7306.
[139] A.N. Kay Lup, F. Abnisa, W.M.A.W. Daud, M.K. Aroua, A review on reaction mechanisms of metal-catalyzed deoxygenation process in bio-oil model compounds, Appl. Catal. A Gen. 541 (2017) 87–106.
[140] J. Zakzeski, P.C.A. Bruijnincx, A.L. Jongerius, B.M. Weckhuysen, The catalytic valorization of lignin for the production of renewable chemicals, Chem. Rev. 110 (2010) 3552–3599.
[141] Y. Zhang, P. Bi, J. Wang, P. Jiang, X. Wu, H. Xue, J. Liu, X. Zhou, Q. Li, Production of jet and diesel biofuels from renewable lignocellulosic biomass, Appl. Energy 150 (2015) 128–137.
[142] H. Wei, W. Liu, X. Chen, Q. Yang, J. Li, H. Chen, Renewable bio-jet fuel production for aviation: a review, Fuel 254 (2019) 115599.
[143] X. Zhang, J. Tang, Q. Zhang, Q. Liu, Y. Li, L. Chen, C. Wang, L. Ma, Hydrodeoxygenation of lignin-derived phenolic compounds into aromatic hydrocarbons under low hydrogen pressure using molybdenum oxide as catalyst, Catal. Today 319 (2019) 41–47.
[144] B. Feng, H. Kobayashi, H. Ohta, A. Fukuoka, Aqueous-phase hydrodeoxygenation of 4-propylphenol as a lignin model to *n*-propylbenzene over Re-Ni/ZrO_2 catalysts, J. Mol. Catal. A Chem. 388–389 (2014) 41–46.
[145] V.M.L. Whiffen, and K.J. Smith, Hydrodeoxygenation of 4-methylphenol over unsupported MoP, MoS_2, and MoO_x catalysts, Energy Fuels 24 (2010) 4728–4737.
[146] H. Ohta, B. Feng, H. Kobayashi, K. Hara, A. Fukuoka, Selective hydrodeoxygenation of lignin-related 4-propylphenol into *n*-propylbenzene in water by Pt-Re/ZrO_2 catalysts, Catal. Today 234 (2014) 139–144.
[147] D. Garcia-Pintos, J. Voss, A.D. Jensen, F. Studt, Hydrodeoxygenation of phenol to benzene and cyclohexane on Rh(111) and Rh(211) surfaces: insights from density functional theory, J. Phys. Chem. C. 120 (2016) 18529–18537.
[148] Q. Sun, G. Chen, H. Wang, X. Liu, J. Han, Q. Ge, X. Zhu, Insights into the major reaction pathways of vapor-phase hydrodeoxygenation of *m*-cresol on a Pt/HBeta catalyst, ChemCatChem 8 (2016) 551–561.
[149] E. Kordouli, B. Pawelec, C. Kordulis, A. Lycourghiotis, J.L.G. Fierro, Hydrodeoxygenation of phenol on bifunctional Ni-based catalysts: effects of Mo promotion and support, Appl. Catal. B Environ. 238 (2018) 147–160.
[150] H. Ohta, H. Kobayashi, K. Hara, A. Fukuoka, Hydrodeoxygenation of phenols as lignin models under acid-free conditions with carbon-supported platinum catalysts, Chem. Commun. 47 (2011) 12209–12211.
[151] S. Velu, M.P. Kapoor, S. Inagaki, K. Suzuki, Vapor phase hydrogenation of phenol over palladium supported on mesoporous CeO_2 and ZrO_2, Appl. Catal. A Gen. 245 (2003) 317–331.
[152] M.S. Zanuttini, B.O. Dalla Costa, C.A. Querini, M.A. Peralta, Hydrodeoxygenation of *m*-cresol with Pt supported over mild acid materials, Appl. Catal. A Gen. 482 (2014) 352–361.
[153] C. Newman, X. Zhou, B. Goundie, I.T. Ghampson, R.A. Pollock, Z. Ross, M.C. Wheeler, R.W. Meulenberg, R.N. Austin, B.G. Frederick, Effects of support identity and metal dispersion in supported ruthenium hydrodeoxygenation catalysts, Appl. Catal. A Gen. 477 (2014) 64–74.
[154] P.M. de Souza, R.C. Rabelo-Neto, L.E.P. Borges, G. Jacobs, B.H. Davis, D.E. Resasco, F.B. Noronha, Hydrodeoxygenation of phenol over Pd catalysts. Effect of support on reaction mechanism and catalyst deactivation, ACS Catal. 7 (2017) 2058–2073.
[155] X. Xiao, H. Bergstrom, R. Saenger, B. Johnson, R. Sun, A. Peterson, The role of oxygen vacancies in biomass

deoxygenation by reducible zinc/zinc oxide catalysts, Catal. Sci. Technol. 8 (2018) 1819–1827.
[156] S.M. Schimming, O.D. Lamont, M. König, A.K. Rogers, A.D. D'Amico, M.M. Yung, C. Sievers, Hydrodeoxygenation of guaiacol over ceria-zirconia catalysts, ChemSusChem 8 (2015) 2073–2083.
[157] K. Kon, W. Onodera, S. Takakusagi, K.I. Shimizu, Hydrodeoxygenation of fatty acids and triglycerides by Pt-loaded Nb_2O_5 catalysts, Catal. Sci. Technol. 4 (2014) 3705–3712.
[158] M. V. Cagnoli, A.M. Alvarez, N.G. Gallegos, J.F. Bengoa, C.D.D. de Souza, M. Schmal, S.G. Marchetti, Mössbauer and XPS spectroscopies studies of SMSI effect on Fe/Nb_2O_5 catalysts for the Fischer-Tropsch synthesis, Appl. Catal. A Gen. 326 (2007) 113–119.
[159] H. Wan, R.V. Chaudhari, B. Subramaniam, Catalytic hydroprocessing of *p*-cresol: metal, solvent and mass-transfer effects, Top. Catal. 55 (2012) 129–139.
[160] J. He, C. Zhao, J.A. Lercher, Impact of solvent for individual steps of phenol hydrodeoxygenation with Pd/C and HZSM-5 as catalysts, J. Catal. 309 (2014) 362–375.
[161] M. Hellinger, H.W.P. de Carvalho, S. Baier, L. Gharnati, J.-D. Grunwaldt, Solvent influence on the hydrodeoxygenation of guaiacol over Pt/SiO_2 and Pt/H-MFI-90 catalysts, Chemie Ing. Tech. 87 (2015) 1771–1780.
[162] S.K. Wu, P.C. Lai, Y.C. Lin, H.P. Wan, H.T. Lee, Y.H. Chang, Atmospheric hydrodeoxygenation of guaiacol over alumina-, zirconia-, and silica-supported nickel phosphide catalysts, ACS Sustain. Chem. Eng. 1 (2013) 349–358.
[163] H.Y. Zhao, D. Li, P. Bui, S.T. Oyama, Hydrodeoxygenation of guaiacol as model compound for pyrolysis oil on transition metal phosphide hydroprocessing catalysts, Appl. Catal. A Gen. 391 (2011) 305–310.
[164] D.A. Ruddy, J.A. Schaidle, J.R. Ferrell III, J. Wang, L. Moens, J.E. Hensley, Recent advances in heterogeneous catalysts for bio-oil upgrading via "*ex situ* catalytic fast pyrolysis": catalyst development through the study of model compounds, Green Chem. 16 (2014) 454–490.
[165] H. Pourzolfaghar, F. Abnisa, W.M.A. Wan Daud, M.K. Aroua, Atmospheric hydrodeoxygenation of bio-oil oxygenated model compounds: a review, J. Anal. Appl. Pyrolysis 133 (2018) 117–127.
[166] Z. Zheng, Z. Luo, C. Zhao, Morphologically cross-shaped Ru/HZSM-5 catalyzes tandem hydrogenolysis of guaiacol to benzene in water, ChemCatChem 10 (2018) 1376–1384.
[167] R.C. Nelson, B. Baek, P. Ruiz, B. Goundie, A. Brooks, M.C. Wheeler, B.G. Frederick, L.C. Grabow, R.N. Austin, Experimental and theoretical insights into the hydrogen-efficient direct hydrodeoxygenation mechanism of phenol over Ru/TiO_2, ACS Catal. 5 (2015) 6509–6523.
[168] K.L. Luska, P. Migowski, S. El Sayed, W. Leitner, Synergistic interaction within bifunctional ruthenium nanoparticle/SILP catalysts for the selective hydrodeoxygenation of phenols, Angew. Chemie. 127 (2015) 15976–15981.
[169] H. Ohta, K. Tobayashi, A. Kuroo, M. Nakatsuka, H. Kobayashi, A. Fukuoka, G. Hamasaka, Y. Uozumi, H. Murayama, M. Tokunaga, M. Hayashi, Surface modification of a supported Pt catalyst using ionic liquids for selective hydrodeoxygenation of phenols into arenes under mild conditions, Chem. – A Eur. J. 25 (2019) 14762–14766.
[170] Anon., Solid biofuels - determination of ash content, FprEN 14775:2009 (E), 2005.
[171] S. Brunauer, P.H. Emmett, E. Teller, Adsorption of gases in multimolecular layers, J. Am. Chem. Soc. 60 (1938) 309–319.
[172] E.P. Barrett, L.G. Joyner, P.P. Halenda, The determination of pore volume and area distributions in porous substances. I. Computations from nitrogen isotherms, J. Am. Chem. Soc. 73 (1951) 373–380.
[173] P. Tarazona, U.M.B. Marconi, R. Evans, Phase equilibria of fluid interfaces and confined fluids, Mol. Phys. 60 (1987) 573–595.
[174] P. Tarazona, Erratum: free-energy density functional for hard spheres, Phys. Rev. A. 32 (1985) 3148–3148.
[175] X. Shen, L. Garces, Y. Ding, K. Laubernds, R.P. Zerger, M. Aindow, E.J. Neth, S.L. Suib, Behavior of H_2 chemisorption on Ru/TiO_2 surface and its application in evaluation of Ru particle sizes compared with TEM and XRD analyses, Appl. Catal. A Gen. 335 (2008) 187–195.
[176] G. Bergeret, and P. Gallezot, Particle size and dispersion measurements, in: G. Ertl, H. Knözinger, F. Schuth, J. Weitkamp (Eds.), Handb. Heteregeneous Catal., 2nd ed., Wiley–VHC Verlag GmbH & Co. KGaA, Weinheim, Germany, 2008: pp. 738–746.
[177] B.M. Babić, S.K. Milonjić, M.J. Polovina, B.V. Kaludierović, Point of zero charge and intrinsic equilibrium constants of activated carbon cloth, Carbon 37 (1999) 477–481.
[178] J.T. Scanlon, and D.E. Willis, Calculation of flame ionization detector relative response factors using the effective carbon number concept, J. Chromatogr. Sci. 23 (1985) 333–340.
[179] A.D. Jorgensen, K.C. Picel, V.C. Stamoudis, Prediction of gas chromatography flame ionization detector response factors from molecular structures, Anal. Chem. 62 (1990) 683–689.
[180] S. Jaatinen, M. Stekrova, R. Karinen, Ni- and CuNi-modified activated carbons and ordered mesoporous CMK-3 for furfural hydrotreatment, J. Porous Mater. 25 (2018) 1147–1160.
[181] C. Prado-Burguete, A. Linares-Solano, F. Rodríguez-Reinoso, C. Salinas-Martínezde de Lecea, The effect of

oxygen surface groups of the support on platinum dispersion in Pt/carbon catalysts, J. Catal. 115 (1989) 98–106.
[182] A. Dandekar, R.T.K. Baker, M.A. Vannice, Carbon-supported copper catalysts: II. crotonaldehyde hydrogenation, J. Catal. 184 (1999) 421–439.
[183] S.L. Yao, C.H. Yang, Y.S. Tan, Y.Z. Han, Deactivation of activated carbon supported nickel-palladium catalyst for vapor phase carbonylation of methanol, J. Fuel Chem. Technol. 34 (2006) 706–711.
[184] J. Huo, H.N. Pham, Y. Cheng, H.H. Lin, L.T. Roling, A.K. Datye, B.H. Shanks, Deactivation and regeneration of carbon supported Pt and Ru catalysts in aqueous phase hydrogenation of 2-pentanone, Catal. Sci. Technol. 10 (2020) 3047–3056.
[185] B. Lin, Y. Guo, J. Lin, J. Ni, J. Lin, L. Jiang, Y. Wang, Deactivation study of carbon-supported ruthenium catalyst with potassium promoter, Appl. Catal. A Gen. 541 (2017) 1–7.
[186] D.D. Laskar, M.P. Tucker, X. Chen, G.L. Helms, B. Yang, Noble-metal catalyzed hydrodeoxygenation of biomass-derived lignin to aromatic hydrocarbons, Green Chem. 16 (2014) 897–910.
[187] M. Behrens, and R. Schlögl, X-ray diffraction and small angle X-ray scattering, in: M. Che, J.C. Védrine (Eds.), Charact. Solid Mater. Heterog. Catal. From Struct. to Surf. React., 1st ed., Wiley-VCH Verlag GmbH & Co., Weinheim, Germany, 2012: pp. 611–652.
[188] N. Li, M. Almarri, X.L. Ma, Q.F. Zha, The role of surface oxygen-containing functional groups in liquid-phase adsorptive denitrogenation by activated carbon, New Carbon Mater. 26 (2011) 470–478.
[189] W. Leitner, J. Klankermayer, S. Pischinger, H. Pitsch, K. Kohse-Höinghaus, Advanced biofuels and beyond: chemistry solutions for propulsion and production, Angew. Chemie - Int. Ed. 56 (2017) 5412–5452.
[190] A. Cho, H. Kim, A. Iino, A. Takagaki, S. Ted Oyama, Kinetic and FTIR studies of 2-methyltetrahydrofuran hydrodeoxygenation on Ni_2P/SiO_2, J. Catal. 318 (2014) 151–161.
[191] A. Rozenblit, A.J. Avoian, Q. Tan, T. Sooknoi, D.E. Resasco, Reaction mechanism of aqueous-phase conversion of γ-valerolactone (GVL) over a Ru/C catalyst, J. Energy Chem. 25 (2016) 1008–1014.
[192] X. Huang, S. Kudo, U.P.M. Ashik, H. Einaga, J.I. Hayashi, Selective hydrodeoxygenation of γ -valerolactone over silica-supported Rh-based bimetallic catalysts, Energy Fuels 34 (2020) 7190–7197.
[193] R.M. Bababrik, B. Wang, D.E. Resasco, Reaction mechanism for the conversion of γ-valerolactone (GVL) over a Ru catalyst: a first-principles study, Ind. Eng. Chem. Res. 56 (2017) 3217–3222.
[194] M.G. Al-Shaal, A. Dzierbinski, R. Palkovits, Solvent-free γ-valerolactone hydrogenation to 2-methyltetrahydrofuran catalysed by Ru/C: a reaction network analysis, Green Chem. 16 (2014) 1358–1364.
[195] J.Q. Bond, D. Martin Alonso, R.M. West, J.A. Dumesic, γ-Valerolactone ring-opening and decarboxylation over SiO_2 /Al_2O_3 in the presence of water, Langmuir 26 (2010) 16291–16298.
[196] L. Faba, E. Díaz, S. Ordóñez, Hydrodeoxygenation of acetone-furfural condensation adducts over alumina-supported noble metal catalysts, Appl. Catal. B Environ. 160–161 (2014) 436–444.
[197] R.W. Jenkins, C.M. Moore, T.A. Semelsberger, A.D. Sutton, Heterogeneous ketone hydrodeoxygenation for the production of fuels and feedstocks from biomass, ChemCatChem 9 (2017) 2807–2815.
[198] L.D. Field, S. Sternhell, J.R. Kalman, Organic Structures from Spectra, 5th ed., John Wiley & Sons, Ltd., West Sussex, UK, 2013. 497 p.
[199] J.L. González Escobedo, E. Mäkelä, J. Neuvonen, P. Uusi-Kyyny, M. Lindblad, R. Karinen, R.L. Puurunen, Hydrodeoxygenation of propylphenols on a niobia-supported platinum catalyst: ortho, meta, para isomerism, reaction conditions, and phase equilibria, Adv. Sustain. Syst. (2020) 1900140.

Aalto-DD 111/2021

ISBN 978-952-64-0479-0 (printed)
ISBN 978-952-64-0480-6 (pdf)
ISSN 1799-4934 (printed)
ISSN 1799-4942 (pdf)

Aalto University
School of Chemical Engineering
Department of Chemical and Metallurgical Engineering
www.aalto.fi

BUSINESS + ECONOMY

ART + DESIGN + ARCHITECTURE

SCIENCE + TECHNOLOGY

CROSSOVER

DOCTORAL DISSERTATIONS